Microbial Mat-Related Structures: Laboratory Experiments and Observations from the Mesoproterozoic Belt Supergroup, Southwestern Montana, U.S.A.

by

Olga Kovalchuk

A thesis submitted in partial fulfillment of the requirements for the degree of

Master of Science

Department of Earth and Atmospheric Sciences
University of Alberta

Abstract

Siliciclastic sediments become biostabilized when benthic bacteria penetrate into the pore spaces and secure grains with filaments and extracellular polymeric substances, forming a microbial mat. The cohesive microbial cover changes typical sedimentary dynamics and leads to formation of diverse microbial mat-related structures. While modern communities are mostly restricted to stressed environments, in the Precambrian through to Ordovician time microbial mats dominated aquatic environments, which is reflected by the abundance of mat-related structures found in strata of this age. Modern day structures are well documented and provide analogs for fossil mat-related structures, but some missing links still exist. Crack-like features are the most common, but also the most puzzling structures. While some are interpreted as shrinkage cracks that form due to desiccation, synaeresis or intrastratal degradation and dewatering of the biomat, others are interpreted as loading structures or remnants of buckled mats. To better understand the influence of microbial mats on desiccation, experiments were carried out using clay-rich and clay-poor substrata. It was observed that the water-rich microbial mat shrinks substantially with desiccation, but its heterogeneous distribution results in an irregular crack network, made up of composite radiating cracks with coiled margins. The shallow penetration of bacteria into the substratum, especially the clay-rich sediment, limits its influence on cracking. The microbial mat modified the orthogonal clay-induced cracks by withstanding crack propagation and by producing curled-up crack polygon margins. The strata of the upper Missoula Group and Spokane Formation (Ravalli Group) of the Mesoproterozoic Belt Supergroup in southwestern Montana were observed to contain well preserved and reoccurring mat-related structures.

Various cracks, were examined in detail, including thin section and scanning electron microscopy analyses. Some cracks intersect in 120º or 90º junctions, providing evidence for shrinkage, while others show soft sediment deformation features and deformed laminae within the crack fill that are the most consistent with an active infill. Other structures were interpreted as kinneyia wrinkles, nodular surfaces and remnants of gas domes. Thin veneers made up of anastomosing argillaceous, carbonaceous and iron-rich fibers were observed to be associated with mat-related structures and interpreted as biolaminae that were formed by the trapping and binding action of ancient bacteria. In addition to mat-related structures, four instance of bilobate structures were found on two bedding surfaces of strata that are currently mapped as the upper Missoula Group. Such structures are interpreted as probable metazoan traces, such as the *Aulichnites*-like trace made by an early bilaterian mollusc-like animal.

Preface

This thesis is an original work of Olga Kovalchuk. Chapter 2 of this thesis has been published as O. Kovalchuk, G. W. Owttrim, K. O. Konhauser and M. K. Gingras, "Desiccation cracks in siliciclastic deposits: Microbial mat-related compared to abiotic sedimentary origin" in Sedimentary Geology, 347 (2017) 67–78. I was responsible for conducting experiments, analysing results and manuscript composition. G. W. Owttrim, K. O. Konhauser and M. K. Gingras were supervisory authors and were involved with concept formulation and manuscript edits. Data collection used for Chapters 3 and 4 has been conducted in collaboration with Dr. J. Brian Mahoney, University of Wisconsin – Eau Claire. Chapters 3 and 4 have not yet been published.

In the loving memory of my stepfather, Sam Doherty.

Acknowledgements

During my academic journey, I was lucky to have the encouragement of many wonderful people. I would like to say a big thank you to my family, your love and support is what keeps me going. A big thank you to my supervisor and mentor Murray Gingras for seeing my potential, and helping me become a more confident geologist and writer. I would like to thank JP Zonneveld for challenging me with insightful discussions and suggesting interesting reading material. Thank you to Kurt Konhauser for sharing his lab with me and his expertise on geomicrobiology. Thank you to George Owttrim for providing bacterial cultures that were essential to the experimental work. I would like to thank Brian Mahoney for guiding us around the Belt outcrops, sharing his expertise of the regional geology, and preparing the most gourmet camping dinners. I really enjoyed staying at the beautiful Dillon KOA, thanks to the owners Bob and Pam for your kind hospitality.

I am thankful for the opportunities that I had as a member of the Ichnology Research Group (IRG), especially going on fun field trips and learning about sedimentology and ichnology from the experts. I enjoyed sharing the office with Alina Shchepetkina and Carolyn Furlong, thanks for always taking the time to give me useful advice. Thanks to Reed Myers for brainstorming ideas and sharing his expert aquarium techniques. Thanks to the rest of the IRG members and alumni for conversations and laughs.

I would like to thank Nathan Gerein whose expertise with the scanning electron microscope have helped me gain a more complete perspective. Thanks to Martin Von Dollen and Mike Labbe for always doing a meticulous job with the thin sections. Thanks to Igor Jakab for his help with scanning, printing and other projects. Thanks to David Chesterman for his assistance with lab equipment. Thanks to the rest of the Earth and Atmospheric Sciences department, Shyra Craig, René Gobeil, Tom Chacko, Lisa Budney, Marilyn Huff and others, for helping me with various things along the way.

Lastly, I would like to thank the Natural Science and Engineering Research Council of Canada, which funded this research through grants provided to Murray Gingras.

Table of Contents

List of Tables

List of Figures

CHAPTER 1: Introduction

Benthic bacteria adhere to solid surfaces forming a thin biofilm that given the right condition develops into a thicker microbial mat (i.e. biomats *sensu* Krumbein, 1983; Krumbein et al., 2003). Mat forming bacteria secrete mucous-like extracellular polymeric substances (EPS) that aid in their attachment to the substrate and survivability (Decho, 1990). In addition to EPS, filamentous bacteria entangle sediment with trichomes, incorporating grains into the mat fabric (Shepard and Sumner, 2010). Bacteria within the microbial mat are organized into horizontal communities based on their geochemical and light needs and tolerances. In the photic zone, the upper microbial mat is dominated by photosynthetic cyanobacteria, while the lower zone consists of anaerobic phototrophic and heterotrophic bacteria, fermenters and methanogens (see Konhauser, 2007 for details). Beyond the reaches of sunlight, microbial mats lack photosynthetic communities, but are still successful at biostabilizing substrata (Bernhard et al., 2000; Bailey et al., 2009).

In siliciclastic environments, the leathery microbial cover changes typical sediment-water and -wind interactions, resulting in a formation of microbial mat-related structures (MRS) (Schieber et al., 2007), also termed microbially induced sedimentary structures (MISS) (Noffke et al., 2001). When in contact with physical stresses, the biostabilized sediment shows cohesiveness that is uncharacteristic of loose sediment, producing wrinkles, tears, roll-ups and buckling (Hagadorn and McDowell, 2012). There is also a biological component to the produced structures, as bacteria trap and bind sediment, produce gases and alter the geochemistry of their surroundings that facilitates mineral precipitation (Noffke et al., 2001; Prat, 2001; Schieber, 2004; Darroch et al., 2012). In environments where carbonate or silica precipitation is favorable, early cementation leads to biogenic domal buildups that have a good preservation potential and are easily detected in the rock record, such as stromatolites (Krumbein, 1983; Allwood et al., 2007; Daza Brunet and Bustillo Revuelta, 2014). While microorganisms are successful at establishing microbial mats in siliciclastic

environments, due to the lack of early cementation such structures have low relief and subtle appearance.

Discoveries of suspected mat-related structures in Archean siliciclastic strata prompted studies of the modern microbial mats in order to provide explanations for the fossil structures. While microbial mats dominated the ancient aquatic environments, the evolution of mat grazing metazoan and damaging vertical burrowing behaviors restricted microbial mats to stressed environments (Seilacher, 1999). Modern siliciclastic microbial studies are mostly limited to tidal flats, lagoons and sabkhas (Cameron et al., 1985; Gerdes et al., 1993, 2000; Noffke 1998, 1999; Gerdes, 2007; Bose and Chafetz, 2009; Cuadrado et al., 2014). While modern mat-related structures of various morphologies have been documented and linked to similar structures seen in the rock record, there are still some missing links between the ancient and the modern structures (Dornbos et al., 2007; Eriksson et al., 2007b; Bouougri and Porada, 2007a; Bottjer and Hagadorn, 2007; Porada et al., 2008). It is suggested that not all microbial mat-related structures may form at the surface, but during burial and early diagenesis, thus are not easily observed (Harazim et al., 2013).

Crack-like feature are among the most commonly observed structures on Precambrian to Ordovician biostabilized bedding surfaces, but the mechanisms responsible for their formation are one of the most debated (Plummer and Gostin, 1981; Pratt, 1998; Tanner, 1998, 2003; Cowan and James 1992; Harazim et al., 2013) . Numerous modern day studies provide evidence that desiccation of heterogeneous microbial mats results in irregular cracks and more regular networks that can be used as analogs for fossil cracks (Gerdes et al., 1993; Porada and Loeffler, 2000; Gerdes, 2007). Shrinkage cracks that are inconsistent with subaerial exposure are proposed to form due to synaeresis or intrastratal cracking processes (Gehling, 1999; Harazim et al., 2013). Alternatively, such networks may not be produced by shrinkage, but are instead mechanical pull-apart structures driven by dewatering and differential compaction (Pflüger, 1999) or remnants of petee structures, which are buckled and deformed microbial mats (Parizot et al., 2005; Gerdes, 2007).

Chapter 2 is an experimental study that provides a direct comparison between desiccation cracks formed in substratum that is biostabilized with a 35-day old microbial mat (i.e. biotic) and those formed in identical, but sterilized (i.e. abiotic) siliciclastic substratum. Different sediment mixtures are used: (1) very fine-sized sand, (2) mixed (ungraded) silt/clay, and (3) normally graded silt/clay. In all of the experiments, the water-rich microbial mat contracted substantially while drying, producing isolated pockets of shallow, but wide cracks, the distribution of which is controlled by heterogeneities in the mat structure and thickness variations of the mat. In the sand-rich substratum, the microbial mat is the only crack-forming mechanism, while in the clay-rich substrata (experiments 2 and 3) desiccation cracks are more strongly influenced by clay shrinkage. The abiotic clay-rich sediment produced a polygonal network of deep cracks intersecting at 90 - 120^{o} junctions. In the biotic clay-rich experiments, the microbial mat modified these desiccation features by withstanding crack propagation or by producing curled-up crack polygon margins. It is concluded, that even though a microbial mat shrinks substantially with desiccation, its cohesive nature and heterogeneous distribution prevents the formation of a regular crack network, while its shallow penetration into the sediment limits its influence on cracking.

Chapter 3 describes diverse mat-related structures that are observed on the bedding surfaces of the Mesoproterozoic shallow-water strata of the upper Missoula Group and Spokane Formation (Ravalli Group), part of the Belt Supergroup in southwestern Montana and proposes mechanisms for their formation. The structures are interpreted as kinneyia wrinkles, nodular surfaces, remnants of gas domes and versatile cracks. Thin argillaceous veneers are observed to be associated with mat-related structures and are predominantly preserved in depressions within the bedding surfaces. These veneers are interpreted as biolaminae produced by trapping and binding activity of ancient mat-forming bacteria, as they have a striking similarity to the "wavy-crinkly" appearance that is characteristic of modern and fossil biomats (e.g. Noffke et al., 2013). Diverse cracks are the most commonly observed structures and are classified based on their morphology and crack fill.

Chapter 4 focuses on suspected trace fossils that were found in the rocks that are currently mapped as Mesoproterozoic upper Missoula Group. Belt stratigraphy is based on

isolated outcrops and is not well delineated. The Neoproterozoic strata is thought to be mostly absent in western Montana, where the middle Cambrian sandstones unconformably overlay the Mesoproterozoic Belt strata. Microbial mats provided food and oxygen needed for evolution of metazoans and it is common that ancient trace fossils are found on biostabilized bedding surfaces (Hagadorn and Bottjer, 1999; Gingras et al., 2011). We propose that some slivers of strata may be misinterpreted as Belt Supergroup, but are in fact younger Neoproterozoic – early Cambrian in age.

In summary, this thesis aims to understand the influence of microbial mats on the formation of sedimentary structures by conducting laboratory experiments and examining fossil mat-related structures. The goals of this thesis is: (1) to understand the microbial influence on desiccation crack development, focusing on biomat-shrinkage versus clay-shrinkage as the crack forming mechanism; (2) to describe and interpret microbial mat-related structures observed on the bedding surfaces of the Belt Supergroup, focusing on the crack-like features and; (3) to describe and interpret possible biogenic traces that are associated with microbial mats.

CHAPTER 2: Experimental desiccation cracks in siliciclastic deposits: Microbial mat-related compared to abiotic sedimentary origin

Introduction

Loose siliciclastic sediment becomes biostabilized once it is colonized by a microbial mat. During biostabilization, cyanobacterial filaments entangle sedimentary grains, and extracellular polymeric substances (EPS) secure grains into a cohesive matrix, protecting the bound grains from hydraulic entrainment and subsequent transport (DeBoer, 1981; Hagadorn and McDowell, 2012). EPS are hydrated polymer chains, approximately 99% water by weight, which are secreted by the microorganisms and play a key role in their survivability (Decho, 1990). Microbial mats (i.e. biomats *sensu* Krumbein, 1983; Krumbein et al., 2003) are thus sheet-like structures composed of diverse microbial communities, EPS and entrapped sedimentary grains (for review of proposed definitions see Gerdes, 2010). Owing to their high cohesiveness, tensile strength and erosional resistance, biomats facilitate exceptional preservation of sedimentary structures, trace fossils and soft tissues (Gehling, 1999; Seilacher, 2008; Gingras et al., 2011; Carmona et al., 2012; Pecoits et al., 2012).

In binding the siliciclastic sediment, biomats leave distinctive structures and micro-impressions, collectively referred to as mat-related structures (MRS) (Schieber et al., 2007). Ubiquitous MRS are described from the siliciclastic rock record throughout the geologic time, but especially in Precambrian through to Ordovician strata, when microbial mats thrived in a wide range of environments (Schieber, 1998; Seilacher, 1999; Noffke et al., 2006a; Noffke et al., 2006b; Sarkar et al., 2006; Sarkar et al., 2008; Porada and Druschel, 2010; Noffke et al., 2013 and others). An assortment of mat-related structures have been documented from modern-day tidal flats, lagoons and sabkhas (Cameron et al., 1985; Noffke 1998; Noffke 1999 and others). While some modern MRS bear a striking resemblance to the structures seen in the rock record, many fossil structures that are thought to be related to

biostabilization do not have clear modern analogs (Dornbos et al., 2007; Eriksson et al., 2007a; Bouougri and Porada, 2007a; Bottjer and Hagadorn, 2007; Porada et al., 2008).

One puzzling category of fossil MRS is the microbial shrinkage cracks. In Precambrian through to Ordovician rocks, cracks of various morphologies and sizes reoccur on bedding planes in siliciclastic strata, ranging from isolated spindle shaped, sinuous cracks, to triradiate morphologies and complex polygonal networks (Porada and Loeffler, 2000; Bouougri and Porada, 2002; Parizot et al., 2005; Harazim et al., 2013). Proximity of such cracks to microbial fabrics, carbonaceous wavy-crinkly laminae, and the presence of authigenic pyrite suggests that the bedding planes were once biostabilized and that the cracks were (at least in part) associated with biomats. Fossil cracks found in clean sand are the most convincing evidence of microbial influence because rigid sand grains do not contract and also lack cohesiveness to form cracks (Eriksson et al., 2007a). The leading interpretation is that such fossil cracks form by subaerially exposed and desiccating microbial mats, such as those observed in the modern intertidal and supratidal biostabilized sediments (Cameron et al., 1985; Gerdes et al., 1993; Gerdes, 2000; Eriksson et al., 2007a; Gerdes, 2007; Bose and Chafetz, 2009; Cuadrado et al., 2014). Since tidal flats are typically characterized by the presence of silt and clay deposited during fair conditions, the microbial cracks are the result of both biomat and clay shrinkage producing an irregular network that is distinct from the orthogonal pattern induced by clay desiccation (Fig. 2-1).

It is difficult to isolate microbial mat influence on crack development and morphology in intertidal and supratidal regions because the observed microbial cracks have a complex history of formation. The desiccation is driven by tidal water table fluctuations causing multiple desiccation and biostabilization cycles during which the pore pressure variations may drive the underlying sediment to infill the cracks or produce petee structures which can serve as loci of cracks (Porada et al., 2007). Evaporation is typically the final step in removing interstitial water and producing desiccation cracks. The goal of this study is thus to determine microbial influence on crack development and morphology by providing a direct comparison of microbial mat- and sediment-related desiccation cracks formed during a single evaporation event. Since desiccation in our experiments is driven by evaporation

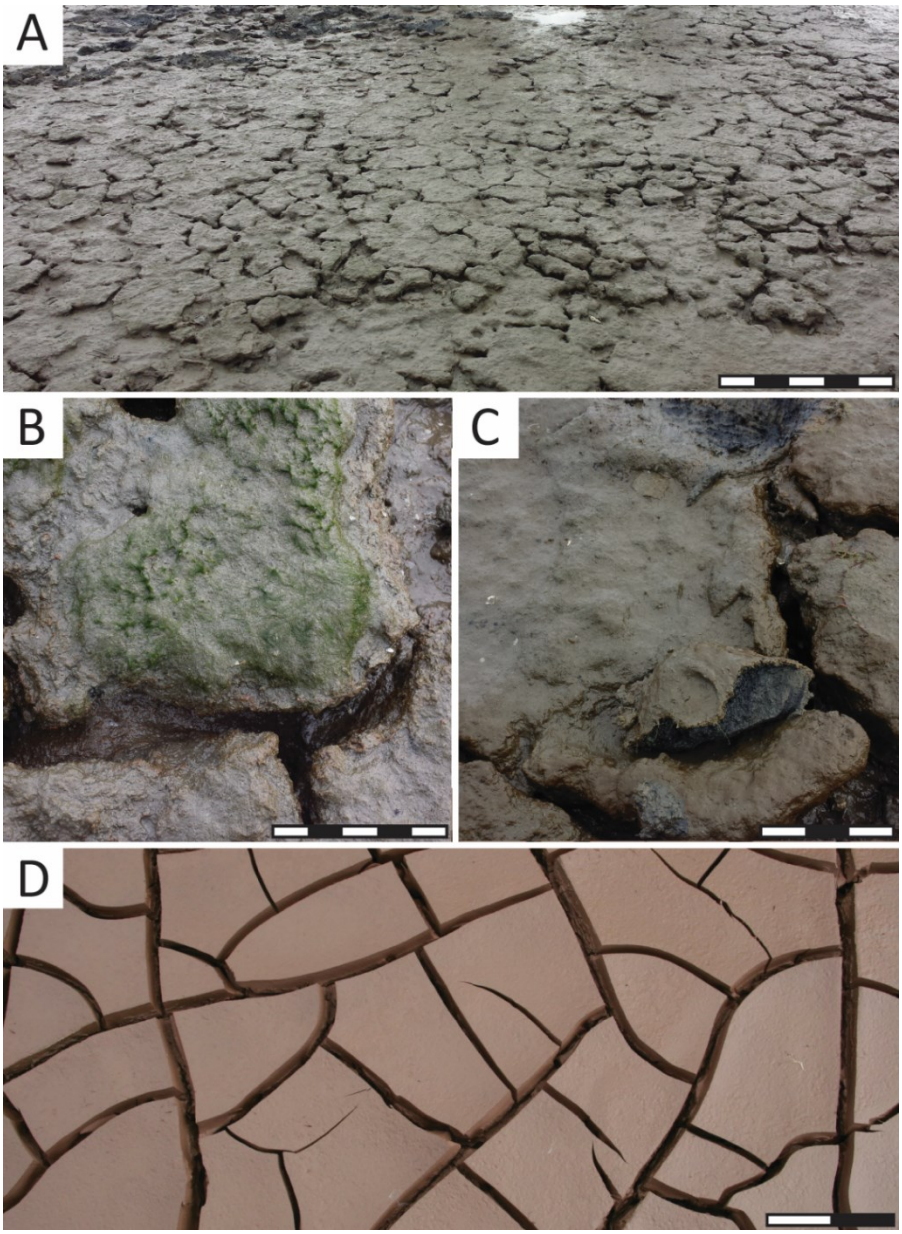

Figure 2-1. Desiccation cracks observed in biostabilized and predominantly abiotic sediments. (A) Desiccation cracks observed in clay-rich sediment colonized by a microbial mat, Fraser River delta, British Columbia. The cracks intersect to form irregular crack-polygons with rounded edges that vary in size 3-40 cm. Microbial mat prevents the features from getting destroyed with flooding, although some crack polygons are eroded forming wide depressions. Scale bar is 50 cm. (B) Bacterial filaments forming reticulated pattern on top of the crack polygon. Scale bar is 5 cm. (C) Cross-section of the biomat, showing thin 1-2 mm layer of photosynthetic bacteria and dark anoxic zone underneath the mat. Scale bar is 3 cm. (D) Orthogonal cracking pattern, typical of desiccated clay-rich sediment, observed on the shores of Petitcodiac River, New Brunswick. Scale bar is 20 cm.

only, the results are most directly comparable to structures produced in temporary pools in supratidal and terrestrial environments. Nonetheless, these findings can also be used as a basis for understanding desiccation in more complex tidal settings and extrapolated to the rock record.

Methods

Preparation of substratum

Sediment was collected at the Fraser River Delta near Vancouver, Canada, and then used as the substrata for the experiments. The sediment was rinsed and then heated in a convection oven at 110^{o}C for 24 hours, drying and sterilizing the sediment. The dry sediment was manually disaggregated using a mortar and pestle and then sieved for 10 minutes using W.S Tyler RX-29 automatic sieve shaker. Sediments collected in sieves No. 120-230 (125-62 μm) were washed with distilled water to reduce the number of residual fines and to produce a sediment dominated by sand sized grains. Sediments finer then coarse silt (<62 μm) were collected in the bottom pan and used as the silt/clay substratum: this fraction was further analyzed using a Micromeritics Corporation Sedigraph 5100, which determined 18-25 wt% clay content (i.e. phylosillicates less than 2-4 μm in diameter) (Fig. 2-2).

Preparation of tanks

Glass tanks, with dimensions of 30 x 30 x 15 cm, were constructed and filled with an even 2 cm layer of sediment. The tanks were paired in the following way: tank-pair 1 was filled with very fine sand (125-62 μm), tank-pair 2 with mixed (ungraded) silt/clay (<62 μm), and tank-pair 3 with normally graded silt/clay (<62 μm) (clay-rich top layer and a silt-rich bottom layer). For each tank-pair, one tank was inoculated with cyanobacteria and left to form a microbial mat over a period of 35 days, whereas the other tank was exposed daily to UV-C radiation to sterilize the sediment and maintain abiotic conditions. Dechlorinated, nutrient spiked tap water and deionized type 1 (ultrapure) water was used for the biotic and abiotic tanks, respectively. The water was slowly siphoned into each of the tanks to prevent

re-sorting of the sediment, except for the normally graded tank, where sediment was stirred and allowed to naturally settle from suspension. During the desiccation experiments, water was left to evaporate naturally in the tanks, and repeated UV-C irradiation kept one tank of each pair sterile throughout desiccation.

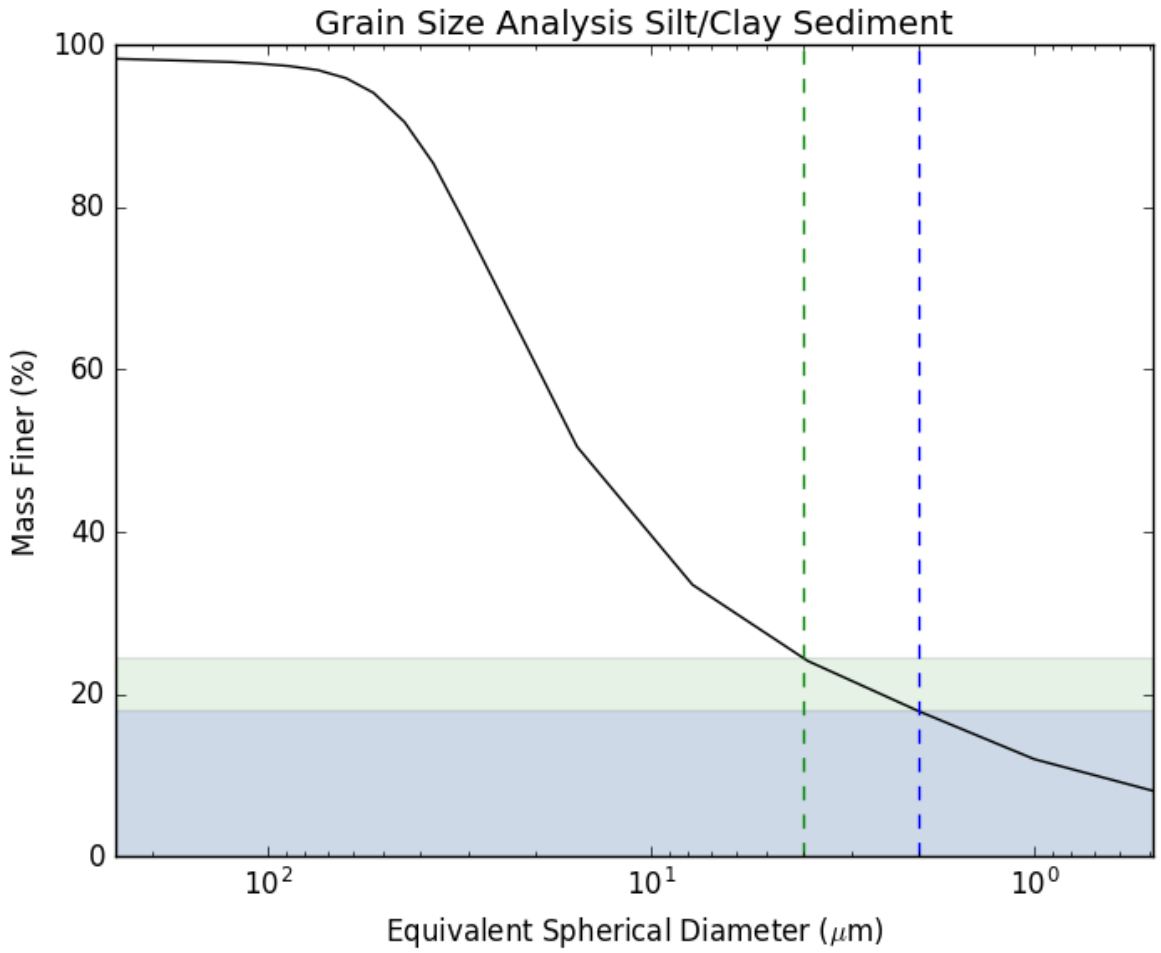

Figure 2-2. Grain size distribution in mixed (ungraded) and normally graded silt/clay sediment. Clay percentage of the bulk composition ranges from 18-25% depending if using 2μm or 4μm as the silt/clay cut-off.

Inoculation and growth of cyanobacteria (biotic tank)

Cultures of non-axenic filamentous cyanobacterium *Leptolyngbya* sp. CPCC 696 (Canadian Phycological Culture Centre: CPCC) were used to establish the biomats in this

study. *Leptolyngbya* were maintained on BG-11 agar plates and inocula grown in liquid BG-11 at 30ºC under a light intensity of 30 microEin/m2/sec (Owttrim, 2012). The tanks were filled with dechlorinated tap water (such as that used in fresh water aquariums, using Seachem Prime Water Conditioner) (Hagadorn and McDowell, 2012), containing dissolved plant fertilizer (Schultz African Violet Liquid Plant Food, 8-14-9, 7 drops/L of water) to which a liquid *Leptolyngbya* culture was introduced. Tank water level was maintained at 3-4 cm above the substrate. The microbial biofilms developed into cohesive microbial mats over a period of 35 days, reaching a thickness of approximately 1 millimeter while wet.

Sterilization of sediment (abiotic tank)

The sterilized tanks were filled with 3-4 cm type 1 purified water from a Barnstead™ Easypure™ II Water Treatment System. Using two Philips 15W mercury-vapor germicidal lamps, the abiotic tanks were subjected to UV-C radiation for 30 minutes daily. The UV-C spectrum peaked at 254 nm with 80 $\mu W/cm^2$ power output (averaged over the UV-C band: 100 nm – 290 nm wavelengths) at the water's surface.

Desiccation experiment

Starting with equal water levels, the biotic and abiotic tanks were left to desiccate *via* evaporation at room temperature (20-22ºC). Desiccation took one week to complete. Observations were recorded daily, focusing on differences between crack formations in abiotic *versus* biomat colonized sediments, specifically the timing of first desiccation crack formation and increases in the density or sizes of the cracks with time. Daily photographs were taken using Canon EOS 50D digital SLR camera placed on a photo stand directly above the tanks. Macro-lens was used to take more detailed photographs of the desiccation features.

In order to quantify the produced crack bounded polygons in clay-rich sediments, the photographs were converted into gray scale images, following a conversion into binary images, where the black pixels represent cracks and the white pixels represent polygons. Crack trajectories in the binary images were corrected and stray pixels were deleted, by overlying the binary image with the original photograph. Photograph processing algorithms were applied to the binary image using Python's Skimage library, which identified polygons

(white pixels) using the bounding cracks (black pixels). The polygon surface areas were calculated, first based on how many pixels each contained and later converted to cm^2. In order to exclude small features that were not representative of the desiccation network, 1 cm^2 filter was applied.

Additionally, the dry samples from each tank were analyzed with a Scanning Electron Microscope (SEM) to observe the bacterial and EPS interactions with the sediment grains. SEM micrographs were taken to document these findings.

Results

Microbial growth and development into a mat

In all of the biotic tank experiments, a visible biofilm formed on the sediment within 48 hours of inoculation. The bacteria first organized themselves into small conical tufts, which then developed into a stringy reticulated pattern as the biofilm matured: this is similar to the growth patterns described in Shepard and Sumner (2010). Development of a microbial mat was accompanied by the production of metabolic gases which were trapped underneath the mat, within the mat fabric, and by the bacterial mucilage water, forming bubbles (Fig. 2-3). Most small bubbles, 1-3 mm in diameter, were stable and remained present throughout the mat's lifecycle, while larger accumulations of gases underneath the domes reached 1 cm in diameter and were often released into the atmosphere (e.g. Bosak et al., 2010).

Sand substratum

The microbial mat effectively biostabilized the sand substratum, forming a 1 millimeter thick, cohesive layer that was flat-laying against the sediment (Fig. 2-3 A, B). SEM analysis shows that bacterial filaments and EPS penetrate into the sand using the space between the grains, reinforcing attachment to the substrate (Fig. 2-9 B). Gas bubbles were observed escaping the mat surface, but they did not cause the mat to become buoyant due to strong attachment of the mat to the substrate.

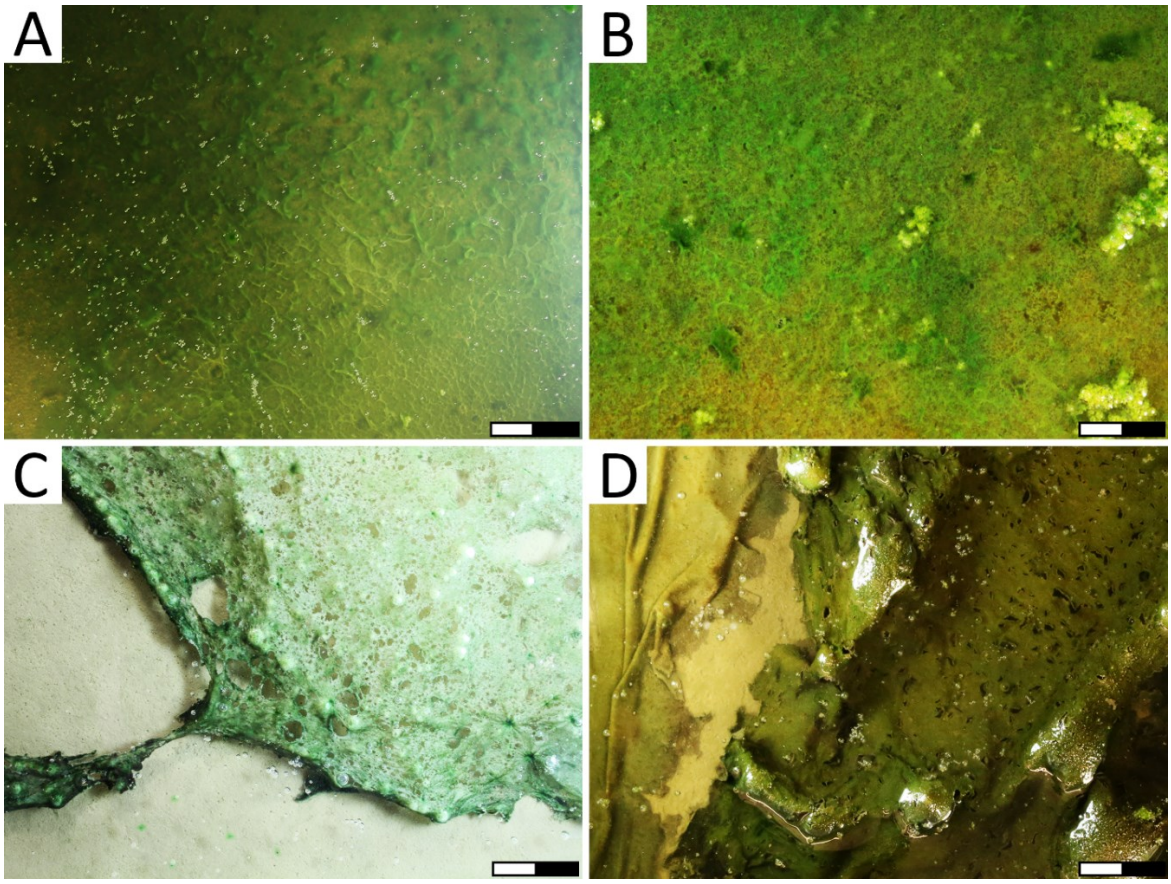

Figure 2-3. Microbial mat growth and development. (A) 10 day old biofilm forming a reticulated surface pattern on the very fine sand substratum, note the small gas bubbles trapped at the water surface. (B) 30 day old microbial mat developed on the very fine sand substratum showing a complex reticulated pattern. (C) Normally graded silt/clay sediment colonized with a 7 day old biofilm showing gas bubbles that are accumulating underneath the biofilm. (D) 30 day old microbial mat developed on the mixed (ungraded) silt/clay substratum. Microbial mat becomes wrinkled due to escape of gases. Scale bar is 2 cm.

Silt/clay substratum

The microbial mat was less successful in biostabilizing the clay-rich substratum and it tended to become suspended in the water column by accumulated metabolic gases forming domal structures (Fig. 2-3 C, D). SEM images show that bacterial filaments and EPS did not penetrate as deeply into the clay-rich substratum due to smaller pore sizes, resulting in a weak attachment (Fig. 2-9 E). Notable wrinkles were developed in the microbial mat, initially at

the slopes of the suspended mat-dome structure, but later over the entire biomat as the domes collapsed due to release of gas (Fig. 2-3 D). The mat did not cover the entire surface area of the tank and mainly concentrated at the center due to suspension and buckling. A new biofilm started to form in the available space at the edges of the tank. The old mat became scared by the escaping gas bubbles giving it a perforated texture (Fig. 2-3 D).

Microbial mat desiccation on sandy *versus* clay-rich substrata

Growth of the microbial mat, in terms of its lateral and vertical colonization of the substrata, had a direct influence on desiccation patterns. Only the thin layer of sediment that was colonized by the cyanobacteria (up to 500 μm in the sand and only about 150 μm in the clay-rich sediment) was involved in the biomat induced desiccation, resulting in shallow cracks. Imperfections in the biomat led to structural weaknesses, such as gas domes and tears, provided the loci for radiating cracks By contrast, regions of greater biomat thickness prevented cracks from propagating and connecting to one another. Table 2-1 summarizes the crack patterns formed in the biotic and abiotic substrata.

Sand substratum

In the sand substratum, the shrinking biomat was the only mechanism that formed desiccation cracks. Initial cracking and coiling of the margins occurred rapidly, but the biomat and attached sediment continued to shrink and curl upwards over the following 24 hours (Fig. 2-4 A-C). Microbially induced desiccation resulted in uneven crack network over the sediment surface. Large portions of the biomat, for example, at the bottom left corner of the tank, remained intact, although the biomat displayed an overall contraction (reduction in surface area) (Fig. 2-4 C). Weaknesses in the biomat, such as scarring by escaping and trapped gas bubbles, provided loci for crack initiation.

The desiccated biomat that colonized sand did not show typical mud crack morphologies, such as polygons, which are completely separated from each other by a rectilinear network of deep cracks. Instead, shallow, radiating cracks that did not propagate far from their point of origin were often isolated from one another or connected to form pockets of composite cracks. Curling at the crack margins obscured the initial crack pattern

and produced wide cracks that exposed the sub-sediment underneath that showed no evidence of cracking (Fig. 2-4 B, C).

	BIOTIC	ABIOTIC
VERY FINE SAND	Underlying sediment (sub-sediment): No cracking. Mat: Radiating, shallow, wide, composite cracks up to 7 cm wide, consisting of microbial mat and attached sediment with margins coiled up to 360°, forming detached curls.	Rare, isolated, thin (hair-like) cracks.
SILT/CLAY (Ungraded, Mixed)	Underlying Sediment (sub-sediment): Flat-laying polygons separated by deep cracks up to 7 mm wide, intersecting in 90 - 120° junctions. Rare tapering cracks forming incomplete polygons. Mat: Top thin layer, consisting of the mat and attached sediment, produced coiling 180-360° at the polygon margins, forming detached curls. Also, shallow radiating cracks with coiled margins independent of the cracked sub-sediment below.	Flat-laying polygons separated by deep cracks up to 7 mm wide, intersecting in 90 - 120° junctions. Rare smaller shallow cracks forming incomplete polygons.
SILT/CLAY (Normally Graded)	Underlying Sediment (sub-sediment): Concave-up polygons separated by deep cracks up to 2 cm wide, intersecting in 90 - 120° junctions. Rare tapering cracks forming incomplete polygons. Mat: Top thin layer, consisting of the mat and attached sediment, produced coiling up to 180° at the polygon margins, forming detached curls. Also, shallow radiating cracks with coiled margins that originated from uplifted gas domes.	Detached concave-up polygons separated by cracks up to 2 cm wide, intersecting in 90 - 120° junctions. Rare smaller shallow cracks forming incomplete polygons.

Table 2-1. Summary of desiccation features produced in biotic and abiotic sediments.

The desiccated abiotic sand of identical composition produced two straight, thin (hair-like) cracks (Fig. 2-4 D), no other contractional features were observed in this abiotic sediment.

Silt/clay mixed (ungraded) substratum

In the clay-rich sediment, both clay and biomat shrinkage contributed to the formation of desiccation cracks (Fig. 2-5 A-C). The clay sub-sediment cracked first while the biomat cover was too moist to crack (Fig. 2-5 B). Initial dilation of the clay induced cracks rapidly, but propagation and widening of the cracks occurred over a 24-hour period. Continuous straight to gently curved cracks penetrated the entire depth of the substratum (except for the top biomat colonized layer) and generally intersected in 90 - 120^{o} junctions, forming square and pentagonal polygons. Also, a few rare and shallow tapering cracks produced incomplete polygons. The crack widths reached up to 7 mm.

At the time of clay desiccation, the biomat remained moist and was either torn by the cracks or was stretched across a crack (bridging the crack) (Fig. 2-5 B). Approximately 24 hours after first appearance of cracks in the clay-rich sub-sediment, the biomat dried and curled upwards along the previously developed crack margins, although a few cracks remained bridged by the biomat, even after drying (Fig. 2-5 C, black arrows). Shallow, wide cracks with coiled margins, similar to those observed in the sand, developed where there were weaknesses in the biomat structures due to gas escape.

Cracks in the abiotic mixed silt/clay substratum were similar to those formed in the biostabilized counterpart. Abiotic cracks penetrated the entire depth of the substratum forming square and pentagonal polygons, with a few smaller shallow cracks forming incomplete polygons (Fig. 2-5 D). Quantitatively comparing the crack bounded polygon surface areas, however, revealed that the mean polygon surface area was larger in the biotic sediment (28.6 cm^2) as compared to the abiotic sediment (19.3 cm^2). Furthermore, less polygons formed the biotic sediment (n = 26) as compared to the abiotic counterpart (n = 40) (Fig. 2-7 A-C).

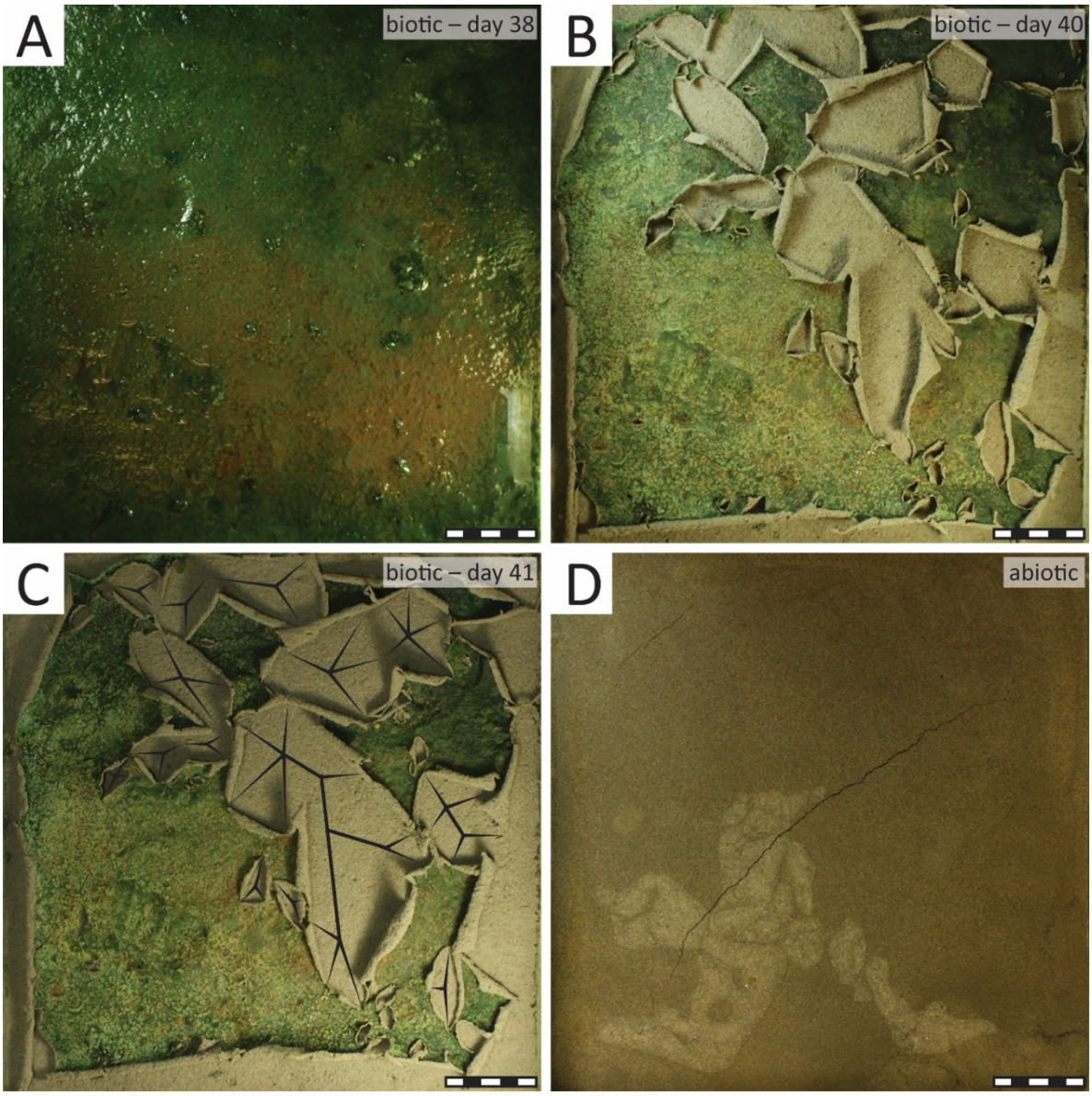

Figure 2-4. Progressive desiccation of the biomat colonized very fine sand and desiccated abiotic very fine sand substrata. (A) 38 day old microbial mat prior to desiccation. (B) Desiccated microbial mat shows irregular cracking pattern characterized by shallow, but wide radiating cracks. (C) Cracks continue to develop over the next 24 hours, characterized by increased coiling of the margins and merging of the cracks, producing composite pockets of cracks. Since curling of the margins obscured the cracking pattern, it is highlighted with black lines. Note that the bottom left corner of the biomat remains mostly uncracked. The underlying sub-sediment shows no cracking, but has a pitted texture. (D) Desiccated abiotic very fine sand substratum produced minor, thin cracks. Scale bar is 5 cm.

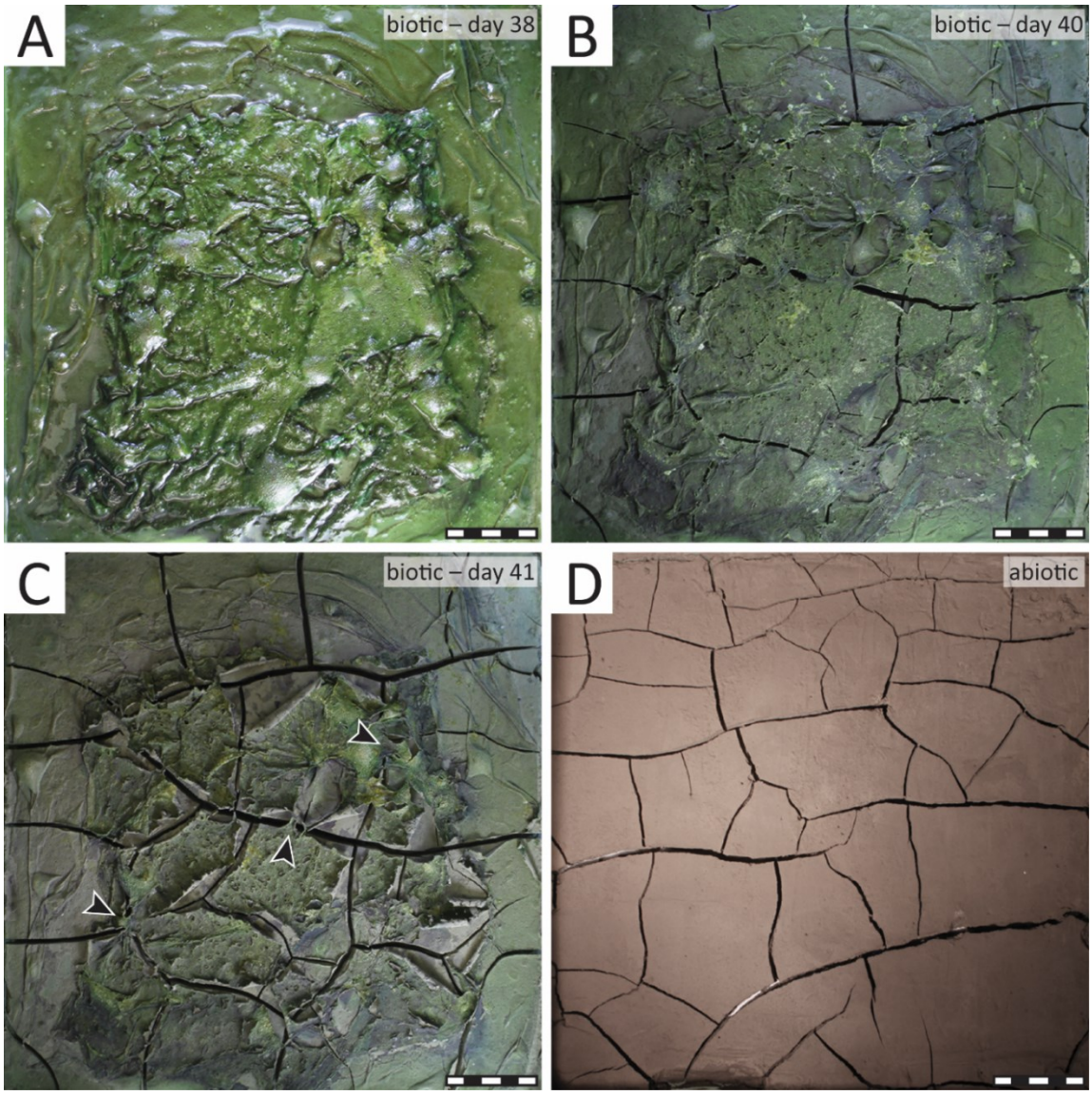

Figure 2-5. Progressive desiccation of the biomat colonized mixed (ungraded) silt/clay and desiccated abiotic mixed (ungraded) silt/clay substrata. (A) 38 day old microbial mat prior to desiccation. Microbial mat is the thickest (oldest) at the center of the tank and becomes thinner (younger) towards the edges. (B) Clay desiccation preceds microbial mat desiccation, where the clay shrinkage rips the still moist microbial mat. Microbial mat shows the ability to withstand crack propagation. (C) 24 hours later, the desiccated microbial mat curls up at the existing crack margins, but also forms shallow cracks that are independent of the sub-sediment. The coiled crack margins are limited to the center of the tank where older microbial mat desiccated. The younger 2 week old biofilm at the edges was not thick enough to curl. Intact microbial mat bridges some of the clay cracks even after drying (black arrows). (D) Desiccated abiotic mixed (ungraded) silt/clay substratum produces a regular network of cracks intersecting in 90-120^{o} junctions forming detached crack polygons. Scale bar is 5 cm.

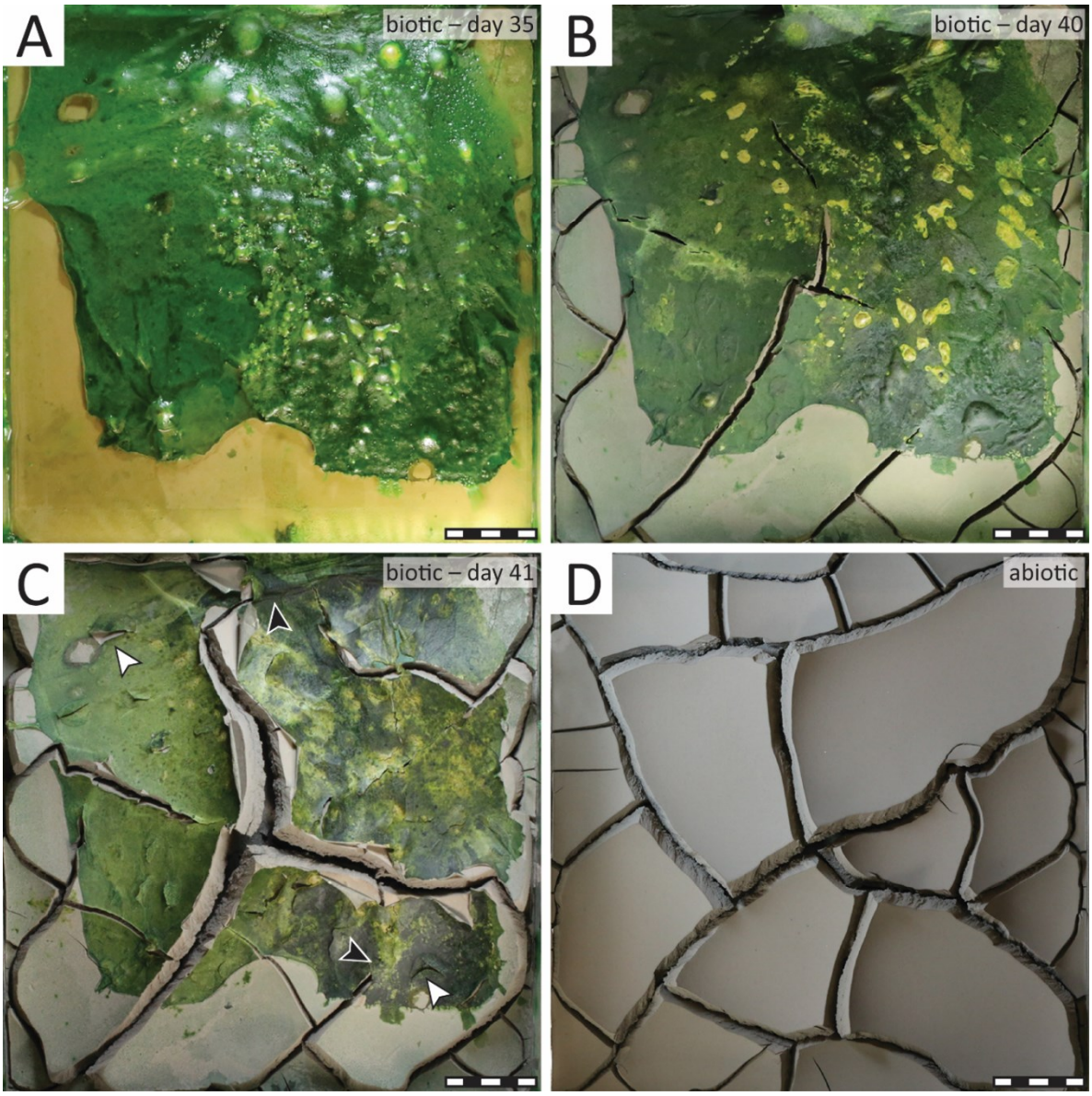

Figure 2-6. Progressive desiccation of the biomat colonized normally graded silt/clay and desiccated abiotic normally graded silt/clay substrata. (A) 35 day old microbial mat prior to desiccation. (B) Clay desiccation preceded microbial mat desiccation, where clay induced cracks rip the still moist microbial mat. (C) 24 hours later, the desiccated microbial mat curls up at the existing crack margins. Dried gas domes became loci of shallow triradiate cracks (white arrows). Microbial mat bridges some of the clay cracks after drying (black arrows). (D) Desiccated abiotic normally graded silt/clay substratum produces a regular network of cracks connecting in 90-120^{o} junctions forming detached crack polygons. Note the concave-up crack polygon margins in both biotic and abiotic substrata, due to the normal grading of the clay-rich sediment. Scale bar is 5 cm.

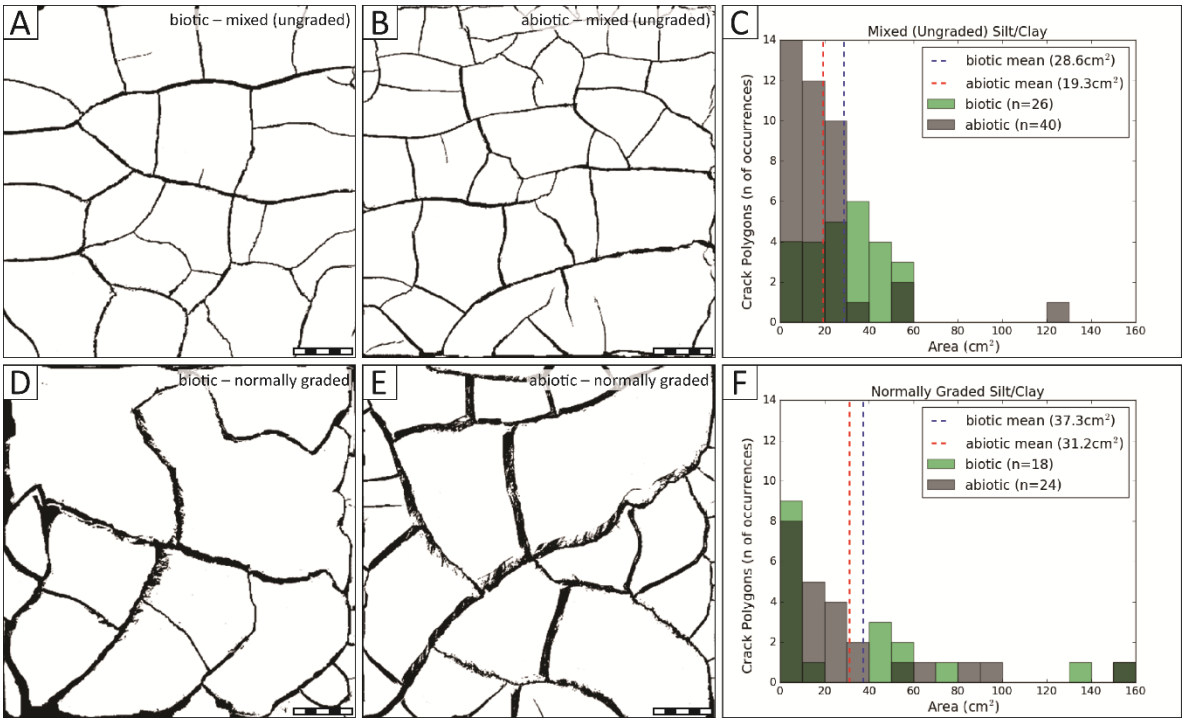

Figure 2-7. Quantitative comparison of biotic and abiotic crack polygons formed in clay-rich substrata. (A, B) Binary images of the desiccated biotic and abiotic mixed (ungraded) silt/clay sediment, respectively. Black pixels represent cracks and white pixels represent crack polygons. (C) Surface areas of crack polygons formed in the sediment are plotted as a histogram. The mean surface area of the biotic and abiotic crack polygons are 28.6 cm^2 and 19.3 cm^2, respectively. In the biotic sediment 26 crack polygons were identified, while in the abiotic sediment 40 crack polygons were identified. (D, E) Binary images of the desiccated biotic and abiotic normally graded silt/clay sediment, respectively. (F) Surface areas of crack polygons formed in the normally graded silt/clay sediment are plotted as a histogram. The mean surface area of the biotic and abiotic crack polygons are 37.3 cm^2 and 31.2 cm^2, respectively. In the biotic sediment 18 crack polygons were identified, while in the abiotic sediment 24 crack polygons were identified. Scale bar is 5 cm.

Silt/clay normally graded substratum

Similar to the mixed (ungraded) silt/clay experiment, the normally graded sub-sediment beneath the biomat cracked first, thereby controlling the ensuing cracking pattern and tearing the still moist biomat (Fig 2-6 A, B). Desiccation of the normally graded clay-rich sub-sediment, produces concave-up crack bound polygons. When the biomat became

dry, 24 hours after the initiation of clay induced cracking, it and attached layer of sediment curled upwards along the existing crack polygon margins, while some of the clay induced cracks remained bridged by the dry biomat (Fig. 2-6 C).

During desiccation of the abiotic and normally graded silt/clay substratum, concave-up polygons with raised margins formed that were separated by deep cracks (Fig. 2-6 D). These structures were similar to those formed by the clay-rich sub-sediment of the biotic tank. The concave-up nature of the polygons produced wide crack separations, up to 2 cm, which is much wider then observed in the mixed silt/clay sediment. As with the mixed silt/clay experiment, the mean crack polygon surface area was larger in the biotic sediment (37.3 cm^2) as compared to abiotic sediment (31.2 cm^2), and less polygons were observed in the biotic sediment (18) as compared to the abiotic counterpart (24) (Fig. 2-7 D-E).

Textures produced by desiccation

The thickness of the siliciclastic layer that was colonized by the biomat varied laterally, resulting in uneven thickness of the desiccated mat curl structure (Fig. 2-8). This differential attachment of grains to the biomat bestowed a pitted and rugose texture to the underside of the biomat curls and on the sub-sediment surface (Fig. 2-8). The texture was more prominent in the mixed clay/silt substratum (Fig 2-8C, D) than in the sand (Fig. 2-8A, B), and it was not visible in the normally graded silt/clay substratum.

SEM imaging

Dry mat curls which formed in the very fine sand and mixed (ungraded) silt/clay were analyzed under SEM. In plan view, the biomat samples from both of these biotic experiments were covered by a cohesive layer of filamentous cyanobacteria characterized by elongated, segmented tube-like bodies about 1 μm in diameter and over 50 μm long, and viscous EPS which coated diatoms, cyanobacteria and the sediment (Fig. 2-9A, D).

A cross-sectional view showed that the cyanobacteria formed a dense 10 μm biomat (dry) on top of the sediment surface, but filaments and EPS penetrated into the pore spaces coating the grains with EPS and entangling the grains with filaments (Fig. 2-9B, E). In the

very fine sand sediment, the cyanobacteria and EPS penetrated as deep as 500 μm (Fig. 2-9B), while the cyanobacteria and EPS only penetrated about 150 μm into the clay-rich sediment (Fig. 2-9E). Cyanobacteria and EPS were scarce on the underside of the biomat curl structures (Fig. 2-9C, F).

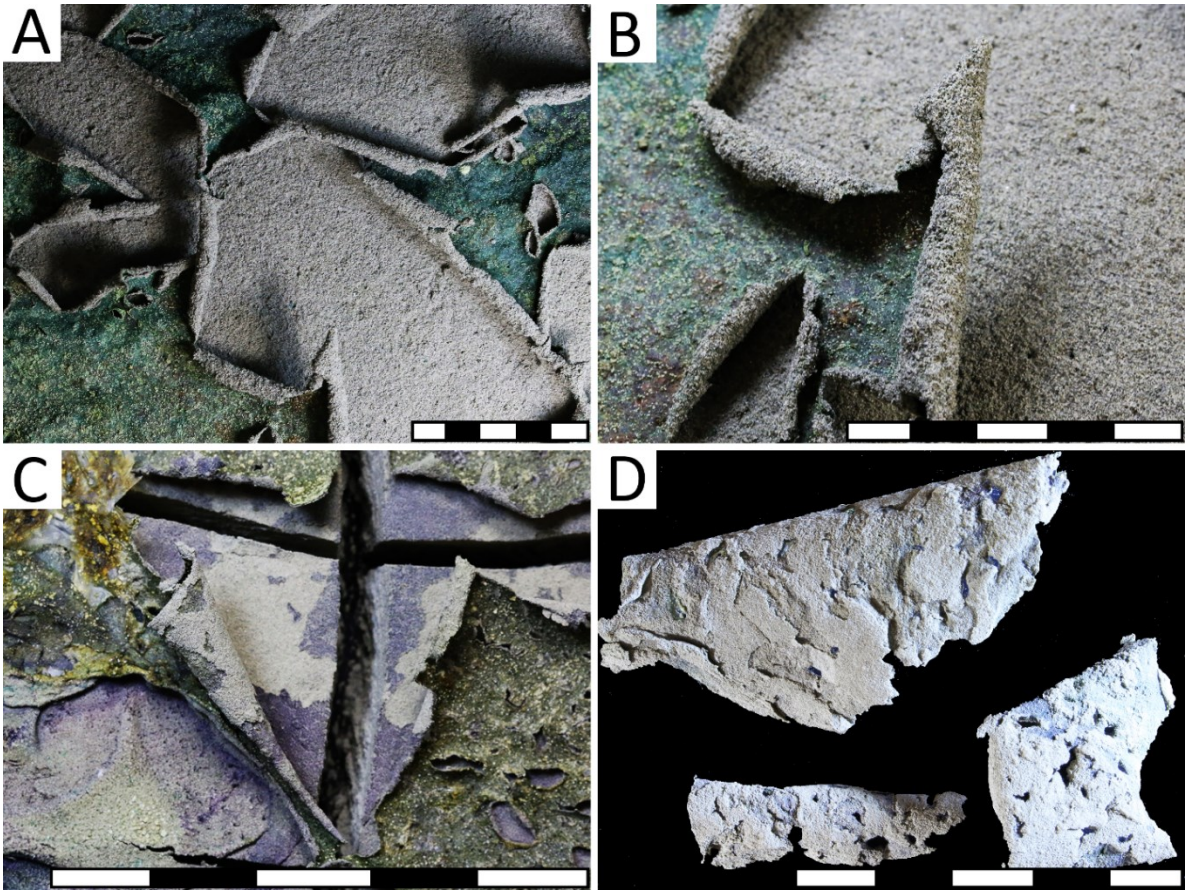

Figure 2-8. Light macrographs of the microbial mat curls and textures left in the underlying sediment. (A) Close-up image showing wide, but shallow cracks formed in the very fine sand substratum. Note the pitted texture that is left behind in the sub-sediment after detachment of the mat curl. (B) Mat curl structure showing coiled margin and pitted texture in the sub-sediment. (C) Uneven, rugged texture in the mixed (ungraded) silt/clay sediment. (D) Rugged texture is also preserved on the underside of the mat curl structure. Scale bar is 5 cm.

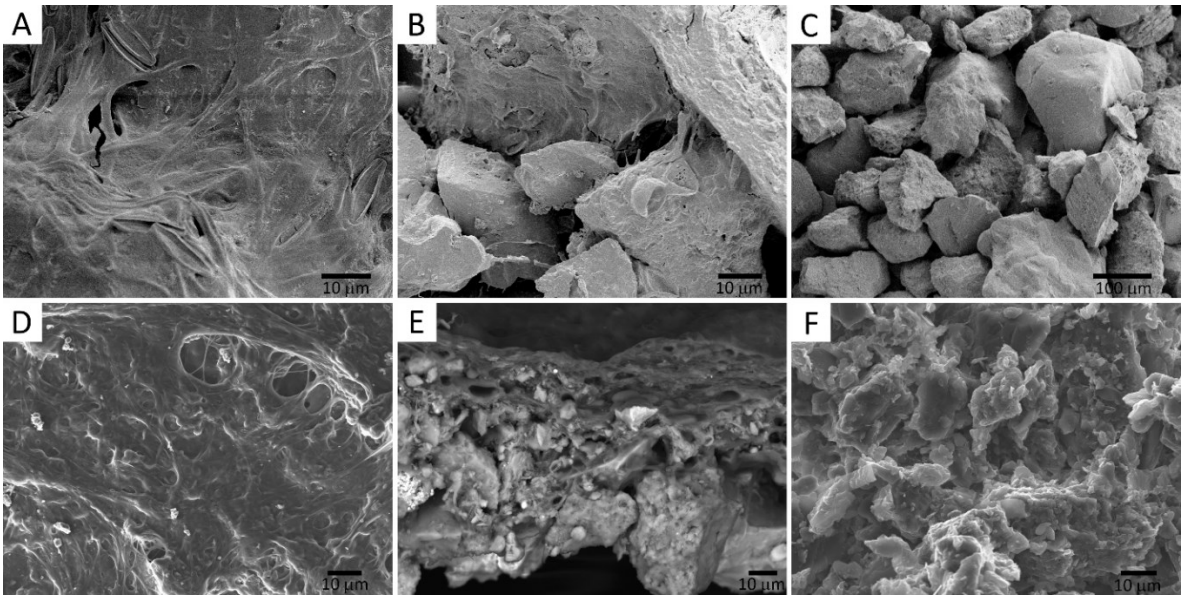

Figure 2-9. SEM micrographs showing biostabilized very fine sand and mixed (ungraded) silt/clay sediment. (A) Plan view of the microbial mat colonized very fine sand showing densely intertwined filamentous cyanobacteria and EPS. (B) Cross sectional view of the dense microbial mat (top right corner) and penetration of cyanobacteria and EPS into the pore spaces. (C) View of the underside of the curl structure formed in the very fine sand, showing rare presence of cyanobacteria and EPS. (D) Plan view of the microbial mat colonized mixed (ungraded) silt/clay sediment showing densely intertwined filaments and EPS. (E) Cross sectional view of the microbial mat and the microbially bound grains developed in the mixed (ungraded) silt/clay sediment. The bacteria and EPS do not penetrate as deeply into the clay-rich sediment as in the sand. (F) View of the underside of the curl structure formed in the mixed (ungraded) silt/clay, showing rare filaments and EPS.

Discussion

Mechanisms behind crack formation

Shrinkage cracks develop when the stress induced from volume loss exceeds the tensile strength of that material (e.g., Bradley, 1933; Groisman and Kaplan, 1994; Shorlin et al., 2000). In the case of desiccation cracks, volume reduction is due to water loss. With microbially stabilized sediments, cracks can form abiotically (due to sediment shrinkage) or biotically (due to biomat shrinkage). The main observed factors that influenced cracking

patterns in our experiments include, the thickness and vertical distribution of the shrinkage-prone materials (i.e. clay minerals or biomat) and physical heterogeneities therein.

Abiotic

The three abiotic sedimentary substrata produced cracks which are distinct from one another, because different grain sizes intrinsically possess characteristic crack-formation patterns. Flake-like clay particles were rearranged and brought closer together by capillary pressures, whereas rigid, spherical sand particles shrink very little with water loss (Bradley, 1933; Eriksson et al., 2007b). As expected, the homogeneous, clay-rich sediments were prone to deep, orthogonal cracking, while clean sand was not prone to cracking, except for minor, thin cracks that can be attributed to residual clay (Fig 2-4D, 2-5D, 2-6D).

In the normally graded, clay-rich sediment the clay was increasingly abundant towards the top of the bed, which means that shrinking intensity of the sediment increased towards the bed-top (Fig. 2-6), resulting in raised crack-polygon margins (concave upwards crack polygons) (Bradley, 1933). In the ungraded, mixed clay-rich sediment, desiccation produced flat laying crack polygons, because clay was distributed evenly throughout the thickness of the sediment (Fig. 2-5). Therefore, the sediment experienced similar shrinkage rates throughout the bed thickness (Bradley, 1933).

In hypersaline lagoons, salt crystal precipitation due to evaporation may have effects similar to those described by Bradley (1933). The larger salt crystals that form on top of the finer clay particles, produce inverse grading that prevents curling of crack margins or even enables convex crack margins that curl inward. Since deionized water was used in these abiotic experiments, there was no visible evaporite precipitation associated with desiccation.

Biotic

As observed under SEM, the topmost portions of the biomat consists of densely intertwined filaments and EPS (Fig. 2-9). Underneath the main biomat structure, filaments and EPS thrive in the pore spaces, but their abundance decreases with depth due to photosynthetic and metabolic limitations. In natural settings the uppermost microbial

community traps and binds grains or is covered by accumulating sediment. In response, the cyanobacteria move upwards to re-establish themselves as a biomat above the sediment. Underneath, the sediment becomes incorporated into the mat fabric (Gerdes et al., 1993), similar to that observed in our experiments.

The water-rich biomat matrix shrunk substantially upon dehydration, bringing the entangled sediment grains into a closer packed arrangement, offering an alternative mechanism for desiccation crack formation. The ability of the uppermost biomat to contract with desiccation is much greater than the sediment below, thus at a certain depth there is a sharp (rather than gradational) change in the physical shear forces of the sediment. Desiccation results in the formation of coiled crack margins (mat curls), where the highly contracted, dry biomat and microbially bound sediment layer become separated from the more rigid sub-sediment below.

In our experiments, the desiccated mat curls are much thicker in the sand (Fig. 4 C), as compared to the clay-rich sediment (Fig. 2-5 C, 2-6 C), due to a deeper colonization of the sand substratum. Thicker mats can be established on porous media, especially quartz rich sediments that allows deeper light penetration (Gerdes, 2007). These experiments show that the thickness of the biomat had to be significant for the biotic cracks to develop: experiments using < 20 day old biofilm did not develop mat curls, even though the sediment surface was covered with a film of cyanobacteria and EPS.

In nature, biomats are thicker stratified communities, where the top few millimeters are largely composed of photoauthotrophs and sulfur-oxidizing bacteria, while the deeper layers below light penetration are composed of various chemoheterotrophic bacteria (see Konhauser, 2007 for details). The biomats may also be vertically discontinuous, due to the repetitive burial by detritus or mineral precipitates (Cameron et al., 1985). Higher curled margins are observed to form in thicker biomats, where the curl height reaches over 3 cm in desiccating mat-sediment laminae that are 1.5 - 2.5 cm thick (Bose and Chafetz, 2009).

Coiled crack margins are one of the most notable indicators of biomat desiccation. This is not a unique property of the biomats, as swelling clays such as smectite are capable

of producing similar coiled margins (Beraldi-Campesi and Garcia-Pichel, 2011). It was shown that the clay content has to be quite high in order for such curls to form: >30% smectite and >40% kaolinite. Only desiccation of smectite results in coiled margins similar to mat curls seen in desiccating biomats (Beraldi-Campesi and Garcia-Pichel, 2011). Also, flip-overs and roll-up structures that are deformational features produced by shear stress acting on a biostabilized bedding plane, have a similar appearance to desiccation mat curls and may be easily misinterpreted in the rock record (Hagadorn and McDowell, 2012).

Salt encrustation in biostabilized sediments may subdue the curling of the margins, similar to the effect observed in abiotic sediment (Bradley, 1933), although it is noted that very abrupt normal grading that results in highly coiled crack margins cannot be easily inverted with salt precipitation. In carbonate settings, crack polygon margins have less developed curled margins, due to early carbonate precipitation (Bose and Chafetz, 2012). Perhaps salt encrustation in highly saline, evaporating conditions would have a similar effect.

Influence of biomats on desiccation crack development and resulting pattern

Cracks in sand substratum

Since the biomat is the only crack forming component in the clean sand, the produced crack pattern is solely controlled by shrinkage of the biomat, where the loci, distribution and propagation of cracks are controlled by regions of higher and lower tensile strength. The latter are ultimately related to mat growth and damage. Thus, fossil, as well as modern microbial desiccation cracks formed in sandy substrata, may have the following characteristics: (1) cracks that radiate from a point of weakness, resulting in pockets of composite radiate (often triradiate) cracks that do not connect to one another; (2) evidence of an irregular and incomplete crack network that produces connected (rather than detached) crack bound polygons; (3) cracks that are unusually wide (often as wide as they are long) due to coiling of the biomat crack margins and evidence of the curled crack margins either preserved *in situ* or as mat chips; and (4) shallow cracks limited by biomat thickness, while sediment underneath shows no cracking, and only an irregular, pitted pattern.

Cracks in clay-rich substratum

In the clay-rich sediments, the limited vertical distribution of the biomat rendered it subordinate to clay as the crack-forming mechanism. The desiccation of biostabilized clay-rich sediment resulted in two cracking patterns superimposed on one another: (1) prominent, deep cracks caused by the shrinkage of the clay and (2) shallow, wide cracks caused by shrinkage of the biomat. These cracking patterns were not completely independent of each other as clay shrinkage, which occurred first, ripped areas of the thinner biomat creating loci for mat cracks. By contrast, the thicker, more cohesive biomat resisted tearing and bridged the clay induced cracks, interfering with the abiotic crack pattern (Fig. 2-5, 6).

Biomats play a secondary role in crack formation in clay-rich sediment, thus cracks in such sediments are not solely due to microbial shrinkage. Microbial influence on cracking, however, can still be recognized as biostabilized clay-rich sediments have cracks that differ markedly from abiotic desiccation cracks and are characterized by: (1) overall deep polygonal crack network that is incomplete or irregular due to biomat bridging and inhibition of crack propagation, particularly if the abiotic cracking is not in line with biomat's own structural weaknesses and strengths; (2) crack polygons that are larger than expected considering the thickness of the cracked bed; and (3) evidence of a secondary shallow crack pattern that shows characteristics of the biomat desiccation described above from the sand-biomat substratum.

The crack polygons in the biomat stabilized clay-rich sediment (both the mixed (ungraded) and normally graded silt/clay) were on average larger than in the abiotic sediment and less crack polygons formed in the biotic sediment as compared to the abiotic counterpart (Fig. 7). The observations are not unusual, as the study done by Bose and Chafetz (2009), showed that crack polygons which are formed in the biostabilized clay-rich sediment of Texas coast tidal flats, reached up to 50 cm in diameter, while the desiccated layer is no thicker than few centimeters. In homogeneous, abiotic sediments, crack polygon size typically increases with thickness of the bed (Plummer and Gostin, 1981), but the cohesive biomat cover subdues crack initiation as well as propagation. The reluctance of biomats to

crack is also observed in the biostabilized sand substratum, where large areas of the desiccated biomat remained un-cracked, although show an overall shrinkage (i.e. reduction in surface area) (Fig. 2-4C).

Comparison to the modern day and fossil microbial cracks

Curled crack margins, wide cracks and irregular networks match well with the general physiology of the cracks produced in modern subaerially exposed microbial mats, especially those formed in temporary pools where evaporation drives desiccation. Clay deposition can be common in such low energy settings and we suspect that clay shrinkage plays the primary role in the resulting polygonal network. The biomat retains moisture longer and plays an important secondary role by interfering with the clay-induced cracking, producing irregularities in the polygons and curled crack margins. Even though the preservation potential of such features is low, especially *in situ* preservation of the mat curls, Eriksson et al. (2000) provide fossil examples of interdune roll-up structures in the 1.8 Ga Waterberg Group fine-grained siliciclastic strata. More commonly the curled crack margins are broken off and transported/deposited elsewhere, producing "mat chips" (Pflüger and Greese, 1996; Eriksson et al., 2007a).

Cracks formed in modern intertidal and supratidal settings are more variable, although are generally polygonal (Gerdes et al., 1993, 2000; Gerdes, 2007; Bose and Chafetz, 2009), even those formed in sandy (clay-poor) biostabilized sediment (Cameron et al., 1985). The polygonal pattern may be the result of a thicker desiccating biostabilized layer, where the bacteria penetrate deeper into the sediment, as compared to our experimental biomat, or because the entrapped or underlying clay fraction is high enough to play a role in crack initiation and distribution. Unfortunately the effect of clay on desiccation is not discussed while describing modern microbial cracks formed in the shrinking "mat-sediment laminae" (Bose and Chafetz, 2009) or simply desiccating "microbial mats" (Gerdes et al., 1993, 2000; Gerdes, 2007). Importantly, cracks that are observed in tidal settings may start out as uplifted petee ridges or gas domes, which rapture with desiccation (Cuadrado et al., 2014). The morphology and distribution of such cracks would be controlled by gas/water overpressure

from below or deformation due to wind or water friction and is different from simple evaporation.

It is proposed that microbial mat genesis can only be accurately ascribed to fossil cracks if they are observed in clean (clay-free) sand (Eriksson et al., 2007a). While fossil "sand cracks" resemble microbial desiccation cracks in a sense that they are polygonal or triradiate (Eriksson et al., 2007a). Moreover many of the cracks tend to be narrow, aligned or overlapping, resembling synaeresis cracks (Porada and Loeffler, 2000; Bouougri and Porada, 2002; Parizot et al., 2005; Bouougri and Porada, 2007a; Harazim et al., 2013). Disconnected, narrow cracks can be explained as incipient cracks that formed during initial stages of desiccation, whereas overlapping cracks should be explained as multiple desiccation and biostabilization events that produce compound generations of cracks. Ability of the biomat to overgrow desiccation cracks was shown to increase their preservation potential and prevent healing during subsequent flooding, allowing the features to survive multiple dry/wet cycles (Gerdes et al., 1993; Gerdes, 2007).

Some authors argue that desiccation struggles to explain the diversity of fossil cracks and facilitate alternative explanations, such as the cracks may have formed intrastratally, where the water is expelled from the water-rich microbial mats with burial and pressure from the overlying sediment (Plummer and Gostin, 1981; Gehling, 1999; Harazim et al., 2013). Another possibility is that such cracks are not produced by shrinkage, but instead are mechanical pull-apart structures formed in gelatinous biostabilized layers under heavy overburden (Pflüger, 1999). Unfortunately, mechanisms of subaqueous and intrastratal crack formation are not that well known, but the differentiation of those and desiccation cracks is important and as such more research on this topic is warranted.

Conclusion

Based on our experiments, we conclude that microbial influence on formation of desiccation cracks can be recognized in clean sand as well as clay-rich sediments. Because the biomat cannot penetrate deeply into clay-rich substrates, the influence of the former on

fine-grained sediment is as a modifying agent of crack-margin and -morphology. In the sand, the biomat penetrates more deeply, forming discernible desiccation cracks, which do not form abiotically. Our work implies that biomats have two roles in the desiccation process depending on the substratum: (1) as the primary crack forming mechanism in sand, and (2) as a modifier of clay cracks in the clay-rich sediment. Key features of identifying a microbial influence on desiccation cracks in the rock record are limited, but include, disconnected, shallow, wide, radiating cracks which produce incomplete polygonal networks and different crack morphologies superimposed on each other.

Fossil microbial shrinkage cracks are identified as such, mainly based on evidence of biostabilization, rather than using the crack morphology itself. Fossil cracking patters are highly variable and some of the characteristics can be linked to desiccation, while others still remain debated. This work provides new insights into the mechanisms underpinning desiccation cracks, and it aids in differentiating between desiccation cracks (i.e. subaerial exposure) and cracks formed by other mechanisms.

CHAPTER 3: Analysis of microbial mat-related structures in the Mesoproterozoic Belt Supergroup, Montana, U.S.A.

Introduction

Precambrian to Ordovician was an especially accommodating time for development of microbial mats, as is reflected by the abundance of microbial mat-related structures found in the strata of this age (Schieber, 1998; Hagadorn and Bottjer, 1999; Bouougri and Porada, 2002; Parizot et al., 2005; Sarkar et al., 2006; Sarkar et al., 2008; Porada and Druschel 2010 and others). Analysis of ancient microbial mat remnants, such as those found in the 3.2 Ga Moodies Group of South Africa (Noffke et al., 2006b), provides insight into the oldest ecosystems on Earth. Ancient microbial mats are linked to key events in the Earth's early history, as they are thought to contribute to increasing oxygen concentrations in the ancient atmosphere and later providing food needed for evolution of complex, mobile animals (Noffke et al., 2006a; Noffke et al., 2006b; Schieber et al., 2007; Gingras et al., 2011).

Microbial mat biolamina consists of bacterial filaments/coccoids, extracellular polymeric substances (EPS) and entrapped sedimentary grains (Gerdes, 2007). In the rock record, biolamina may be preserved as argillaceous iron-rich layers containing isotopically light, elemental carbon fibers that entangle sedimentary grains (Noffke et al., 2006b). The presence of iron in the form of pyrite crystals/framboids or as oxidized iron bands is good indicator of past microbial growth, as pyrite tends to form in the lower anoxic layers as the by-product of sulfate-reducing metabolism; these layers may be subsequently oxidized.

Cohesive microbial cover prevents typical sediment-water or sediment-atmosphere interactions, resulting in formation of characteristic microbial mat-related structures (MRS) (Schieber et al., 2007). MRS are typically a physical phenomenon, resulting from deformation or destruction of the microbial mat, partially preserved as wrinkle marks, cracks, tears, mat rip-ups and roll-ups (Hagadorn and MacDowell, 2012). There is also a biological component to the structures, as bacteria trap and bind sediment out of the water column,

produce gases, alter the geochemistry of their surroundings and facilitate mineral precipitation (Noffke et al., 2001). MRS are typically small scale and low relief features that are most noticeable on bedding surfaces (Schieber et al., 2007).

Understanding the formation and distribution of microbial mat-related structures has important implications for sedimentology and stratigraphy. The presence of widespread microbial mats is a good indicator of low sedimentation rates (Gerdes, 2007). It may also give insight into hydrodynamics of the system, as establishment of a biofilm requires calm waters (i.e. minimal sediment movement), although well-established mats are able to tolerate currents that move as rapidly as 160 cm/s (Noffke, 2009). Thus the low erodibility of the biostabilized sedimentary surfaces by deep or shallow currents may facilitate aggradation rather than the expected erosion (Catuneanu, 2007; Sarkar et al., 2014).

It can be difficult to determine if microbial mat-related structures are formed under unique set of conditions and thus are useful in refining paleoenvironmental interpretations. Modern studies of biostabilized peritidal settings show that microbial structures are diverse, and are generally organized into zones based on water depth and subaerial exposure (Bose and Chafetz, 2009; Sarkar et al., 2014). However, not all MRS have modern analogues. Modern siliciclastic microbial mats studies are mostly limited to shallow-water environments, such as tidal flats, lagoons and sabkhas. However, many ancient biomats were well established in shallow- and deep-water settings. Unfortunately the formation of mat-related structures in deeper water is not well understood. It has further been suggested that not all microbial mat-related structures form at the surface, and that some develop during burial and early diagenesis, thus not easily observable (Harazim et al., 2013).

Diastasis cracks are among the most commonly observed biomat-associated structures on Precambrian bedding surfaces, and their origin is heavily debated (Gehling 1999; Pflüger 1999; Porada and Loeffler, 2000; Bouougri and Porada, 2002; Parizot et al., 2005; Eriksson et al., 2007a; Porada and Druschel, 2010; Harazim et al., 2013). Numerous studies of modern peritidal microbial mats show that desiccation alone can produce versatile array of cracks that are variable in size and shape and can be used as modern analogues for

fossil structures (Gerdes, 2007; Cuadrado, 2013). If cracks can be linked to desiccation, it would make them excellent indicators of shallow paleoenvironments and subaerial exposure.

However, there are several examples of diastasis cracks that are inconsistent with subaerial exposure, particularly non-orthogonal, irregular networks that give rise to alternative interpretations. It has been proposed that such cracks may be formed by "synaeresis" or "intrastratal cracking", where the water-rich microbial mats expel water due to changes in water chemistry or degradation of the biomat due to burial, producing irregular openings (cracks) that are infilled by the overlying or underlying sediment (Harazim et al., 2013; Gehling 1999; Plummer and Gostin 1981; Parizot et al., 2005). Experiments carried out by Jungst (1934), White (1961), Burst (1965), Donovan and Foster (1972), indicate that subaqueous synaeresis shrinkage is possible under laboratory conditions, especially successful when using swelling clays (Barclay et al., 1991). Alternatively, some linear and polygonal features may not be driven by shrinkage, but instead are intrastratal pull-apart structures that form due to rupturing of the microbial mat by denser overburden (Pflüger, 1999).

The goal of this paper is to describe and interpret a range of microbial mat-related structures, including various diastasis crack morphologies that are observed on the bedding surfaces of the Mesoproterozoic Belt Supergroup. The purpose of the research is to contribute to the current knowledge of microbial mat-related structures in the rock record.

Geological Setting

Belt Supergroup is a thick and widespread package of Middle Proterozoic sedimentary strata that range in age from 1470 to 1400 Ma (Ross and Villeneuve, 2003). Belt Supergroup outcrops throughout north-central U.S.A., including Montana, Idaho, Utah, Washington and reaches into southern Canada where it is called the Purcell Supergroup (Fig. 3-1). In western Montana, the Middle-Cambrian sandstones unconformably overly the Mesoproterozoic Belt strata, representing a widespread 900 Ma unconformity followed by

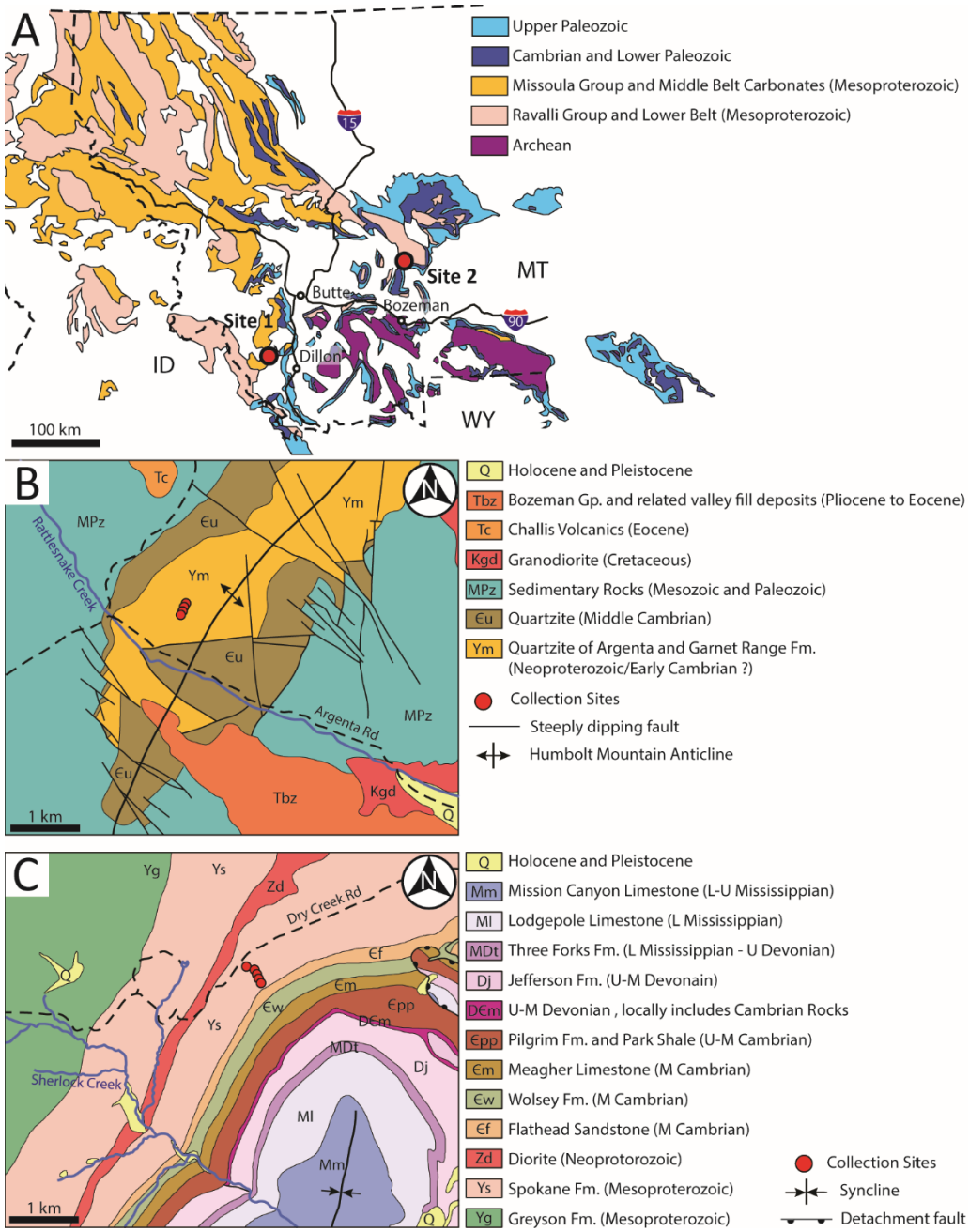

Figure 3-1. Geological map of the outcropping Belt-Purcell Supergroup, surrounding strata and collection sites. (A) Extent of the Belt-Purcell Supergroup. The study locations 1 and 2 are indicated on the map. Modified from Ross and Villeneuve (2003). (B) Geological map of the study area 1, 20 km northwest of Dillon, MT. The outcropping upper Missoula Gp. was studied in the indicated collection sites. Modified from Pearson (1996). (C) Geological map of the study area 2, 60 km north of Bozeman, MT. The outcropping Spokane Fm. of the Ravalli Gp. was studied in detail in the indicated collection sites. Modified from Geological Maps of Montana made available by the Montana Bureau of Mines and Geology.

the transgression of the Cambrian sea that drowned much of the North American craton (Macke, 1993; Ross and Villeneuve, 2003).

Mesozoic orogenic activity shortened most of the Belt Basin, resulting in thrust faults and high-angle reverse faults (Ross and Villeneuve, 2003). The Belt strata is overprinted by low-grade metamorphism that reaches sub greenschist facies, except for the outcropping southern and westernmost strata. However, the Belt strata has well preserved sedimentary features that were not destroyed by the onset of metamorphism, allowing for sedimentological analysis (Schieber, 1998).

The sedimentary succession is predominantly composed of shales, siltstones, sandstones, as well as argillaceous limestones and dolomites (Schieber, 1998). Belt stratigraphy is generally divided into four categories: the Lower Belt, the Ravalli Group, the Middle Belt Carbonates and the Missoula Group (Fig. 3-2). The environment of deposition of the Belt strata, as well as the basin architecture, are debated, but it is generally agreed that lower Belt consists of deep-water submarine fan deposits succeeded by shallow water to subaerially exposed sediments deposited in epicontinental sea or lacustrine type settings (Cressman, 1989); the latter shallow-water strata conditions were ideal for microbial mat development.

Abundant microbial mat-related structures throughout the Belt strata have been observed and documented by Schieber (1998), in both the sandy and argillaceous sediments that were deposited in marginal marine to calm-offshore environments. Fossils of eukaryotic algal filaments have also been observed (Walter et al., 1976; Horodyski, 1993).

Methods

Belt Supergroup strata, just below the overlying Cambrian sandstone, were examined for this study in outcrop. Exposed strata of the upper Missoula Group were examined 20 km northwest of the town of Dillon, MT (Fig. 3-1 B). Outcropping strata of the Spokane Formation (part of Ravalli Group) were examined in the Devil's Fence Anticlinorium 60 km north of Bozeman, MT (Fig. 3-1 C). Field photographs were taken and samples were brought

back to the lab for analysis. Due to the recessive nature of the studied units, the samples were in part collected from scree and were not in their original stratigraphic position. Thin sections were made perpendicular to the bedding surfaces and examined under transmitted light microscope and scanning electron microscope (SEM).

Collection site 1: Rattlesnake Creek, Beaverhead National Forest– upper Missoula Group

In this location, the upper Missoula Group consists of 3 Units, Unit 1 and 3 are silicified, well sorted, fine to medium grained trough cross-stratified quartz arenite beds, interpreted to have been deposited in a high energy environment, such as an upper shoreface. The middle, Unit 2 is dominated by recessive, light grey-tan, quartzites, siltites and argillites. Very-fine sand- and silt-sized quartz and feldspar grains are interlaminated with mica-rich argillite, contributing to an overall fissility. Sedimentary structures include wave ripples, low angle cross lamination and coarser grained sand lenses. This unit was interpreted to have been accumulated in a lower energy setting, such as in the proximal offshore. Missoula Group has been interpreted to represent a distal alluvial apron that includes subaerial and subaqueous facies (Ross and Villeneuve, 2003). It is in Unit 2 where microbial mat-related structures are observed on bedding planes. Silicified sandstones of Units 1 and 3 have poorly developed bedding surfaces, and no visible microbial structures in cross-section.

Collection site 2: Devil's Fence Anticlinorium - Spokane Formation (Ravalli Group)

The sedimentary succession of the Spokane Formation in the Devil's Fence Anticlinorium comprises mainly red siltstones with local sand lenses. Sedimentary structures include small-scale trough cross-stratification of combined flow ripples or small-scale dunes, and wave ripples preserved on bedding surfaces. The environment of deposition is interpreted as lower shoreface. Northward current directions have been reported, but in some locales the orientations are variable, leading to interpretation of tidal influence (McMechan, 1981). Numerous microbial mat-related structures were observed on bedding surfaces throughout the strata.

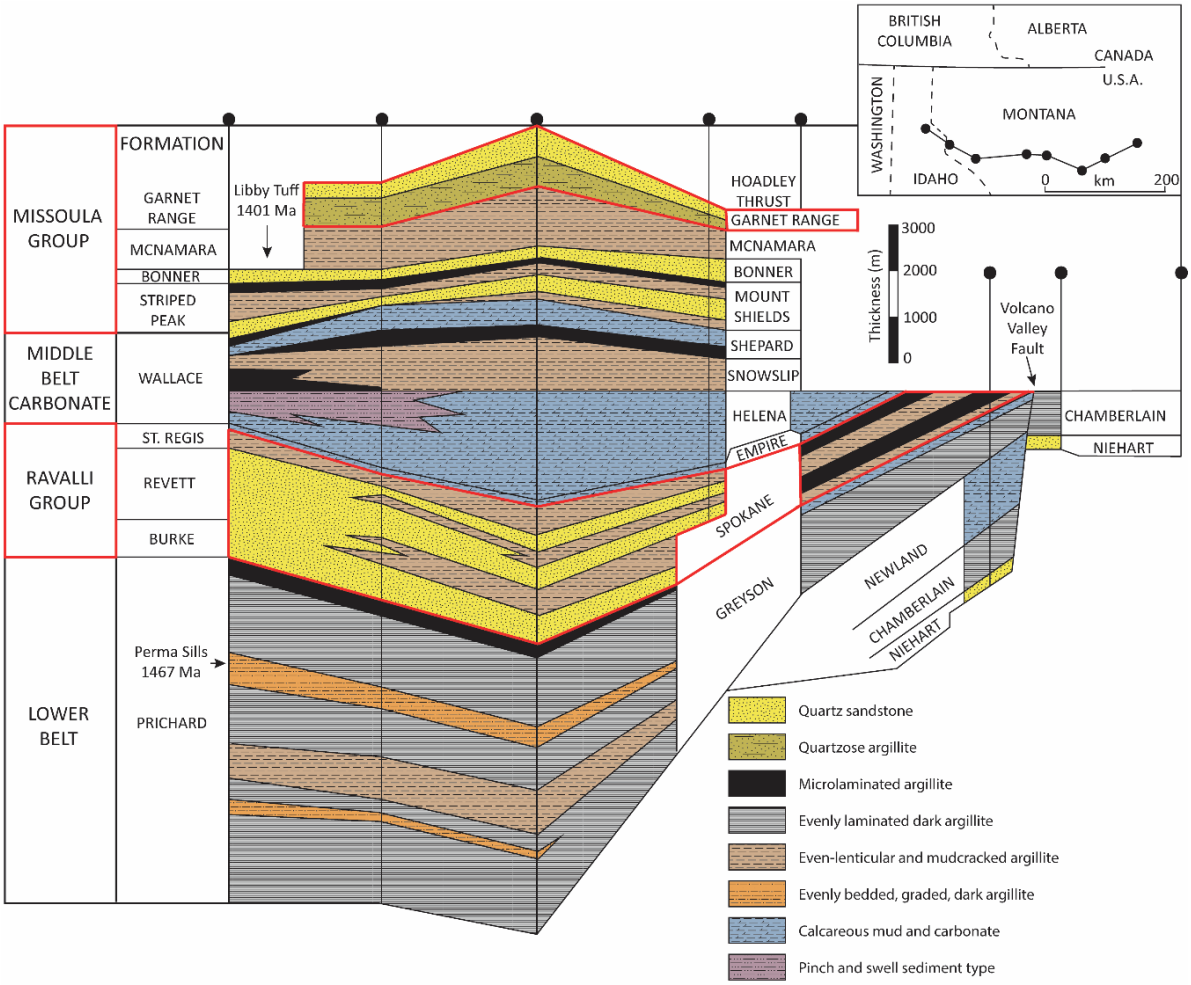

Figure 3-2. Cross-section through northern Idaho and Montana, indicating the typical stratigraphy of the region. Modified from Ross and Villeneuve (2003).

Description and Interpretation of Mat Related Structures

Many structures that are atypical of sediment water interaction were found on bedding planes of the Belt strata in both locales. The bedding surfaces were often nodular, wrinkled or cracked. The interpreted microbial-mat related structures are described in detail below.

Biolaminae

The bedding surfaces from the two locales had in common a thin argillaceous veneer that was only preserved in small depressions within the surface, such as those formed by the protruding mat-related structures. Argillaceous laminae are also preserved within the sample, as both continuous layers and discontinuous "mud chips". Frequent soft sediment deformation features are observed between the sand/silt unit and the argillaceous laminae.

Under transmitted light microscope, it was apparent that the argillaceous lamina are composed of sand- and silt-sized grains that were floating in an argillaceous, fibrous matrix that is highly indicative of microbial biolamination (Scieber et al., 1998) (Fig. 3-3 A, B). The morphologies of the biolaminae are nearly identical to those observed in the modern microbial mats (Gerdes, 2007) and the rock record (Bouougri and Porada, 2002; Noffke et al., 2013) and are interpreted to form as a result of trapping and binding activity of ancient bacteria. Biolaminae have previously been observed to be associated with mat-related structures, such as the kinneyia wrinkles (Porada et al., 2008).

SEM analyses revealed that the laminae contain elongated iron precipitates and iron halos that surrounded carbon-rich grains (Fig. 3-3 C-H). The biolaminae are also enriched in heavy minerals such as rutile and zircon. The iron was present as an oxide phase (limonite/goethite/hematite) and is interpreted as the weathered by-product of pyrite, which is indicative of anoxic degradation of organic matter (Schieber, 2007; Darroch et al., 2012).

Kinneyia Structures

Description

Structures that resemble small-scale interference ripples are observed on the bedding planes at both study locales (Fig. 3-4 A, B). The structures are low relief, steep sided, flat-topped ridges. The ridges are less than 1 mm in height, 1-2 mm wide and interfinger with one another. The 1-2 mm wide depressions between the ridges range in shape from isolated, ovate pits (Fig. 3-4 A) to elongate troughs that wind alongside the ridges, resulting in less interconnectivity (Fig. 3-4 B).

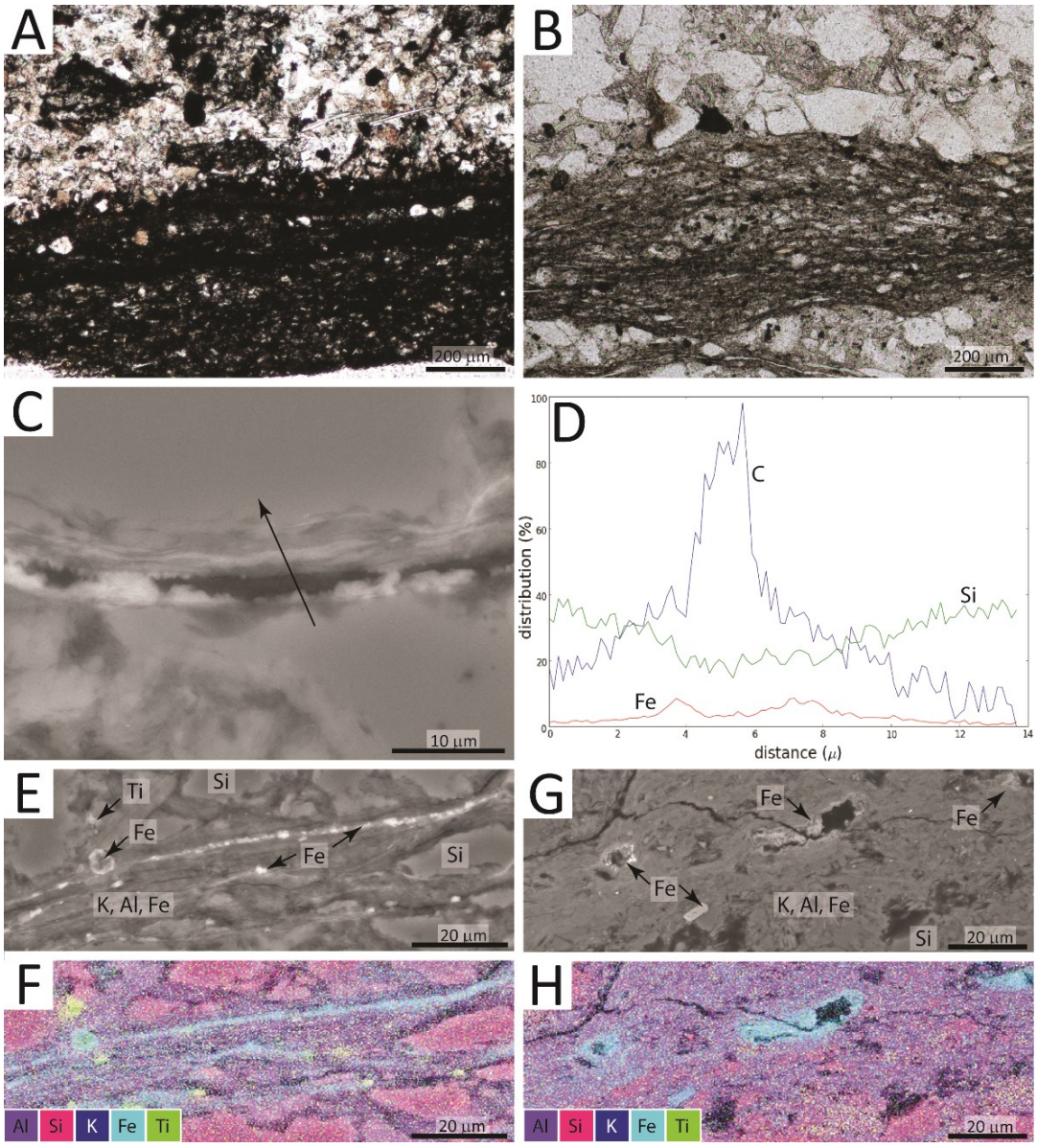

Figure 3-3. Transmitted light and SEM micrographs of the biolaminae. (A) Transmitted light micrograph showing dark fibrous material surrounds silt and very-fine sand sized quartz grains, Spokane Fm. (B) Transmitted light micrograph similarly shows the darker fibers surround very-fine sand sized quartz grains, Missoula Gp. (C) SEM micrograph showing a carbon rich fiber that is surrounded by iron oxide precipitate. (D) Line graph through the carbon rich fiber, showing element distribution which includes carbon-rich center and iron-rich rims. (E) SEM micrograph showing fibrous iron-oxide precipitates in a matrix of clay rich laminae and quartz grains. (F) Map that breaks down elemental composition into different colours, associated with panel F. (E) SEM micrograph showing carbon rich grains that have an iron-rich rim. (F) Map that breaks down elemental composition into different colours, associated with panel G.

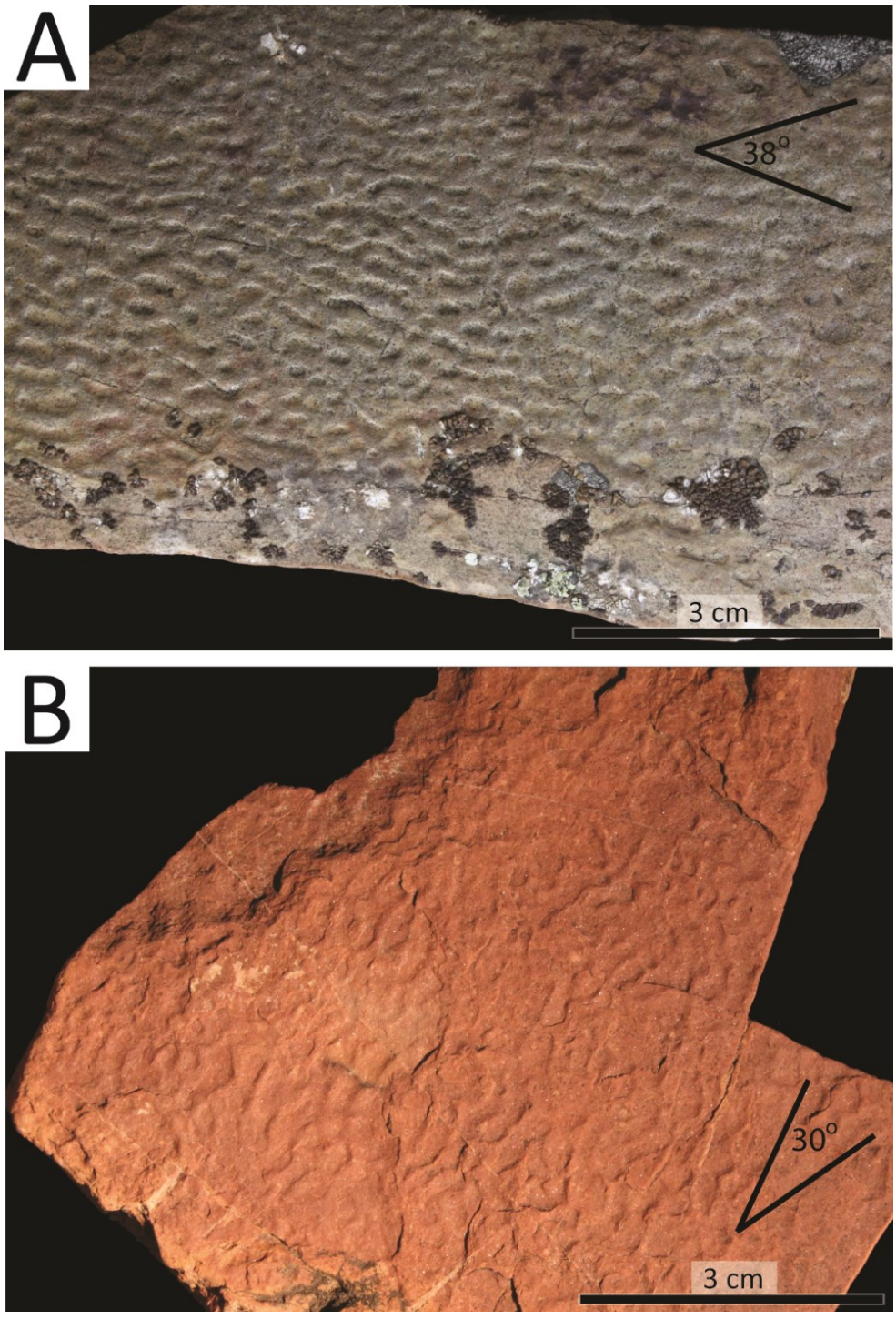

Figure 3-4. Kinneyia structures. (A) Typical kinneyia pattern consisting of interconnected flat-topped ridges separated by ovate pits, upper Missoula Gp. The ridges tend to bifurcate at an average 38° in the directions indicated. (B) Kinneyia structure showing less interconnectivity, where the narrow depressions wind alongside the ridges, observed in the Spokane Fm. strata. The ridges tend to bifurcate at an average 30° in the directions indicated.

Interpretation

These distinct structures are identified as "kinneyia" or "runzelmarken" that are commonly observed in Proterozoic and early Cambrian strata (Hagadorn and Bottjer, 1999; Bouougri and Porada, 2007a; Porada and Bouougri, 2007). The term Kinneyia was introduced by Walcott (1914), who suggested that the structures are formed by a new algal genus *Kinneyia* (Porada, 2008). Subsequent efforts by Hagadorn and Bottjer (1997, 1999), Pflüger (1999), Noffke (2002, 2003); Porada (2008) and others, showed that formation of kinneyia is likely associated with microbial mats. Especially convincing are the over-steepened sides of the ridges that are well above angle of repose of loose sand would not be stable at the sediment-water or -air interface (Pflüger, 1999).

Kinneyia is proposed to be a surface wrinkle structure caused by flooding, where the shear flow of the overlying water causes corrugation of the microbial mat (Hagadorn and Bottjer, 1999; Thomas et al., 2013). However, since such flat-topped, millimeter scale wrinkles are not observed in modern biomats, a more convincing theory is that they are formed underneath a microbial mat cover either at the surface or intrastratally.

Pflüger (1999) proposed that kinneyia are formed by arrangements of metabolic gases, which are trapped underneath the microbial mat where the gas bubbles coalesce and leave depressions in the sediment which get preserved as the troughs of the kinneyia structure. Linear arrangements of gasses were documented from the modern Bahar Alouane coast of southern Tunisia (see their Fig. 7) and those structures do resemble kinneyia (Gerdes, 2007). A major difference is that the bubbles, in this case, produce the "ripple" crests rather than the troughs. This can be attributed to the pliable nature of microbial mats, which cannot constrain accumulated gases. As such, intrastratal formation of kinneyia provides a better explanation for these structures, where the overlying sediment prevents the mat from being uplifted by the escaping gases that are produced due to mat decay, with gases forming the channel-like pockets below the confining surface (Noffke, 2002, 2003).

The linear alignment of the ridges and troughs suggests that there may also be a flow component to the formation of kinneyia. Porada et al. (2008) observed that kinneyia ridges

typically bifurcate in two preferential orientations, in average 45^{o} angles from one another, proposing that porewater oscillation formed by wave or tidal-current hydrodynamics, causes small scale interference ripples in the liquefied sediment confined underneath a microbial mat. The kinneyia samples in the Belt Strata also align in a similar orientation, where the ridges split in 35^{o} angles with relation to one another (Fig. 3-4 A, B), possible supporting a flow component to their formation.

Petee Structures

Description

Linear wrinkles protruding from the bedding plane are observed at both study sites (Fig. 3-5 A, B). Two types of morphologies are recognized, the first type consists of elongate positive relief ridges that are 3 mm wide and up to 1.5 cm long and have steep, near vertical sides (Fig. 3-5 A). These features are aligned nearly parallel with respect to one another, and are typically rounded on top, although some are flat-topped and resemble non-intersecting kinneyia (Fig. 3-5 A). The second type consists of low relief, linear ridges, which are less than 0.5 mm wide and branch out in 60-120 ^{o} angles (Fig. 3-5 B). These features do not form a complete polygonal networks, but isolated pockets of branching wrinkles.

Interpretation

These structures are interpreted as petee structures rather than diastasis cracks, because the structures are continuous with the bedding plane; i.e., there is no crack and the structures are rounded on top. The term "petee" was first introduced by Gavish et al. (1995) to differentiate between inverted U-shaped folds formed in biotic sediment from the similar inverted V-shaped tepee structures which form in abiotic sabkha sediments. Petee structures were later classified by Reineck et al. (1990), into alpha, beta and gamma petees, where the alpha petees and beta petees are formed by gases ascending from buried decaying organic matter. The buoyant gasses elevate parts of the mat creating sinuous or polygonal patterns (Porada et al., 2007; Gerdes, 2007). Gamma petees are formed when the mat fabric is torn, folded or over thrusted by water or wind friction acting along the mat surface (Gerdes, 2007).

Petee structures can rupture making them difficult to differentiate from cracks in the rock record (Gerdes et al., 1993).

It is not possible to say if these structures observed in the Belt Supergroup strata were caused by gas deformation or due to wind or water friction, as those processes can produce both linear and more polygonal forms and sometimes work together to form the petee (Gerdes, 2007). Because the linear structures are aligned, it is possible that they are formed by a unidirectional flow induced shear, rather than gas uplift alone (Fig. 3-5 A).

In slippery evaporitic or clay-rich sediments the petee structures are especially common, as the microbial mat layer detaches quite easily, forming polygonal ridges or linear petee structures (Gerdes, 2007). It is expected that the petee ridges are filled from below, by the same sediment as the bedding plane. However when petee crests are ruptured, the structures can be filled from above by wind-blown sediment or by the next sedimentation event, making them hard to differentiate from cracks (Bouougri and Porada, 2002). Modern petee structures are described from sea-marginal hypersaline ecosystems, such as the salt evaporation ponds of Lanzarote, Canary Islands, salt evaporation ponds of Bretagne coast, France and Gavish Sabkha of Gulf of Aqaba, Egypt and may be common in high-sabkha settings (Gerdes, 2007), however petee structures are likely to form subaqueously, due to the tendency of the microbial mat to fold and buckle with shear stress.

Nodular Surfaces

Description

Positive relief, rounded and elongate mounds were observed on bedding planes giving an irregular appearance. The mounds were observed to protrude 1-2 mm above the bedding plane and were up to 2 cm in length (Fig. 3-6). Some of the features are nearly hemispherical, while others are more linear in shape. The elongated features change in thickness and/or direction and some are made up of nested rounded mounds. The sides are quite steep, sometimes over steepened and bulge out of the bedding plane.

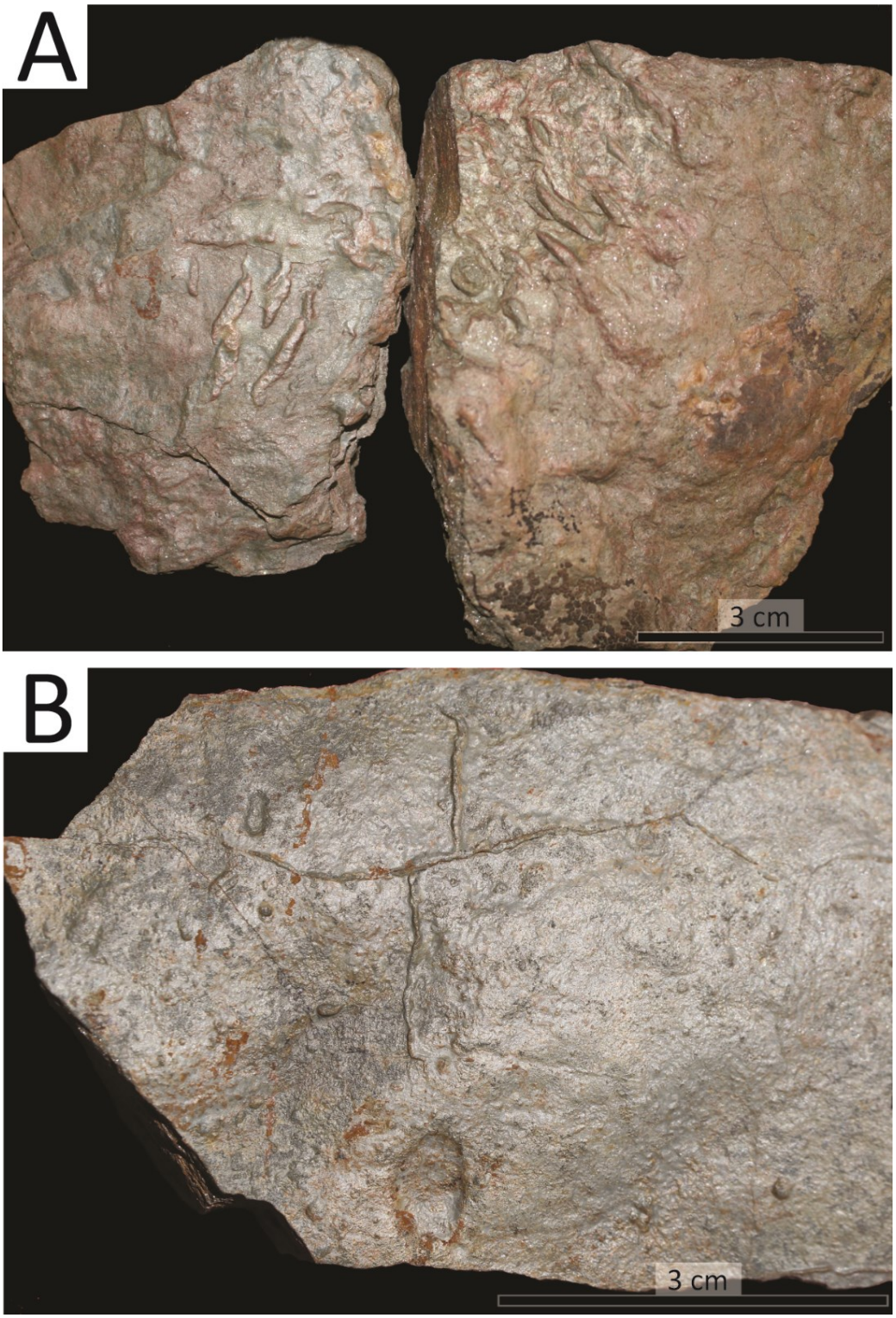

Figure 3-5. Petee structures. (A) Linear, near parallel ridges that are interpreted as petee structures, upper Missoula Gp. (B) Thin branching wrinkles that are interpreted as petee structures, upper Missoula Gp.

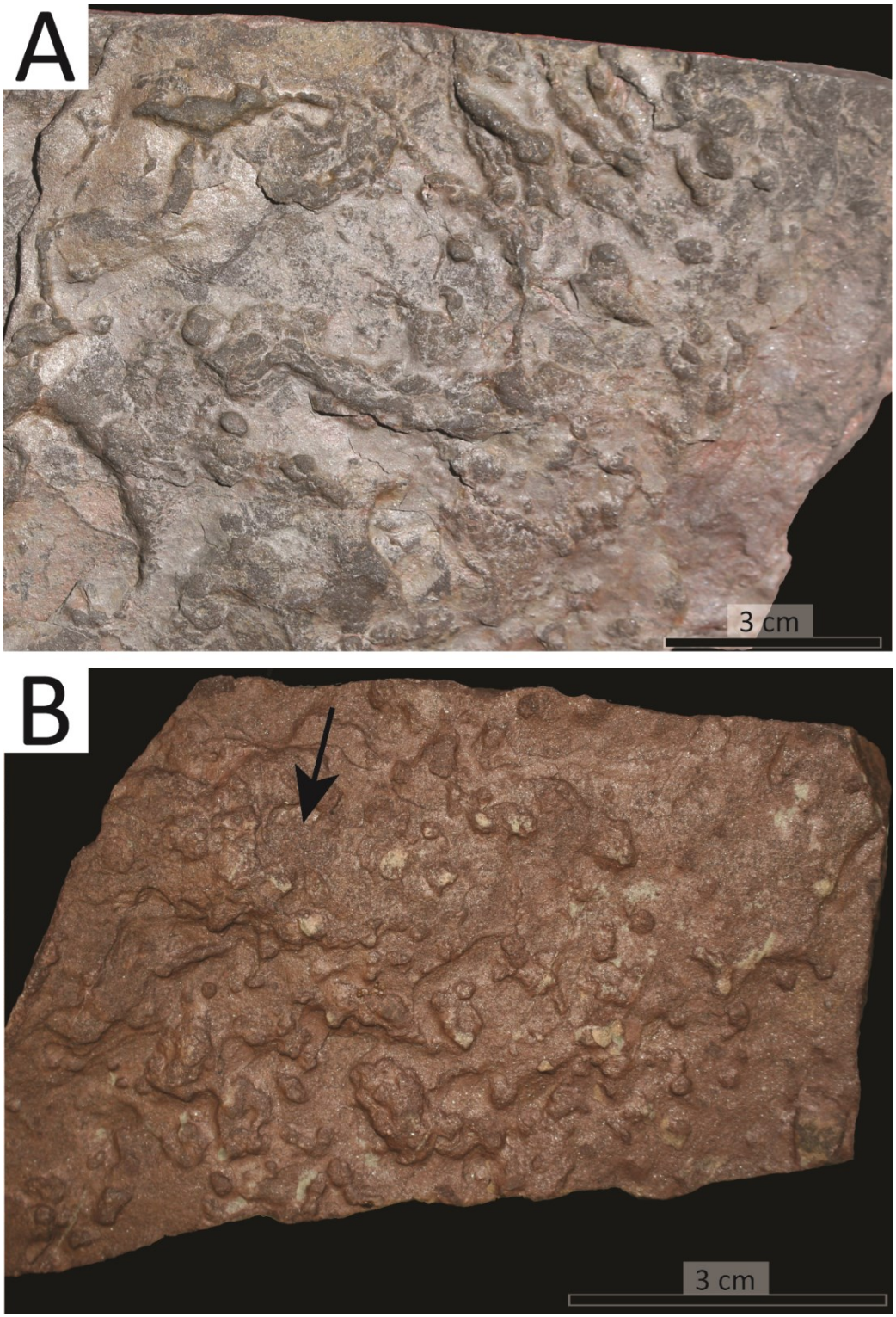

Figure 3-6. Nodular surfaces. (A) Irregular bedding plane consisting of rounded and elongate nodules, upper Missoula Group (B) Nodular surface that are deformed in a similar orientation, perhaps indicative of a flow direction, Spokane Fm.

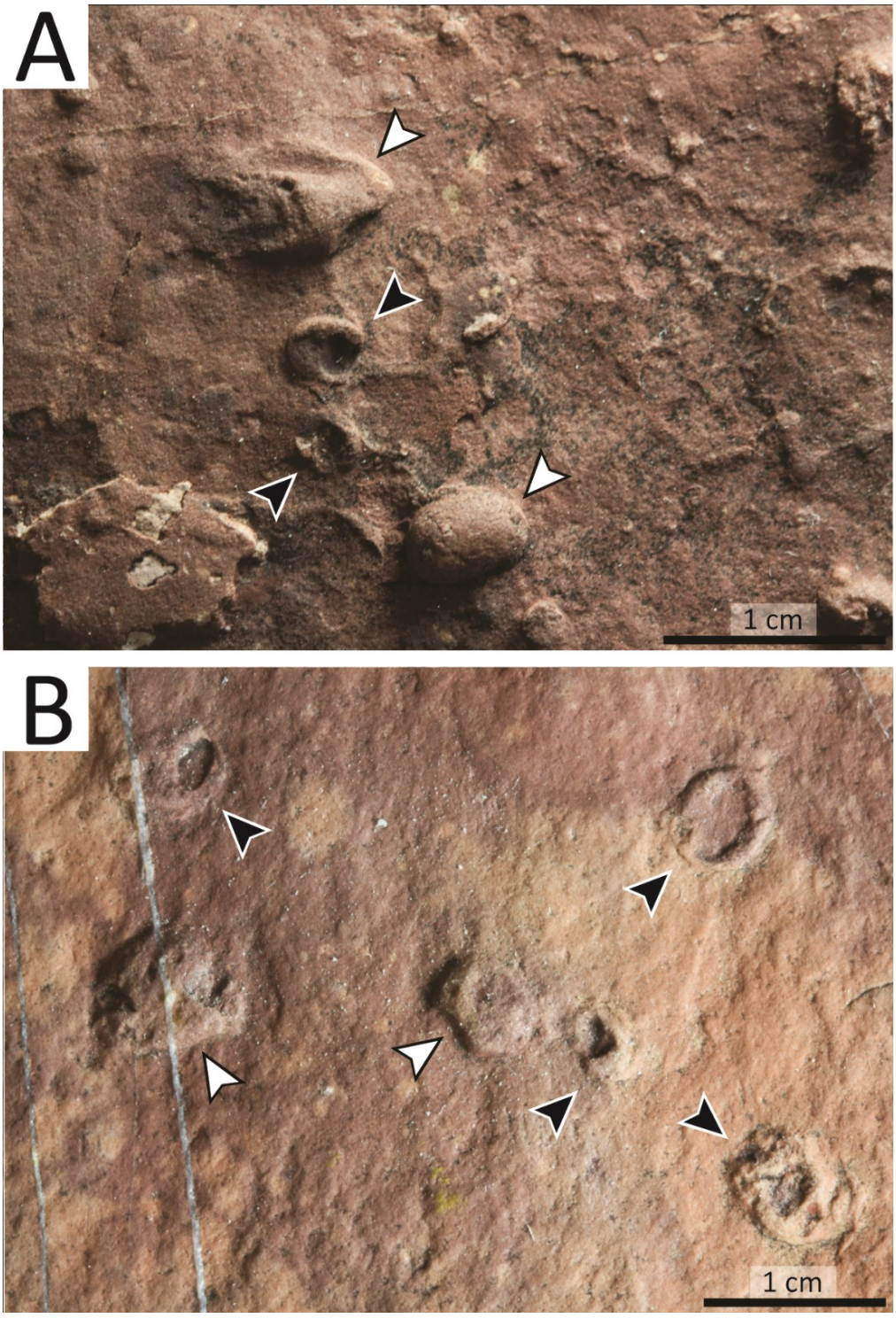

Figure 3-7. Gas domes. (A) Doughnut-shaped structures that are interpreted as deflated gas domes, indicated with black arrows, hemispherical domes, white arrows, Spokane Fm. (B) Doughnut-shaped structures on an otherwise smooth bedding plane, indicated with black arrows and small domes indicated by white arrows, Spokane Fm.

Interpretation

Such structures are proposed to have formed due to uneven trapping and binding of the sedimentary grains by the microbial mats, forming irregular clusters called sand stromatolites and algal balls (Bottjer and Hagadorn, 2007). Schieber (1998) also noted "pustular-crinkled surface relief" on bedding planes of the Belt Supergroup. Similar "knobby surfaces" are described by Bose and Chafetz (2009), from the upper supratidal region of the Texas Coast, where the uneven bacteria growth is caused by seagrass and roots. Gerdes (2007) noted that microbial mats rich in coccoid cyanobacteria often lead to "an irregular surface topography".

One sample was observed to be asymmetrical where the mounds were steeper sloped in one direction, perhaps due to deformation by a current or wind (Fig. 3-6 B). Such structures have been reported to be quite soft and malleable, as they are easily deformed by animal trackways (Bottjer and Hagadorn, 2007).

Gas Domes and Bubbles

Description

Semispherical and doughnut-shaped structures are observed on the bedding surfaces and are sometimes associated with the nodular surfaces, but are smoother. The outer rim diameter of the doughnut-shaped structures ranges from 3-5 mm and the central portion is approximately coplanar with the bedding surface (Fig. 3-7 A, B, black arrows). The hemispherical features are of similar dimensions and are present among the doughnut features (Fig. 3-7 A, B, white arrows).

Interpretation

These structures are interpreted as deflated gas domes or bubbles that are produced by the microbial mats due to accumulating photosynthetic gases or gases released by mat decay. The gases are observed to uplift the flexible, semipermeable microbial mat as they are trying to escape into the atmosphere, producing hemispherical gas domes (Gerdes, 2007). Some of such domes are long lived, especially in arid settings, where the domes are stabilized

by gypsum (Gerdes, 1993). In modern day mats the gas domes were observed to predominantly form in the upper and lower supratidal zones (Chafetz et al., 2009), although underwater observations may be lacking due to accessibility.

Even though such gas domes are fragile, their hemispherical shape can be preserved as positive relief protuberance structures (Fig 3-7 A, B, white arrows), where the slow gas escape causes release in pressure that allow the sediment to move upwards and infill the gas dome (Bououdri and Porada, 2002; Gerdes, 1993). Gas domes can also be preserved as collapsed doughnut-shaped structures such as those found in the Lower Pleistocene sandstone/sandy tuff bedding surfaces of NW Milos Island Greece (Kilias, 2012) or the 1.6 Ga Chorhat sandstones, India (Sarker at al., 2006).

Microbially Mediated Diastasis Cracks

Microbially Mediated Diastasis Cracks (MMDS) are the most commonly observed features on the bedding surfaces of the upper Missoula Group and the Spokane Formation (Ravalli Group), forming triradiate and orthogonal networks, and more commonly irregular networks or linear cracks that are disconnected from one another. The crack fills are predominantly preserved as positive relief structures on the sole of the bed, protruding 1-2 mm below the bedding surface. The crack-fill height may be related to the thickness of the cracked microbial lamina (Tang et al., 2012), but compaction of the microbial mat should be considered (Harazim et al., 2013).

Taking into consideration the connectivity of the cracks and network morphology, the structures were divided into 4 groups (purely descriptive classification): (1) triradiate cracks; (2) orthogonal cracks; (3) irregular polygonal cracks; (4) linear cracks. Separating cracks into categories was not always simple, as cracks transition from one group to the next. The mechanisms of crack formation are poorly understood and in this context the different types of observed MMDS are discussed below.

Triradiate cracks

Description

Triradiate cracks are observed on the bedding surfaces of the Spokane Fm. (Ravalli Gp.), where three linear cracks branch out from a point of origin, in 120^{o} between the trajectories (Fig. 3-8 A, B). The equidimensional triradiate cracks are observed to be approximately homogeneously distributed on bedding planes (Fig. 3-8 A). The cracks are thickest at the center and only propagate 5-9 mm before tapering at their terminus. The triradiate cracks sometimes intersect, but are typically separate from one another. Also, triradiate cracks and isolated aligned cracks (discussed below) can observed on the same bedding plane (Fig. 3-8 B).

The thin section analysis permits the observation of planar- and cross-laminated silt-sized quartz grains (Fig. 3-8 C). The crack fills are preserved as positive relief features on the sole of the bed. The crack fill is the widest at the base and tapers downwards, eventually terminating with a flat edge (Fig. 3-8 D, E). The cracks are filled with the same material as the cracked sedimentary bed and argillaceous cusps are preserved on either side of the crack.

Interpretation

The triradiate cracking is indicative of initial response to tension caused by contraction. The tension is released by rupturing the shrinking layer, where cracks isotropically propagate from a point of weakness in a tri-radial manner (e.g. Sholin, 2000). With progressive shrinkage, the cracks grow in length and in numbers, and the newer generation of cracks spread perpendicularly from the parent crack. Following the initial rupture, the cracks tend to connect and branch out in 90^{o}, resulting in an approximately orthogonal network, where triradiate junctions are likely to be the oldest (Sholin, 2000).

Triradiate cracks have been observed in desiccating microbial mats, where the cracks originate at the apexes of gas domes, since these high regions are the first to dry out, while the lower-laying microbial mat remains wet (Cuadrado et al., 2014). Synaeresis triradiate

cracks have also been generated in the laboratory, where the ratio of swelling to non-swelling clay is lower than that needed for the development of a complete crack network (Burst, 1965).

The argillaceous material that is preserved around the crack features, is interpreted to be the biolaminae that cracked upon contraction. In this study's examples, the cracking was initiated, but never progresses into a mature network. Radiating cracks are typical of microbial mat shrinkage as cohesive microbial meshwork tends to restrict crack propagation (see Chapter 2). The cracks were likely filled from above, since crack fill widens upwards.

The regular, equal dimensions of the cracks is indicative of isotopic tensile stress. While the aligned cracks indicate that the maximum tension is perpendicular to the crack propagation, perhaps indicating a directional drying/dewatering front (Sholin, 2000). Long axes of the cracks have been observed to align parallel to ripples which were linked to paleoshoreline orientation and downslope creep (Donovan and Foster, 1972). Orientations of aligned cracks have also been linked to regional faulting and stress regime (Donovan and Foster, 1972).

Studies have shown that contraction, whether it is due to desiccation (water loss due to drying) or synaeresis (water loss due to increased salinity), will follow similar pathways in crack formation and propagation, making it very difficult to distinguish desiccation from synaeresis origin (Burst, 1965; Tanner, 1998; Tanner, 2003). However the cracks that are interpreted as synaeresis in the rock record are often more disconnected (linear or triradiate), hence synaeresis interpretation for similar triratiate cracks has been used (Parozot et al., 2005; Porada and Druschel 2010). Even though the triradiate cracks in this study do not display clear sediment injection or soft sediment deformation features, like some of the samples discussed below, it seems most likely that these features were produced by intrastratal processes, rather than synaeresis. Microbial mats are embedded in EPS, which protects the community from environmental stresses, such as salinity variations (Decho, 1990), thus biomat burial is the most likely mechanism for biomat degradation and cracking.

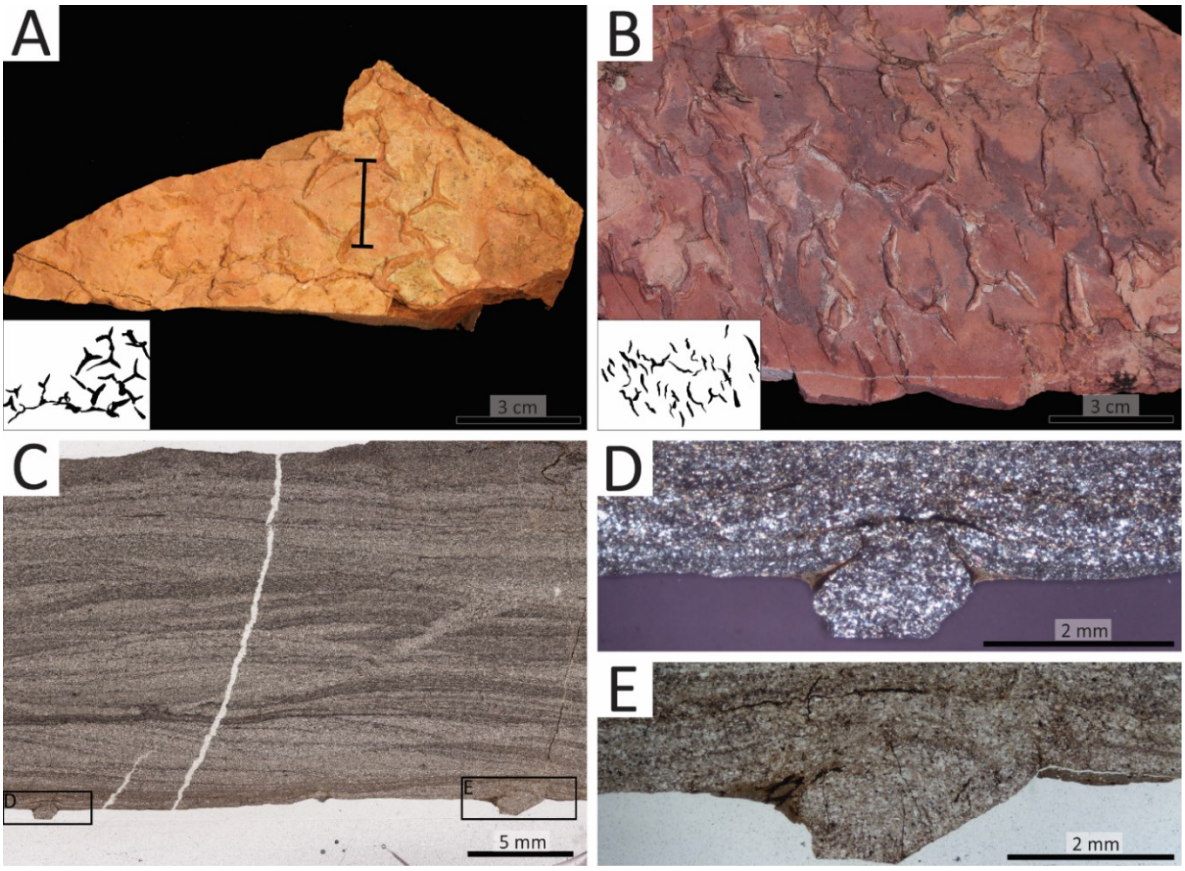

Figure 3-8. Triradiate cracks. (A) Triradiate cracks on a bedding surface, Spokane Fm. (Ravalli Gp.). The black line indicates the thin section location that is shown in panel C (B) Isolated, aligned cracks that transition into triradiate cracks. (C) Cross-laminated siltstone with main crack features protruding from the bottom bedding surface. (D) Crack feature in cross-polarized light, showing quartz rich silt-sized deposit. The crack fill is the same as the rest of the sample. (E) Crack feature in plain polarized light, showing biolamina preserved in the depression between the crack and the bedding surface. The crack fill consists of silt-sized quartz grains, similar to the rest of the bed.

Orthogonal cracks

Description

Straight to semi-curved cracks that intersect to form a polygonal network (Fig. 3-9 A, B). The crack widths are consistent, ranging from 9 to 2 mm, with few tapering cracks. Commonly 3 or 4 cracks intersect at 120° or 90° junctions, respectively, forming an

approximately orthogonal and equidimensional crack-polygons. This crack morphology is the most similar to a mature network of desiccated mudcracks.

The thin section analysis reveals very-fine to fine sand-sized quartz grains that are suspended in argillaceous matrix (Fig. 3-9 C). Very coarse sand sized grains, up to 1 mm in diameter, are scattered through the bed. Thin, argillaceous laminae, that are parallel with respect to the bedding plane, are present throughout the section. Fracturing along the argillaceous layers is common.

There are evidences of soft sediment deformation between the sand-dominated laminae and the thin argillaceous laminae (Fig. 3-9 C-E), i.e. sand descends downwards and is emplaced in the mud, and thin mud cusps extend upwards into the sand bed. The argillaceous material is composed of anastomosing dark fibers that entangle silt and very fine sand grains.

The crack is filled with sediment that is finer than the overlying material and the sediment inside the crack shows poor sorting, including some coarser grains (Fig. 3-9 C). Argillaceous material is preserved in the depressions around the crack.

Interpretation

The "floating grain" texture is observed in the argillaceous laminae and is consistent with the biolaminae produced by microbial mats (Noffke et al., 2006b). Shrinkage of this layer played the main role in formation of the crack network. This is evidenced by the presence of triple and orthogonal junctions that are indicative of shrinkage cracks. The sand is observed to infill the cracks from above. The mud cusps on either side of the crack fill indicate that soft sediment deformation and loading took place, but it likely played a secondary role in producing the resulting crack network morphology.

Although such cracks are typically interpreted to be desiccation in origin, based on their regular polygonal morphology (Barclay et al., 1991), a well-developed network of microbially mediated desiccation cracks will have upturned crack polygon margins. This produces cracks that are unusually wide and the curled margins are preserved *in situ* or

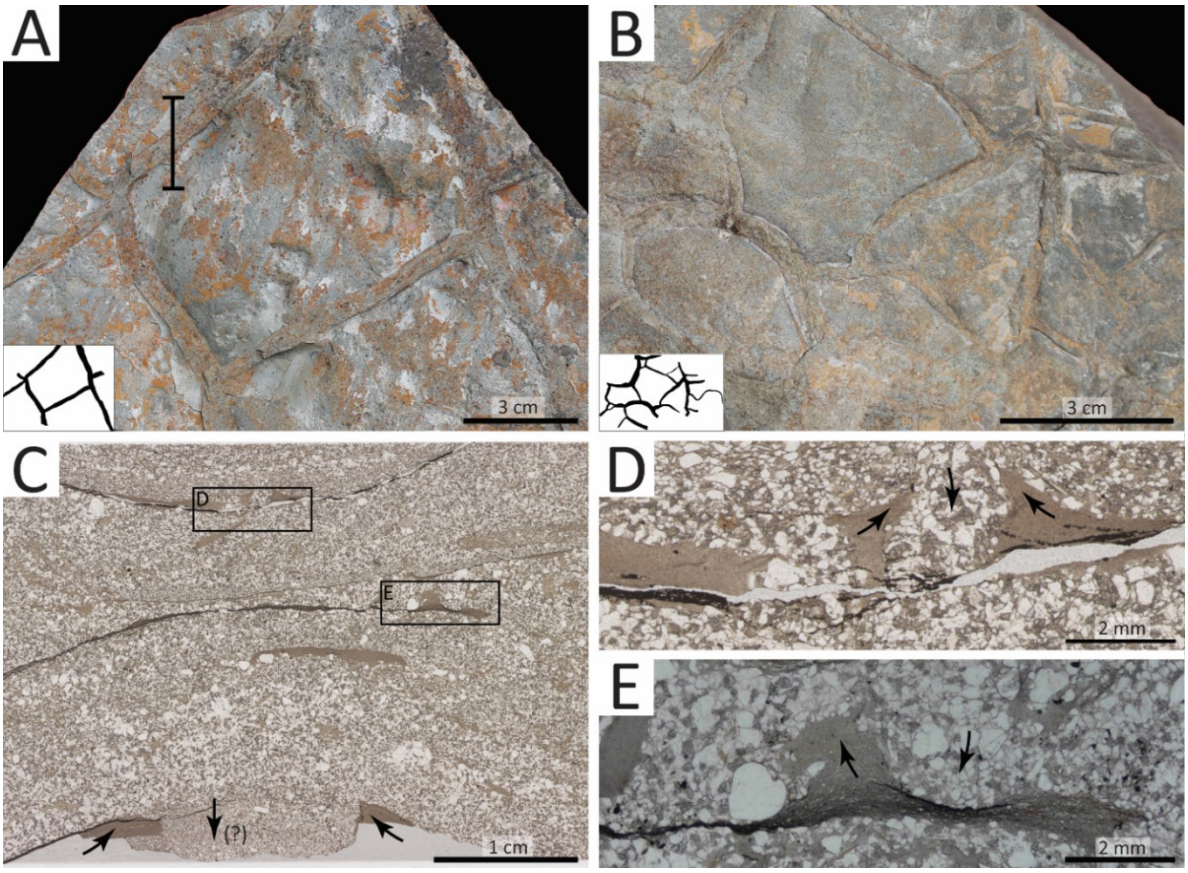

Figure 3-9. Orthogonal cracks. (A) Plan view of polygonal cracks, where 3 cracks intersect in 120^{o} junctions or 4 cracks intersect in 90^{o} junctions, upper Missoula Gp. The black line indicates where the thin section was taken that is shown in panel C. (B) Plan view of semi-curved cracks forming a polygonal network, upper Missoula Gp. (C) Cross-section through the cracked bedding plane showing crude lamination of fine and very-fine quartz grains in argillaceous matrix. Crack fill consists of similar sediment as the bedding plane and has dark argillaceous material preserved on each side. The directions of sediment movement is indicated by black arrows. (D, E) Soft sediment deformation, where the black arrows indicate the sediment movement.

redeposited nearby (Pflüger and Gresse, 1996). In our samples there is no evidence of curled crack margins that would suggest desiccation took place. In fact, rock record examples of curled crack polygon margins and "true" desiccation cracks are rare (Eriksson et al., 2007a see their Fig. 4(c)-5 E, F, Neoproterozoic Im n-Tizi Formation), hence the need for other crack forming mechanisms (Harazim et al., 2013).

The random distribution of grains in the crack fill is more consistent with active infill, such as that during intrastratal crack formation, where the downward movement of the overlying sand would infill cracks and fissures produced in the biolaminae. The shrinkage of the biomat is likely caused by dewatering and degradation of the buried organic layer, rather than subaerial exposure.

Irregular-polygonal cracks

Description

Straight to semi-curved cracks produce a branching network in the plan view. The cracks are variable in width, ranging 1-4 mm, often intersect at acute angles (30-60^{o}) and form irregular polygonal networks. Lone cracks are also present on the bedding surface that are the thickest at the center and taper outwards (Fig. 3-10, Fig. 3-11). Way up indicators based on ripple cross-lamination and scour surfaces show that the structures are preserved as positive relief features on the sole of the bed (Fig. 3-10 B, C).

The bed comprises of quartz-rich siltstone with euhedral to subhedral muscovite grains that are oriented parallel to the bedding surface, and iron oxide and rutile grains present as dark laminae. The crack fill consists of highly convoluted biolaminae, while the rest of the sample is planar- or cross-laminated. Just like in previous examples, the dark laminae are present on either side of the protruding crack fill (Fig. 10 D, Fig. 11 D-F).

An irregular dark 2 mm thick lamina in the middle of the bed indicates another microbial horizon (Fig. 10 D). The biolamina contains a sole crack that was filled with silt material from above and underwent significant amount of shortening (Fig. 11 B, C). The crack does not penetrate the entire thickness of the biolamina, but is only present in the upper argillaceous unit that has little intertwined quartz grains. Disarticulated microbial mat fragments are also present in layers though out the beds (Fig. 3-11 B, D).

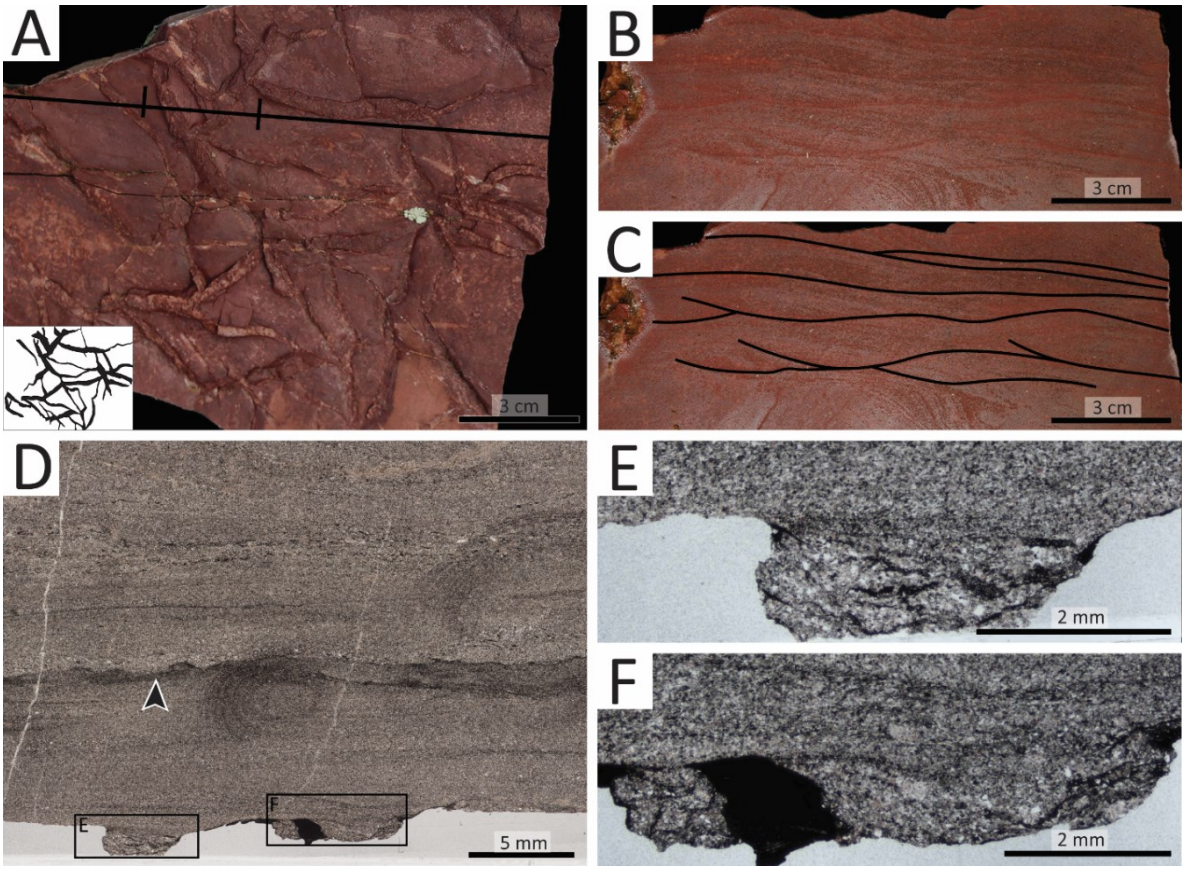

Figure 3-10. Irregular network of cracks, sample 1. (A) Plan view of the cracks, Spokane Fm. (Ravalli Gp). The black line shows the location where the rock was cut, panel B and C, and the perpendicular lines indicate the location of the thin-section cut, panel D. (B) Cross-section through the sample showing ripples and scour surfaces. (C) The ripples and scour surfaces highlighted and interpreted as way-up indicators. (D) Thin section of the sample showing a possible irregular biolamina (black arrow), and two crack features protruding from the bottom bedding plane. (E) Close-up view of the crack fill, showing convoluted laminae. (F) Close-up of a smaller and larger crack features that also show convoluted laminae. The dark argillaceous layer that is preserved between the cracks is interpreted as biolamina.

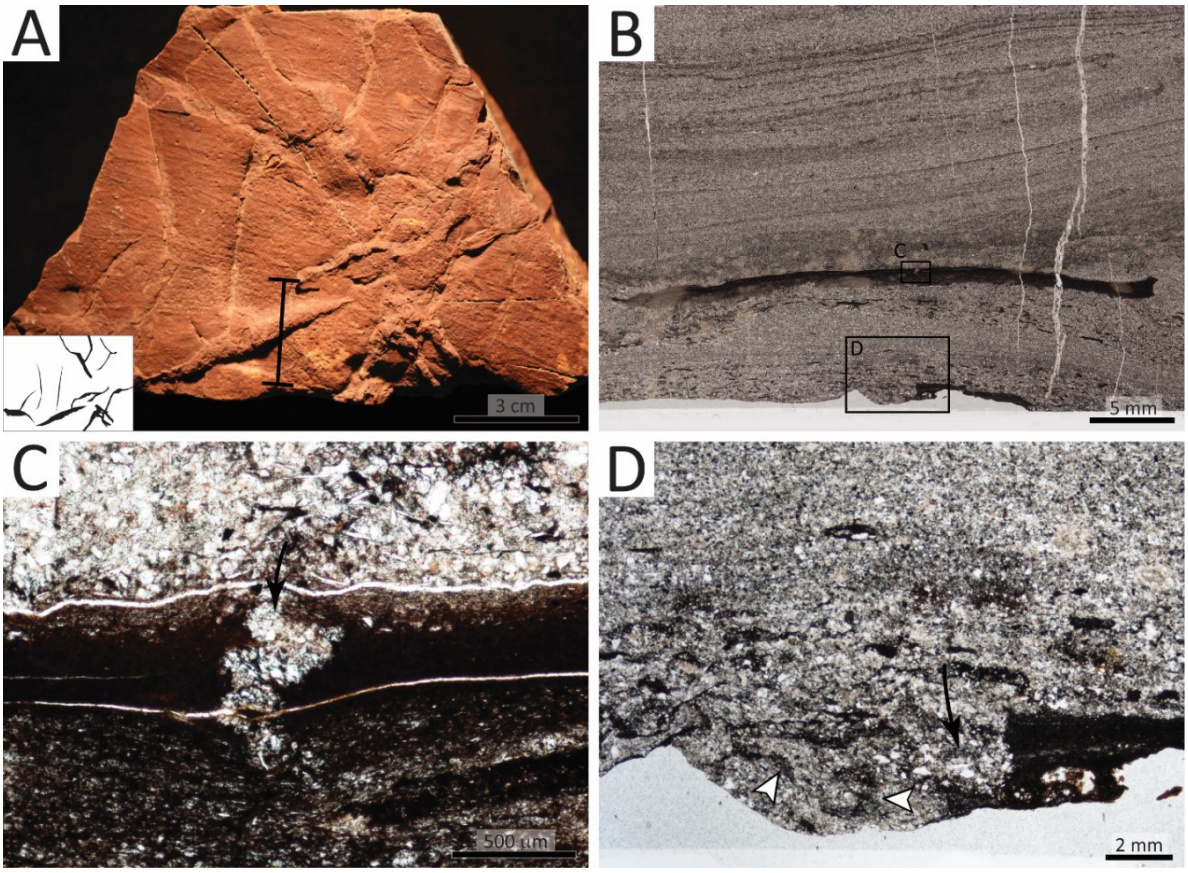

Figure 3-11. Irregular network of cracks, sample 2. (A) Plan view of the cracks, Spokane Fm. The black line indicates the location of the thin-section shown in panel B, C and D. (B) Thin section through the crack feature showing laminated silt-sized quartz sediment with a large "mat chip" and crack feature that is protruding from the bottom bedding plane. (C) Close-up of a compressed crack, sediment infill direction is indicated by the back arrow. (D) Close-up of the crack feature, the convoluted, spiral shaped laminae is highlighted by white arrows. Black arrow indicates possible sediment movement. Dark biolamina is preserved on the right side of the crack fill.

Interpretation

The branching, irregular morphology is not typical of cracks formed during shrinkage, although microbial cover tends to be heterogeneous and has been shown to effect crack structure (Gerdes, 2007). There are two main factors that contribute to crack morphology: the heterogeneities in the mat structure such as thickness variations that drives crack initiation and propagation; and the amount of contraction (for example due to longevity

of subaerial exposure) which is related to crack connectivity and width (see Chapter 2). The irregularity of our cracks is indicative of a heterogeneous shrinking medium.

The convoluted bedding is highly suggestive of soft sediment deformation and active crack infill (Frey et al., 2009). Similar features are sometimes interpreted as petee structures, where the convoluted bedding is interpreted as the remnant of a buckled microbial mat (Parizot et al., 2005). Such features tend to be preserved as positive features on the underlying bedding surface protruding upwards, whereas in our samples the crack-fill protrudes downwards, indicating infill from above that is not consistent with petee interpretation.

The small crack that underwent shortening is an order of magnitude smaller than the main crack features and isolated (Fig. 3-11 C). By straightening the crack, it is apparent that the biolamina contracted 2-3 times its original thickness. Since the crack was infilled prior to any significant compaction, intrastratal cracking may be an early diagenetic process that only requires shallow burial by storm deposition. With further burial the biolamina becomes compacted, while the rigid crack fill buckles under the weight.

Linear cracks

Description

Some cracks are observed to be isolated from one another and do not form a network. Such cracks are up to 10 cm in length and are variable in width, ranging from 2 mm to 1 cm (Fig. 12 A). Others are shorter and have bulbous appearance (Fig. 12 B). The linear cracks are often aligned.

A thin section through an example reveals planar lamination of fine quartz sandstone, muscovite and chlorite and layers containing anastomosing dark fibers, which were enriched in opaque iron minerals, rutile and zircon. The way up is not obvious in mostly planar laminated bedding, but the best interpretation seems to be that the crack fill is preserved as a positive relief feature on the sole of the bed.

The crack fill comprises of fine- to very fine-sand sized quartz grains that are suspended in argillaceous matrix. The dark fibers within the biolamina are parallel to the

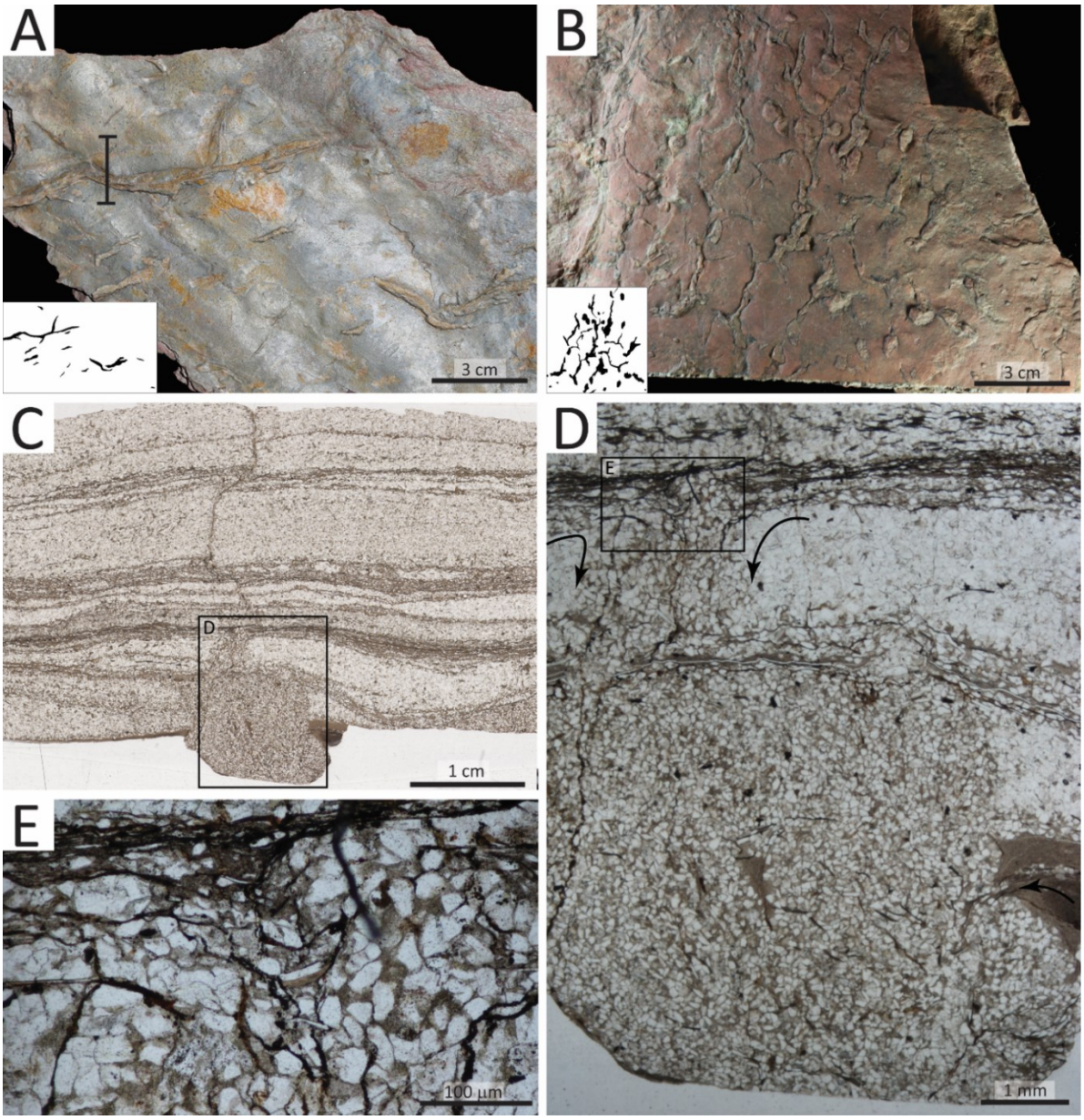

Figure 3-12. Isolated linear and irregular cracks. (A) Plan view of the linear cracks, upper Missoula Gp. The black line indicates the location of the thin section, panel C. (B) Highly irregular cracks that have a bulbous appearance, Spokane Fm. (Ravalli Gp.). (C) Thin section scan showing laminated nature of the sample, where grain supported quartz is interlaminated with quartz grains that are embedded in fibrous matrix. (D) Close-up view of the main crack feature. The crack fill is made up of very-fine sand sized quartz grains that are suspended in argillaceous matrix, while the surrounding sediment is grain supported. The biolamina above the crack is disrupted and the movement of sediment is indicated by the black arrow. (E) Close-up view of the fibrous laminae that change orientation from horizontal to vertical.

bedding plane, except for just above the crack feature, where the fibers change their orientation to vertical (Fig 12 C-E). The elongated fibers within the crack fill are oriented randomly (Fig. 12 D). There is a thin fracture that runs vertical across the entire bed starting at the base of the crack-fill feature, offsetting some of the lamina and acting as a steeply dipping microfault. There is fine grained material present on either side of the crack. On one side the argillaceous material swirls together with the sand forming a soft sediment deformation structure.

Interpretation

Typically soft sediment deformation is associated with rapidly deposited sediments that have low internal shear strength (Frey et al., 2009). Even though biomats start out as cohesive layers with high shear strength, following burial the biolaminae degrades, producing openings that are intruded and filled from above or below (Harazim et al., 2013).

Based on the orientation and bending of the linear fibers within the biolamina (Fig. 12 D, E), the sediment that infills the crack-like feature was squeezed downwards, or injected, rather than pushed up (in its current orientation). In addition the elongated fibers within the crack fill are oriented randomly, some have vertical orientation, indicating that the crack-like feature was filled by active injection, rather than passive sedimentation. The swirl between the crack fill and the argillaceous material preserved on the side of the crack further supports intrastratal formation, where the sediment above has been deposited, prior to crack formation. Such features contain the least evidence for shrinkage, and may be interpreted as mostly influenced by sediment loading and injection.

Discussion

Paleoenvironmental interpretation

Due to the absence of damaging mat burrowing and grazing metazoans, the low-gradient Precambrian seafloors hosted widespread microbial mats (Seilacher, 1999). Even though modern observations of microbial mats and mat-related structures are largely limited

to peritidal settings, it can be argued that the higher energy marginal marine settings (including, but are not limited to tidal flats) will result in the most diverse array of microbial structures due to physical forces acting on the cohesive organic cover. While microbial mats are observed to thrive in deep hydrodynamically quiet siliciclastic environments, down to 500 m depth, they are best characterized by carbonaceous biolaminae in clay-rich sediment, though gas and water escape structures may also be important (Laflamme et al., 2012).

Diverse microbial mat related structures and remnants of biolaminae provide convincing evidence that the sediment of the Spokane Formation and upper Missoula Group were repeatedly colonized with microbial mats. The discontinuous microbial mat fragments "mat chips" observed within the samples are indicative of higher energy events that redeposited the cohesive layer in fragments (Pflüger and Gresse, 1999). It can be interpreted that sand-rich sediments were deposited during higher energy sedimentation, while the microbial mats overgrew these storm deposits and thrived in times of quiescence and lower rates of sedimentation (Bouougri and Porada, 2002).

Biolamina remnants

It is suggested that diastasis cracks are best interpreted as microbial in origin if they are observed in clean sands, where there is an absence of a shrinking argillaceous layer (Eriksson et al., 2007a). However, it was observed that argillaceous veneers accompany many of the features in the Belt strata. This argillaceous layer shows the typical "floating grain" or "wavy-crinkly" anastomosing texture that is highly suggestive of biolaminae (Schieber, 1998; Gerdes, 2007; Noffke et al., 2013). The biolamina acts as a plain of weakness, contributing to the easy separation along bedding surfaces. The biolaminae are mostly weathered away and are only preserved in depressions within the bedding surface or within the bed. Such layers are often only detectable under higher magnifications.

Microbial mats are the most successful at biostabilizing very fine to fine grained quartz rich sands (Noffke, 2009) and prefer low sedimentation rates (Gerdes, 2007). Formation of microbial mat requires time of quiescence, thus it is likely that during this time the microbial mat will acquire fine grained sediment, including clay material out of the water

column, thus be preserved as an argillaceous layer, rather than only be associated with clean sand. In addition, it has been shown that anoxic degradation of organic matter will facilitate precipitation of argillaceous aluminosilicates that accompanies pyrite precipitation, thus adding to the evidence that biolaminae tend to be argillaceous (Darroch et al., 2012).

Intrastratal cracking mechanism

Crack networks that have orthogonal or triradiate elements are best interpreted as shrinkage cracks. Shrinkage cracks can be due to desiccation (Bradley, 1933; Gerdes et al., 1993, 2000) synaeresis (White, 1961; Burst, 1965; Donovan and Forster, 1972) or intrastratal dewatering and mat degradation (Tanner, 1998; Harazim et al., 2013). Synaeresis cracking has been proven to be a valid crack forming mechanism in sediments rich in swelling clays (Burst, 1965). It is unlikely that salinity changes will lead to cracking of a microbial mat, as the bacteria within a microbial mat are cocooned in exopolymers that act as buffers, protecting the cells from environmental changes, including pH, salinity and toxins (Decho, 1990).

The intrastratal crack formation in is proposed form in the following way: (1) the microbial mat is buried by a storm deposit and with time begins to degrade; (2) the weakened microbial mat contracts (due to dewatering ?) leading to formation of polygonal fractures (3) the sediment intrudes from above or below into the weakened organic layer, the active injection may lead to convoluted laminae within the crack fill and soft sediment deformation features; (4) the bed easily splits along the argillaceous biolamina, which weathers away, except for small remnants that are preserved in depressions within the bedding surface (Fig. 3-13). Intrastratal cracking is the better explanation for diastasis crack formation.

MMDC observed in Belt Supergroup strata lack evidence of desiccation, such as wide cracks with upturned margins that are preserved *in situ*, or redeposited nearby (Gerdes, 1993; Gerdes, 2007; Eriksson et al., 2007a). The larger “mat chips” observed in the cross-section have straight, rather than curled edges. There are evidence of active infill in the form of convoluted laminae that suggest that the best interpretation is intrastratal cracking. While

triradiate and orthogonal networks were caused by shrinkage, the linear cracks may have been caused by rapture of the biolaminae by the denser overburden (Pflüger, 1999). Both shrinkage and soft sediment deformation played some part in formation and modification of the structures.

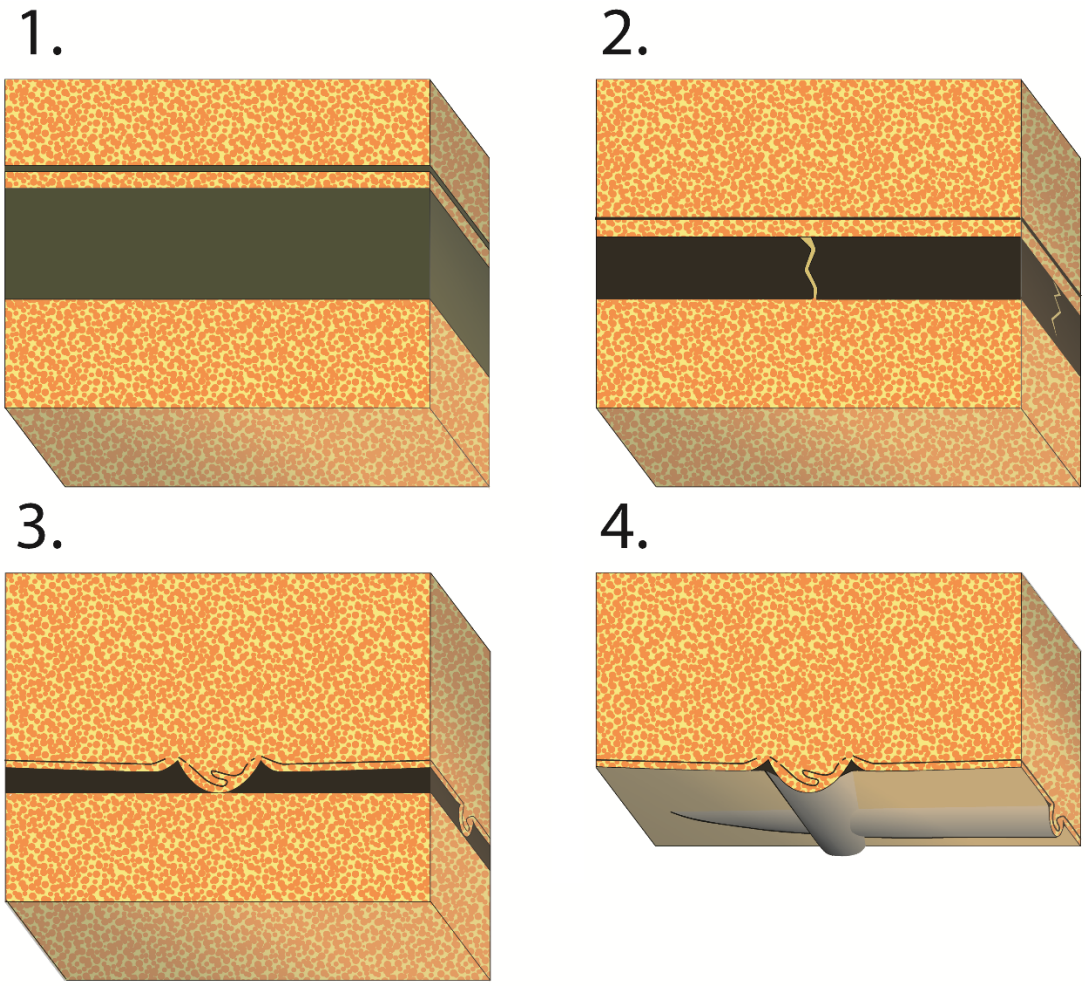

Figure 3-13. Intrastratal crack formation schematic. (1) The microbial mat gets covered with sediment. (2) Further burial leads to compaction and degradation of the biomat. The equal distributions of pressure and approximately evenly distributed mat contraction, may lead to the formation of polygonal fractures. (3)The sediment intrudes from below or above into the weakened biomat. The active infill may produce convoluted laminae within the crack fill. (4) The crack features, produced by the combination of mat degradation and contraction, sediment injection and differential compaction, are preserved as positive features on the bedding surface or on the sole of the overlying bed. The argillaceous biomat layer acts as a natural plain of weakness. The biomat is mostly weathered away except for within depressions, such as the pockets in between protruding crack and the bedding plane.

Conclusions

Abundant microbial mat related structures are observed on closely spaced horizons of both the upper Missoula and the Spokane Formation (Ravalli Group), including kinneyia wrinkles, petee structures, nodular bedding surfaces, remnants of gas domes, and versatile diastasis cracks. Thin carbonaceous veneers that are consistent with biolaminae interpretation, such as the "anastomosing floating grain" or "wavy-crinkly" appearance, provide evidence for microbial origin of the features. Studying the interaction of biolaminae with the sediment using thin sections, gives better insight into origin and formation of the structures.

Even though the strata are interpreted to have been deposited in a shallow water environment, it is not likely that the sediment was subaerially exposed, as there is no evidence of desiccation. The diastasis cracks are interpreted to have been formed due to intrastratal processes, such as biomat degradation, dewatering and shrinkage, as well as sediment loading.

CHAPTER 4: Probable metazoan traces in the currently mapped upper Missoula Group, southwestern Montana, U.S.A.

Introduction

Neoproterozoic to middle Paleozoic strata of north-central United States and western Canada represent a basin-style transition from a rift basin to a passive margin, during and subsequent to the breakup of the supercontinent Rodinia (Meert and Torsvik, 2003; Lund, 2008). Strata of this age are rare to absent in east-central Idaho and throughout most of western Montana, which represents a gap in general north-south trending miogeoclinal successions (Fig. 4-1) (Lund, 2008).

Recent analyses of the miogeoclinal and volcaniclastic rocks, including stratigraphy, geochronology and detrital zircon studies, suggest complex multi-phase rifting along-strike of the western Laurentian margin (Yonkee, 2014). Due to the current incomplete understanding of geological complexities of the western Laurentian margin, including spatial and temporal distribution of strata and the tectonic setting, it is possible that Neoproterozoic strata are in fact present in fault bounded, isolated pockets throughout southwestern Montana, but are misinterpreted as part of the Mesoproterozoic Belt Supergroup (Lund, 2008).

In our study areas the Mesoproterozoic Belt Supergroup is overlain by shallow-marine middle Cambrian sandstone. The contact between these two packages is mapped as an unconformity, which represents erosion and 900 Ma of non-deposition. The youngest formations within the upper Missoula Group, such as the Quartzite of Argenta, Garnet Range and Libby formations, are considered by some authors to be a part of a younger post-Belt succession (Smith and Barnes, 1966; Kidder, 1988; Pearson, 1996). The presence of mica along bedding surfaces and beds with hummocky cross-stratification, differentiates these formations from the rest of the Missoula Group strata.

The upper Missoula Group and Spokane Formation (part of the Ravalli Group), which are currently mapped as rocks of the Mesoproterozoic Belt package below the

Mesoproterozoic – Cambrian unconformity, were assessed in two locations (Fig. 4-3). Abundant microbial mat-related structures were identified, including microbial diastasis cracks, kinneyia (runzelmarken) and other microbial impressions (see Chapter 3). Distinct and reoccurring bilobate structures are observed on bedding planes of the upper Missoula Group and interpreted as probable metazoan traces. While microbial mat features are common in both Proterozoic and Phanerozoic successions, the discovery of metazoan burrowing or grazing behaviors would limit the age of these rocks to Ediacaran. In the Spokane Formation study area, microbial mat impressions are commonly found on the bedding surfaces and are shown here to help differentiate between bilobate traces and trichome impressions.

Geological History

The Belt Supergroup is a thick and widespread package of Middle Proterozoic sedimentary strata which range in age from 1470 to 1400 Ma (Ross and Villeneuve, 2003). Belt Supergroup outcrops throughout north-central U.S.A., including Montana, Idaho, Utah, Washington and reaching into southern Canada where it is called the Purcell Supergroup (Fig. 4-1). Mesozoic orogenic activity shortened most of the Belt Basin, resulting in thrust faults and high-angle reverse faults (Ross and Villeneuve, 2003). In fact the Belt terrane is largely allochthonous, as it was transported eastward by the Cretaceous-Eocene Rocky Mountain fold and thrust belt, followed by extensional relaxation (Harrison, 1972; Harrison et al., 1980).

The Belt strata are overprinted by low-grade metamorphism that reaches sub greenschist facies, except for the southern and westernmost outcrops (Ross and Villeneuve, 2003). The Belt strata contain well preserved sedimentary features that were not destroyed by the onset of metamorphism, allowing for sedimentological analysis (Schieber, 1998).

The sedimentary succession consists predominantly of shale, siltstone, sandstone, as well as argillaceous limestone and dolomite (Schieber, 1998). Belt stratigraphy is generally divided into four categories: the Lower Belt, the Ravalli Group, the Middle Belt Carbonates

and the Missoula Group (Fig. 4-2). The environment of deposition of Belt strata as well as the basin architecture are debated, but it is generally agreed that lower Belt consists of deep-water submarine fan deposits succeeded by shallow water to subaerially exposed sediments deposited in epicontinental sea or lacustrine type settings (Cressman, 1989); the latter shallow-water conditions were ideal for microbial mat development. Abundant microbially mat related structures throughout the Belt strata were observed and documented by Schieber (1998). Fossils of eukaryotic algal filaments have also been observed (Walter et al., 1976; Horodyski, 1993), but fossils or trace fossils of animals have not been reported.

Cryogenian to Devonian rifting formed a passive western Laurentian margin, which accumulated Neoproterozoic – Cambrian succession of volcanic and miogeoclinal strata, found today throughtout north western United States and western Canada (Lund, 2008). However this rifting event was non uniform, reflected by the absence of Neoproterozoic strata in east-central Idaho and most of western Montana (Fig. 4-1).

Middle Cambrian Sandstones that was deposited during the earliest transgression of the Cambrian sea, overlie Belt strata in southwestern Montana. Proposed depositional environments include braided fluvial, for the oldest coarse grained, immature feldspathic and conglomeritic sediment and nearshore marine for the younger, well sorted, quartz-rich sediment (Macke, 1993). A wide array of trace fossils have been observed in this unit including *Skolithos*, *Diplocraterion*, *Corophioides*, *Corophium*, *Cruziana*, *Sabellarifex*, *Phycodes*, and *Plagiogmus* (Macke 1993). Inarticulate brachiopods have also been reported *(Lingulepis* sp.) (Macke, 1993).

Methods

Formations mapped as the youngest preserved strata of the Belt Supergroup, just below the overlying middle Cambrian Sandstones were examined in two locations, to determine if there are any evidences of biogenic sedimentary structures that would indicate strata younger than Mesoproterozoic. Outcropping upper Missoula Group was examined 20 km northwest of the town of Dillon, MT (Fig. 4-3A). Outcropping Spokane Formation (part of Ravalli Group) was examined in the Devil's Fence Anticlinorium, 60 km north of

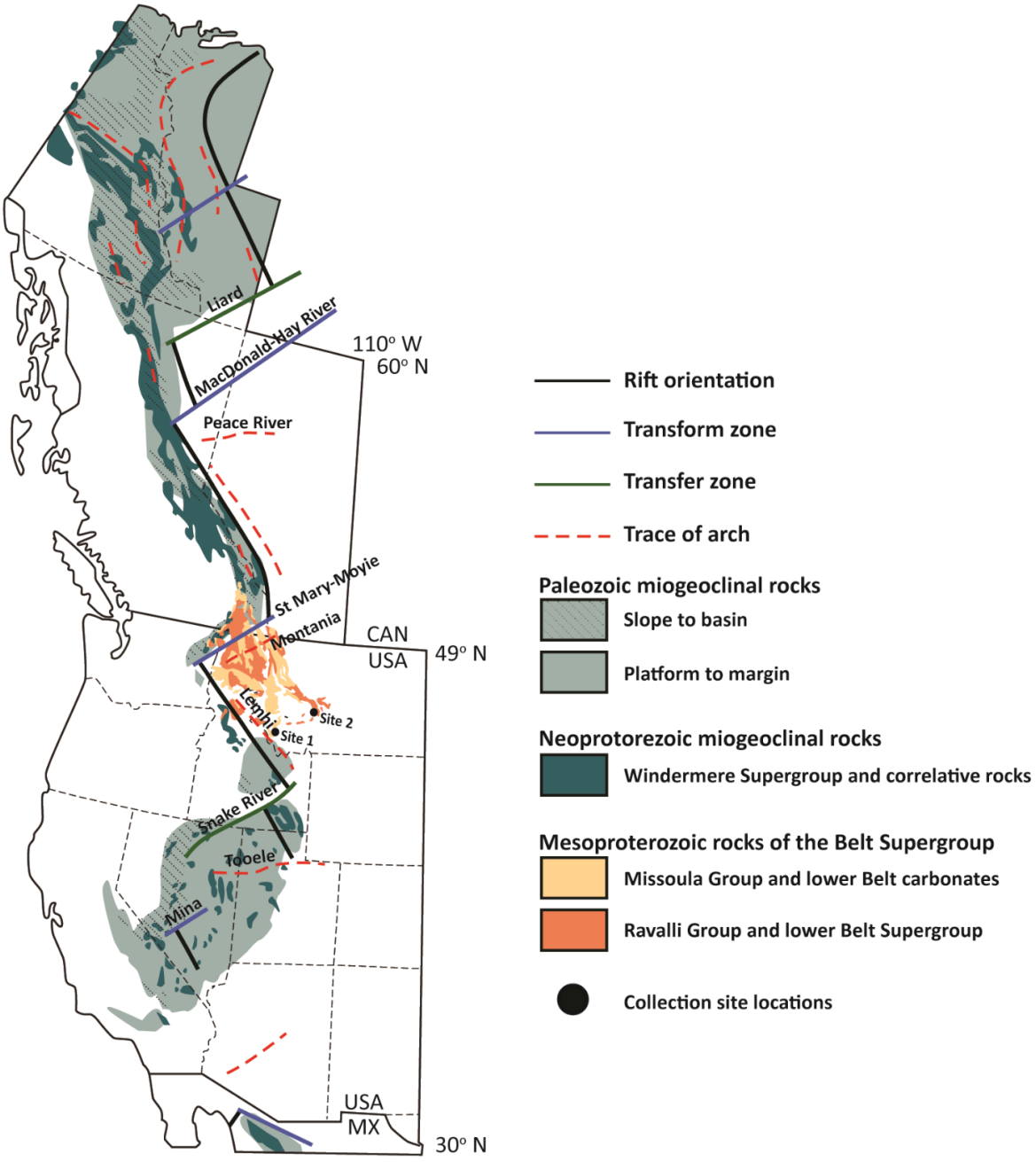

Figure 4-1. Regional map showing outcropping Belt Supergroup and Neoproterozoic and Paleozoic miogeoclinal strata including structural elements. Schematic representation of segmented rifting, including transform and transfer zones, forming separate basins where miogeoclinal strata accumulated. Note the absence of miogeoclinal strata in northern Idaho and western Montana. Modified from Ross and Villeneuve (2003) and Lund (2008).

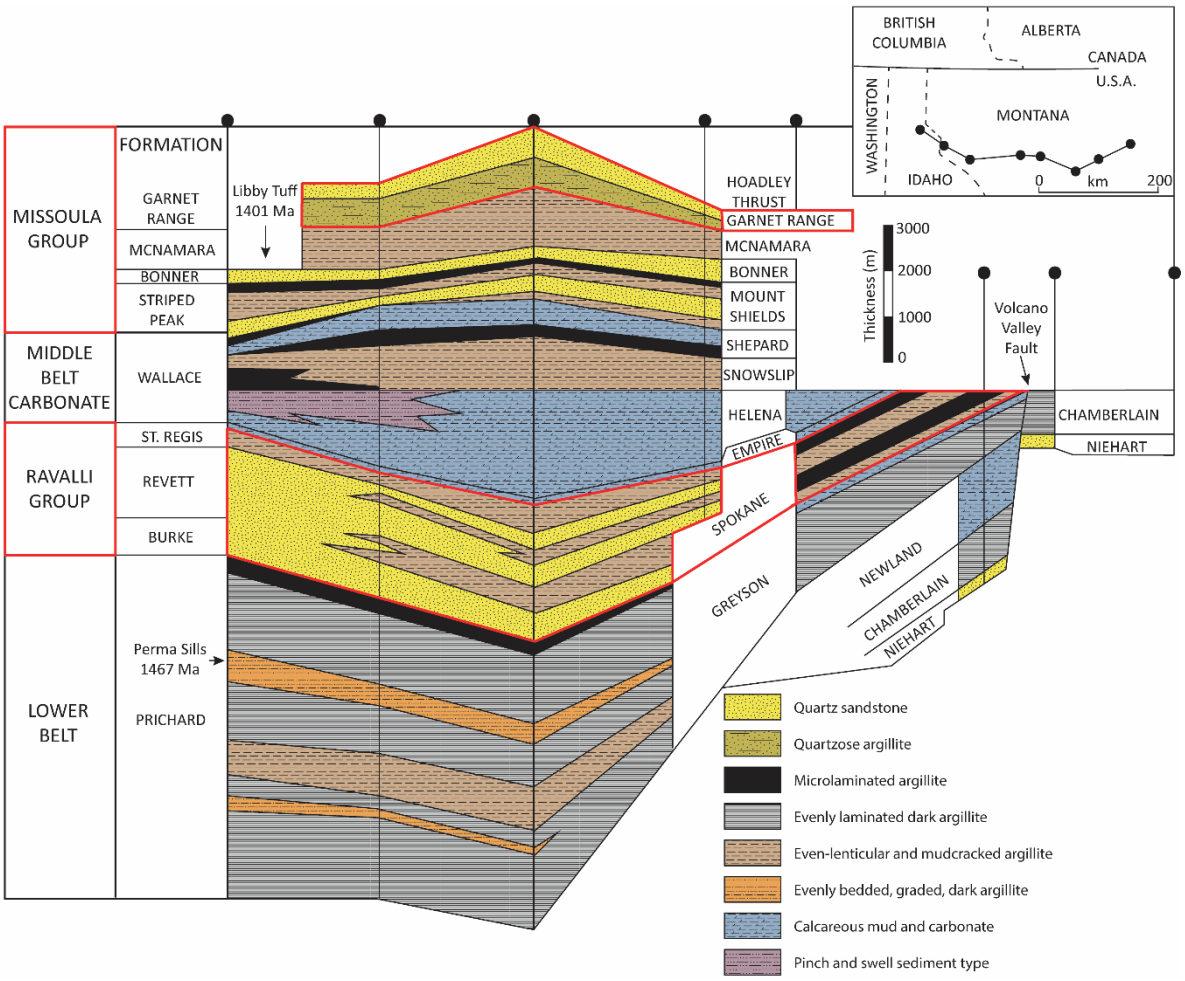

Figure 4-2. Cross-section through northern Idaho and Montana, indicating the typical stratigraphy of the Belt Supergroup. Modified from Ross and Villeneuve (2003).

Bozeman, MT (Fig. 4-3B). Field photographs were taken and samples were brought back to the lab for closer analysis. Due to the recessive nature of the Belt units, the samples were often collected as weathered slabs that were not in their original stratigraphic position.

Collection site 1: Rattlesnake Creek, Beaverhead National Forest– upper Missoula Group

In this area, the upper Missoula Group consists of 3 Units, Unit 1 and 3 are silicified, well sorted, fine to medium grained trough cross-stratified quartz arenite beds, interpreted to have been deposited in a high energy environment, such as an upper shoreface. The middle Unit 2 is dominated by recessive, light grey-tan, sandstones, siltites and argilites. Very-fine sand- and silt-sized quartz and feldspar grains are interlaminated with mica-rich argillite, contributing to an overall fissility. Sedimentary structures include wave ripples, low angle cross lamination and coarser grained sand lenses. This unit was interpreted to have accumulated in a lower energy setting, and resembles proximal offshore deposits. It is in Unit 2 where microbial mat-related structures are observed on bedding planes (see Chapter 3). Silicified sandstones of Units 1 and 3 have poorly developed bedding surfaces, and no visible microbial structures in cross-section.

Collection site 2: Devil's Fence Anticlinorium - Spokane Formation (Ravalli Group)

The sedimentary succession of the Spokane Formation in the Devil's Fence Anticlinorium comprises mainly red siltstones with local sand lenses. Sedimentary structures include small-scale trough cross-stratification of combined flow ripples or small-scale dunes and wave ripples preserved on bedding planes. The sedimentary features best resemble a lower shoreface environment. Northward current directions have been reported, but in some locales the orientations are variable, leading to interpretation of tidal influence (McMechan, 1981). Numerous microbially induced sedimentary structures are observed on bedding surfaces throughout the strata (see Chapter 3).

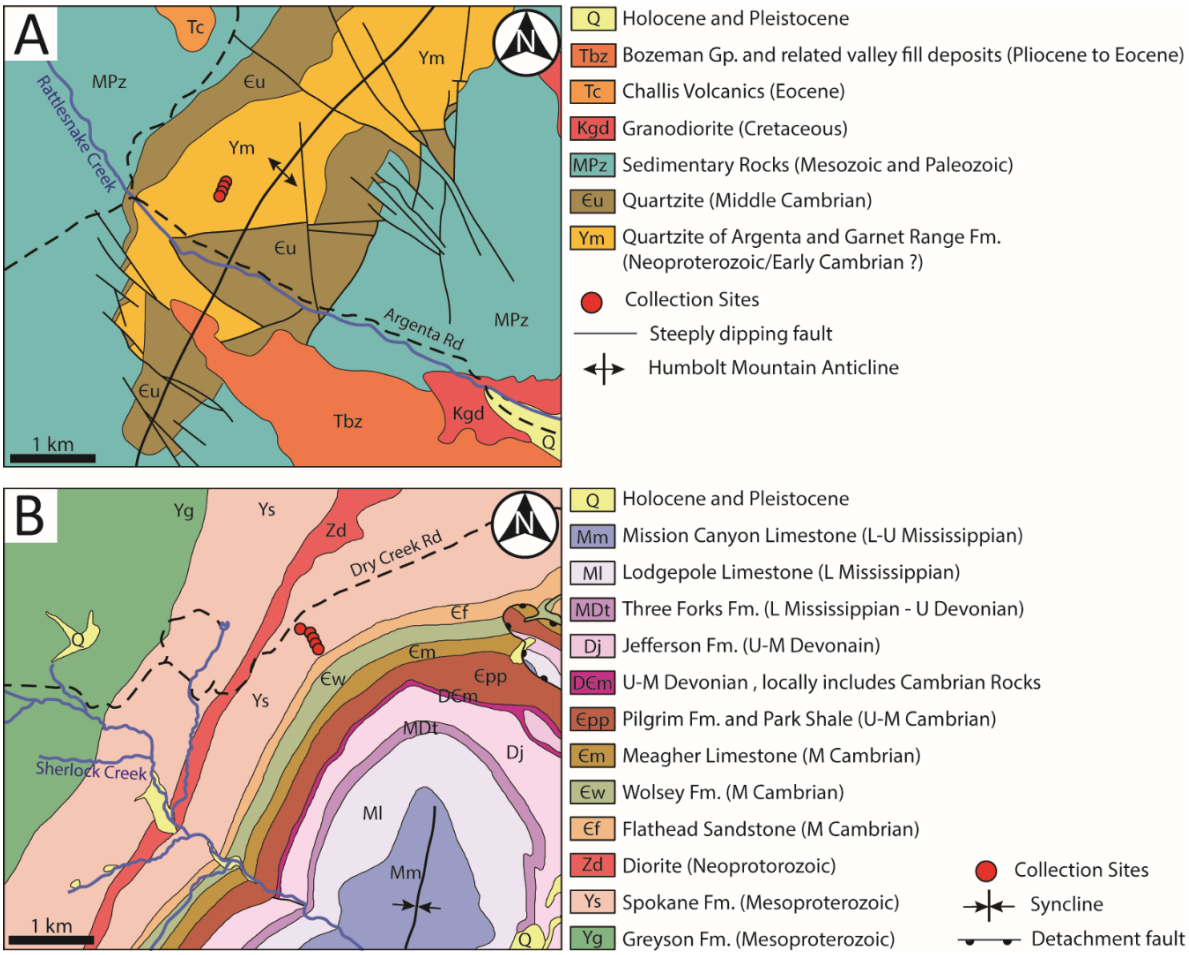

Figure 4-3. Regional maps of the collection sites 1 and 2. (A) Geological map of the study area 1, 20 km northwest of Dillon, MT. The outcropping upper Missoula Gp. was studied in the indicated collection sites. Modified from Pearson (1996). (C) Geological map of the study area 2, 60 km north of Bozeman, MT. The outcropping Spokane Fm. of the Ravalli Gp. was studied in detail in the indicated collection sites. Modified from Geological Maps of Montana made available by the Montana Bureau of Mines and Geology.

Results

Bilobate structures, upper Missoula Group

Rare, but reoccurring bilobate structures of consistent width distinctly stand out from the microbial shrinkage cracks. Four instances of such bilobate structures were observed on two different bedding surfaces in Unit 2 of the upper Missoula Group (Fig. 4-4, 4-5). The structures are preserved as upward-protruding (convex epirelief) bilobate ridges which are separated by a thin, central grove. The individual lobes are 1-1.2 mm in width with a total width of the structure of approximately 2-2.5 mm. The length of a continuous structure is typically 0.6 – 1.5 cm, but may be as long as 3 cm where the trail porpoises in and out of the bedding plane: in such cases, convex epirelief lobes leave the bedding plane and reappear as a downward protruding (concave hyporelief) groves separated by a thin central ridge (Fig. 4-4 A, B). The two preservation styles indicate that the structure is emplaced within the sediment and a top and bottom of the structure are preserved.

Microbial mat impressions, Spokane Formation (Ravalli Group)

Several bedding surfaces of the Spokane Formation (Ravalli Group) display linear fabric, consisting of straight, often intersecting at low angle, ridges and grooves that are 0.5 mm thick and can be traced on the surface for several centimeters (up to 5 cm long) (Fig. 4-6). There is no evidence that the linear structures go in and out of the bedding plane, they simply terminate with a rounded edge. Such fabric is interpreted as impressions left by ancient encrusting filamentous bacteria or algae that once grew on the sediment surfaces. Structures with a similar relief and size are described from the bedding surfaces of the red mudstone of the Snowslip Formation, Belt Supergroup and are interpreted as microbial mat impressions formed in an upper intertidal to supratidal setting (Horodyski, 1993).

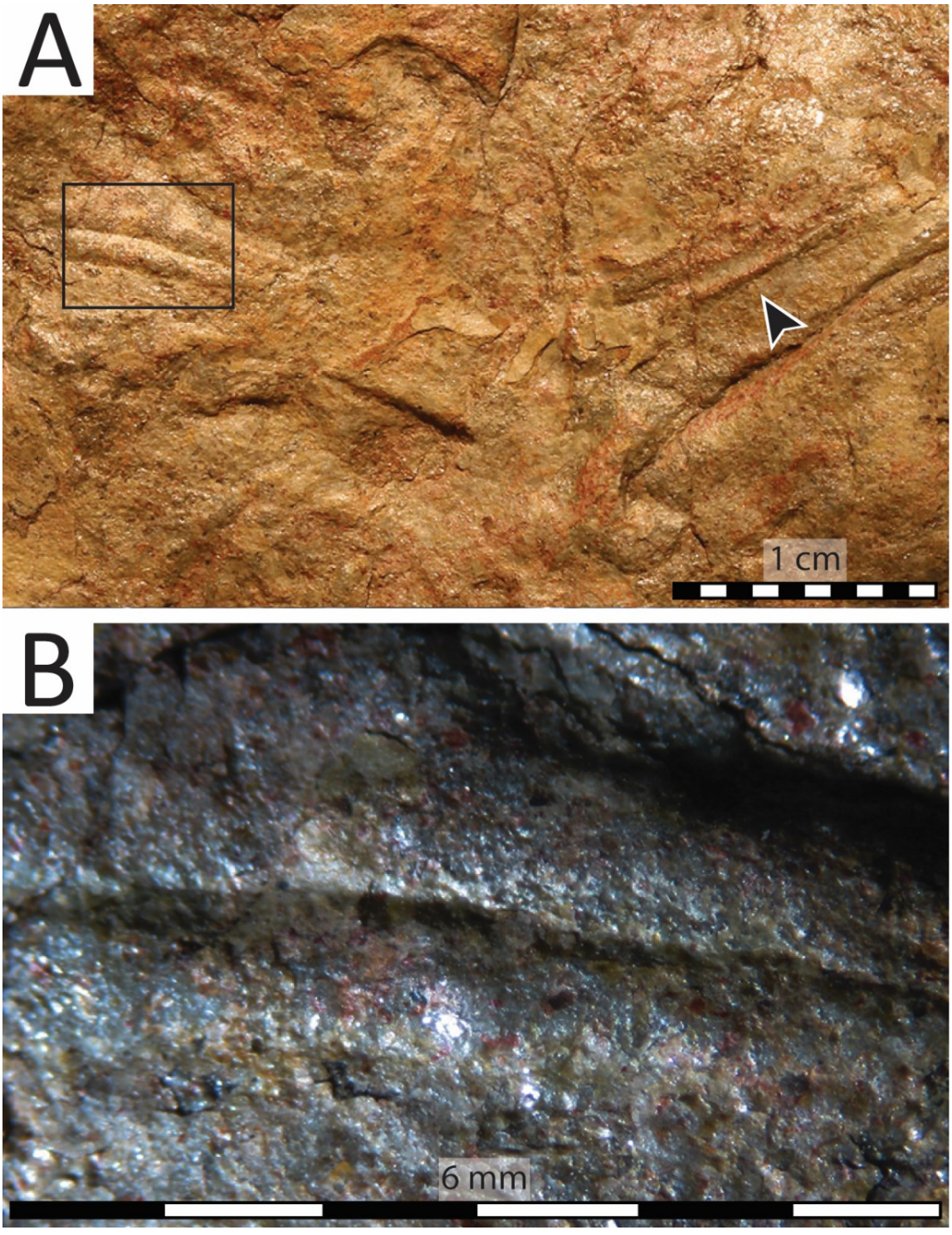

Figure 4-4. Probable metazoan traces, sample 1. (A) Upwards-protruding bilobate ridges which appear to leave the bedding plane and reappear as a downward-protruding bilobate groves as indicated by the arrow, upper Missoula Group. (B) Close-up micrograph of the bilobate feature in panel A, observed under a stereo microscope.

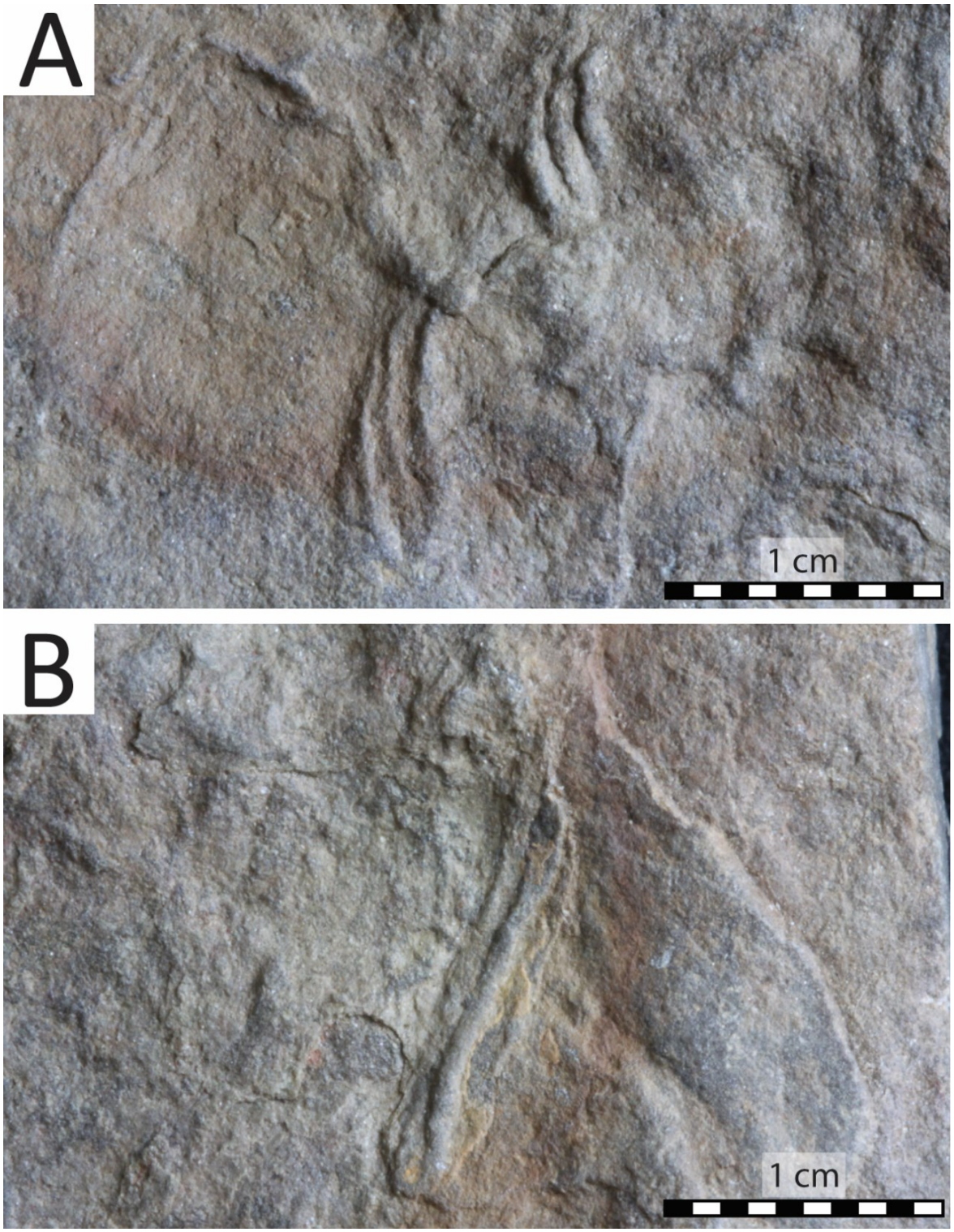

Figure 4-5. Probable metazoan traces, sample 2. (A) Bilobate structures observed on a second bedding surface. (B) Slightly sinuous, bilobate structure observed on the same bedding surface as the structures in panel A, upper Missoula Group.

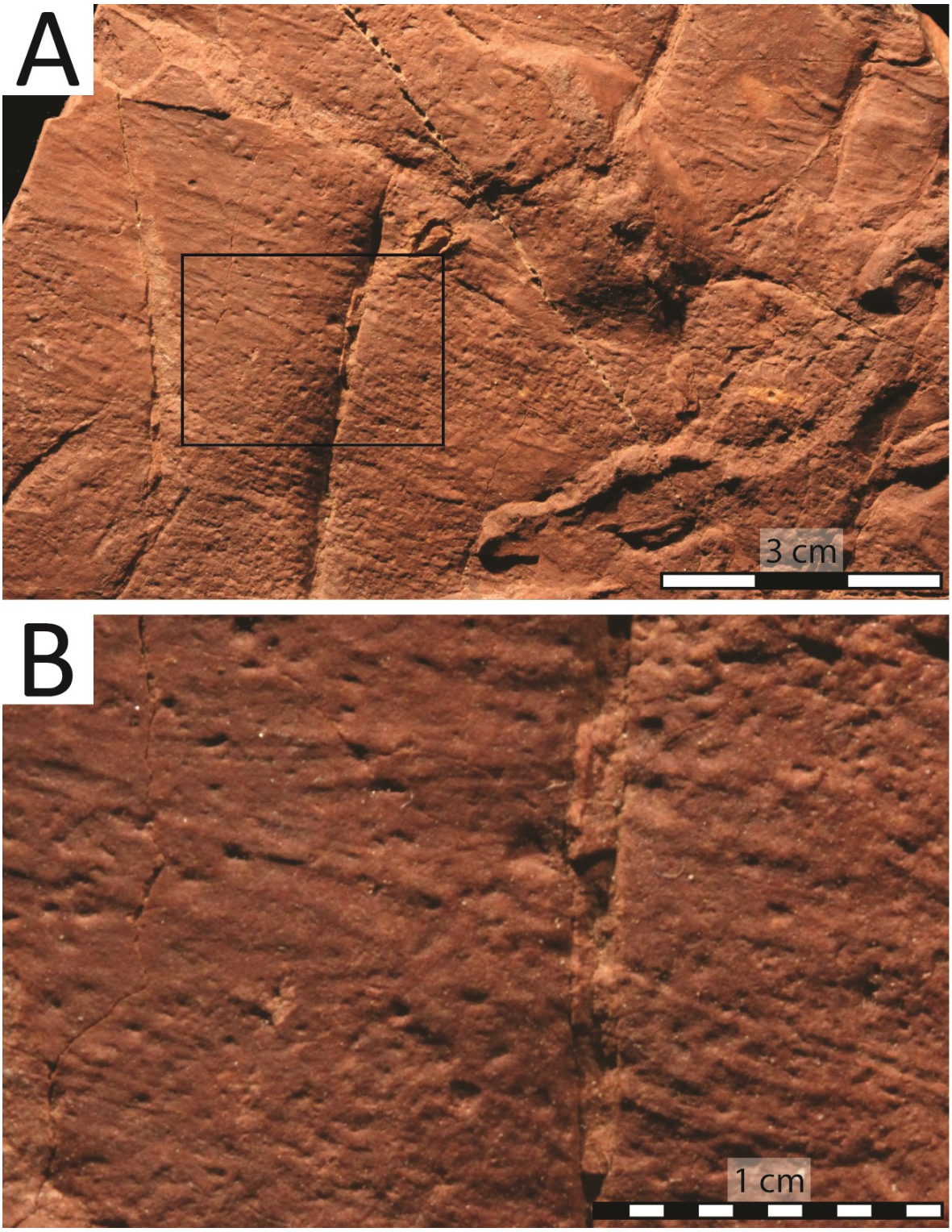

Figure 4-6. Microbial mat impressions. (A) Fabric forming straight and intersecting ridges and grooves that can be traced on the surface for several centimeters. (B) Close-up view of the linear structures, the individual widths of the ridges are about 0.5 mm.

Discussion

Precambrian time was conductive to proliferation of microbial mats, this is reflected by the abundance of mat-related structures found in siliciclastic strata of this age (Schieber, 1998; Noffke et al., 2006a; Noffke et al., 2006b; Sarkar et al., 2006; Bouougri and Porada, 2007a; Bouougri and Porada, 2007b). Metazoan lifestyles in the Ediacaran time were not damaging to the microbial mats and were limited to mat encrusters, mat scratchers, mat stickers and undermat miners (Seilacher, 1999). Microbial mats were an important source of food and oxygen for early animals and it is common that ancient traces are found alongside microbial mat impressions (Hagadorn and Bottjer, 1999; Gingras et al., 2011).

Some of the oldest identified trace fossils are Ediacaran in age, living just before the Cambrian Explosion (Pecoits et al., 2012). The bilobate burrows described by Pecoits et al. (2012) from >585 Ma Tacuari Formation, Uruguay, have strikingly similar appearance to the bilobate structures described above from the upper Missoula Group. Such burrows are interpreted to form by early metazoans with bilateral symmetry of the body (Pecoits et al., 2012). The bilaterian *Aulichnites*-like traces from the Cambrian-Vendian Great Basin, U.S.A., are observed among microbial kinneyia wrinkles and are essentially identical in dimensions and appearance to the bilobate traces of the upper Missoula Group (Hagadorn and Bottjer, 1999). The traces are interpreted to have been formed by a mollusk-like animal and may be related to the younger *Scolicia* (Mangano et al., 2003).

Determination of whether the elongate structures were biogenic traces, abiotic tool marks or microbial impressions were based on the tubular and bilobate nature of the structure and evidence of leaving and reappearing on the bedding surface. There are other mechanisms that can form structures similar to animal burrows, however tool marks often show angularity, cracks taper at their terminus, and microbial wrinkle structures are not tubular. Impressions of bacteria filament or algae poses the greatest challenge (Fig. 4-6) to the metazoan trace interpretation, however the evidence of the linear trails going in and out of the bedding plane and consistent bilaterian nature of the structures imply burrowing behaviors and body symmetry. Structures that are interpreted as algal impressions form the

Spokane Formation (Ravalli Group) produce a continuous fabric (Fig. 4-5), while the structures that are interpreted as trace fossils are isolated (rather than fabric-forming) (Fig. 4-4). Structures that are interpreted as the metazoan traces are also much thicker than those interpreted as microbial mat impressions.

Conclusion

The model which suggests a major unconformity between the Mesoproterozoic Belt Supergroup and the middle Cambrian Sandstones does not seem to hold true in our study area in southwestern Montana. We propose some of the strata that are currently mapped as the upper Missoula Group, are much younger, Ediacaran to early Cambrian in age and may be conformable with the overlying middle Cambrian strata. The evidence of probable metazoan life, provide a convincing argument in favor of reclassifying certain strata of the upper Missoula Group from Mesoproterozoic to Ediacaran or early Cambrian. Further mapping, ichnological and geochemical analysis is needed to isolate and delineate these younger pockets of strata.

CHAPTER 5: Conclusions

This thesis investigates structures produced from microbial mat-sediment interactions, by conducting laboratory experiments and observing fossil microbial mat-related structures on the bedding surfaces of the Mesoproterozoic Belt Supergroup. The focus is to provide a detailed study of the poorly understood microbially mediated diastasis cracks and interpret the mechanisms responsible for their formation. In addition, various mat-related structures and bilobate traces associated with early biomats are discussed and interpreted.

Similarly to clays, water-rich microbial mats have the ability to shrink, making them an excellent catalyst in crack formation. Since desiccation is the most popular mechanism that is used to explain cracks in the rock record, experiments were performed in order to provide an additional laboratory analog. The experiments showed that that the water-rich microbial mat contracts rapidly with desiccation, producing an irregular network of radiating crack clusters. Weaknesses in the mat act as loci for crack initiation, however the cohesive mat withstands crack propagation leading to cracks that do not propagate far from their point of origin. Curled crack-polygon margins are readily formed as a result of tremendous shrinkage of the top microbial layer as compared to sediment underneath. Curled margins produce unusually wide cracks, where the original cracking pathways may become unresolvable.

The diastasis cracks observed on the bedding surfaces of the Belt Supergroup, both upper Missoula Group and Spokane Formation (Ravalli Group), have different morphologies, ranging from regular triradiate and orthogonal networks to irregular and isolated crack-like features. The best characteristics of shrinkage cracking is triradiate junctions that represent the initial response to shrinkage and orthogonal junctions, since cracks tend to connect and branch out in 90^{o} angles (Sholin, 2000). However the cracks do not show the expected desiccation features, such as wide cracks with curled-up crack-polygon margins. Instead the cracks show evidence of an active infill and soft sediment deformation, and are thus best interpreted as intrastratal. The isolated linear cracks show the least evidence of shrinkage and are best interpreted as dewatering and loading features, based

on the intrusive crack fill (Pflüger, 1999). While the studied Belt sediments were deposited in a shallow water environment, there is no evidence of subaerial exposure.

While desiccation is the most prevalent mechanism for crack formation in the modern peritidal settings, it should not be automatically assumed that cracks in the rock record are formed by the same method and thus underwent subaerial exposure. As discussed above, the versatile Mesoproterozoic cracks tend to agree more with intrastratal formation, an early diagenetic process that cannot be easily observed, where the biolaminae get degraded with burial and is intruded by sediment from above or below. Shrinkage of the biomat is certain as orthogonal and triple junctions are common, but in few instances the cracks may be purely mechanical features formed as loading structures due to differential compaction.

Synaeresis is used as an alternative mechanism for crack formation in abiotic sediments. Laboratory experiments show that subaqueous shrinkage is possible whether using man made materials or natural sediment containing swelling clays (White, 1961; Burst, 1965; Donovan and Foster, 1972). While synaeresis is a valid mechanism for clay containing sediments, it does not seem a likely crack forming mechanism for biostabilized sediments. It is unlikely that the microbial mat will be shocked by salinity variations and crack, as the extracellular polymeric substances attenuate bacterial exchange with its surroundings. Modern microbial mats grow in subaerially exposed tidal flats that are subjected to sea water flooding and fresh rainwater runoff (Gerdes, 2007). For this reason, intrastratal cracking is the favored mechanism when it comes to biostabilized sediments, because microbial mats, especially the photosynthetic communities degrade with burial (Harazim et al., 2013).

In addition, we propose some of the strata that is currently mapped as the upper Missoula Group is in fact younger in age. The discovery of bilaterian traces suggests that certain slivers of the strata are Ediacaran to early Cambrian and may be conformable with the overlying middle Cambrian sandstone. Further mapping, ichnological and geochemical analysis is needed to isolate and delineate these younger pockets of strata.

References

Allwood, A. C., Walter, M. R., Burch, I. W., Kamber, B. S., 2007. 3.43 billion year old stromatolite reef from the Pilbara Craton of Western Australia; ecosystem scale insights to early life on Earth. Precambrian Research 158, 198–227.

Bailey, J. V., Orphan, V. J., Joye, S. B., Corsetti, F. A., 2009. Chemotrophic microbial mats and their potential for preservation in the rock record. Astrobiology 9, 843–859.

Beraldi-Campesi, H., Garcia-Pichel, F., 2011. The biogenicity of modern terrestrial roll-up structures and its significance for ancient life on land. Geobiology 9, 10–23.

Bernhard, J. M., Buck, K. R., Farmer, M. A., Bowser, S. S., 2000. The Santa Barbara Basin is a symbiosis oasis. Nature 403, 77–80.

Bosak, T., Bush, J.M., Flynn, M.R., Liang, B., Ono, S., Petroff, A.P., Sim, M.S., 2010. Formation and stability of oxygen-rich bubbles that shape photosynthetic mats. Geobiology 8, 45–55.

Bose, S., Chafetz, H.S., 2009. Topographic control on distribution of modern microbially induced sedimentary structures (MISS); a case study from Texas coast. Sedimentary Geology 213, 136–149.

Bose, S., Chafetz, H.S., 2012. Morphology and distribution of MISS; a comparison between modern siliciclastic and carbonate settings. Special Publication - Society For Sedimentary Geology 101, pp. 3–14.

Bottjer, D., Hagadorn, J.W., 2007. Mat growth features. In: Schieber, J., Bose, P.K., Eriksson, P.G., Banerjee, S., Altermann, W., Catuneanu, O. (Eds.), Atlas of Microbial Mat Features Preserved Within the Clastic Rock Record. Elsevier, pp. 53–71.

Bouougri, E., Porada, H., 2002. Mat-related sedimentary structures in Neoproterozoic peritidal passive margin deposits of the West African Craton (Anti-Atlas, Morocco). Sedimentary Geology 153, 85–105.

Bouougri, E., Porada, H., 2007a. Mat-related features from the Neoproterozoic Tizi n-Taghatine Group, Nnti-Atlas belt, Morocco. In: Schieber, J., Bose, P.K., Eriksson,

P.G., Banerjee, S., Altermann, W., Catuneanu, O. (Eds.), Atlas of Microbial Mat Features Preserved Within the Clastic Rock Record. Elsevier, pp. 198–207.

Bouougri, E., Porada, H., 2007b. Mat related features from the Terminal Ediacaran Nudaus Formation, Nama Group, Nambia, Schieber. In: J., Bose, P.K., Eriksson, P.G., Bannerjee, S., Sarkar, S., Altermann, W., Catuneanu, O., (Eds.), Atlas of Microbial Mat Features Preserved within the Siliciclastic Rock Record, Elsevier, pp. 214–221.

Bradley, W.H., 1933. Factors that determine the curvature of mud-cracked layers. American Journal Of Science 26, 55–71.

Burst, J. F., 1965. Subaqueously formed shrinkage cracks in clay. Journal Of Sedimentary Petrology 35, 348-353.

Cameron, B.W., Cameron, D., Jones, J.R., 1985. Modern algal mats in intertidal and supratidal quartz sands, northeastern Massachusetts, U.S.A. Special Publication - Society Of Economic Paleontologists And Mineralogists 35, 211–223.

Carmona, N., Bournod, C., Ponce, J.J., Cuadrado, D., 2012. The role of microbial mats in the preservation of bird footprints; a case study from the mesotidal Bahia Blanca Estuary (Argentina). Special Publication - Society For Sedimentary Geology 101, 37–45.

Catuneanu, O., 2007. Sequence stratigraphic context of microbial mat features. In: Schieber, J., Bose, P.K., Eriksson, P.G., Banerjee, S., Altermann, W., Catuneanu, O. (Eds.), Atlas of Microbial Mat Features Preserved Within the Clastic Rock Record. Elsevier, pp. 276–283.

Cressman, E.R., 1989, Reconnaissance stratigraphy of the Prichard Formation (Middle Proterozoic) and the early development of the Belt basin, Washington, Idaho, and Montana. U.S. Geol. Surv. Prof. Pap. 1490, 80 pp.

Cowan, C. A., James, N. P., 1992. Diastasis cracks; mechanically generated synaeresis-like cracks in Upper Cambrian shallow water oolite and ribbon carbonates. Sedimentology 39(6), 1101-1118.

Cuadrado, D.G., Perillo, G.E., Vitale, A.J., 2014. Modern microbial mats in siliciclastic tidal flats; evolution, structure and the role of hydrodynamics. Marine Geology 352, 367–380.

Darroch, S. F., Laflamme, M., Schiffbauer, J. D., Briggs, D. G., 2012. Experimental formation of a microbial death mask. Palaios, 27, 293–303.

Daza Brunet, R., Bustillo Revuelta, M. A., 2014. Exceptional silica speleothems in a volcanic cave; a unique example of silicification and sub-aquatic opaline stromatolite formation (Terceira, Azores). Sedimentology 61, 2113–2135.

De Boer, P.L., 1981. Mechanical effects of micro-organisms on intertidal bedform migration. Sedimentology 28, 129–132.

Decho, A., 1990. Microbial exopolymer secretions in ocean environments - their role(s) in food webs and marine processes. Oceanography And Marine Biology 28, 73–153.

Donovan, R. N., Foster, R. J., 1972. Subaqueous shrinkage cracks from the Caithness Flagstone Series (middle Devonian) of northeast Scotland. Journal Of Sedimentary Petrology 42, 309–317.

Dornbos, S. Q., Noffke, N., Hagadorn, J.W., 2007.Mat-decay features. In: Schieber, J., Bose, P.K., Eriksson, P.G., Banerjee, S., Altermann, W., Catuneanu, O. (Eds.), Atlas of Microbial Mat Features Preserved Within the Clastic Rock Record. Elsevier, pp. 106–110.

Eriksson, P.G., Simpson, E.L., Eriksson, K.A., Bumby, A.J., Steyn, G.L., Sarkar, S., 2000. Muddy roll-up structures in siliciclastic interdune beds of the c. 1.8 Ga Waterberg Group, South Africa. Palaios 15, 177–183.

Eriksson, P.G., Porada, H., Banerjee, S., Bouougri, E., Sarkar, S., Bumby, A. J., 2007a. Mat-destruction features. In: Schieber, J., Bose, P.K., Eriksson, P.G., Banerjee, S., Altermann, W., Catuneanu, O. (Eds.), Atlas of Microbial Mat Features Preserved Within the Clastic Rock Record. Elsevier, pp. 76–105.

Eriksson, P.G., Schieber, J., Bouougri, E., Gerdes, G., Porada, H., Banerjee, S., Bose, P.K., Sarkar, S., 2007b. Classification of structures left by microbial mats in their host sediments. In: Schieber, J., Bose, P.K., Eriksson, P.G., Banerjee, S., Altermann, W., Catuneanu, O. (Eds.), Atlas of Microbial Mat Features Preserved Within the Clastic Rock Record. Elsevier, pp. 39–52.

Frey, S. E., Gingras, M. K., Dashtgard, S. E., 2009. Experimental studies of gas-escape and water-escape structures; mechanisms and morphologies. Journal Of Sedimentary Research 79, 808-816. doi:10.2110/jsr.2009.087

Gavish, E., Krumbein, W. E., Halevy, J., 1985. Geomorphology, mineralogy and groundwater geochemistry as factors of the hydrodynamic system of the Gavish Sabkha Ecological studies; analysis and synthesis. Federal Republic of Germany: Springer-Verlag : Berlin, Federal Republic of Germany, 186-217.

Gehling, J.G., 1999. Microbial mats in terminal Proterozoic siliciclastics: Ediacaran death masks. Palaios 14, 40–57.

Gerdes, G., 2007. Structures left by modern microbial mats in their host sediments. In: Schieber, J., Bose, P.K., Eriksson, P.G., Banerjee, S., Altermann, W., Catuneanu, O. (Eds.), Atlas of Microbial Mat Features Preserved Within the Clastic Rock Record. Elsevier, pp. 5–38.

Gerdes, G., 2010. What are microbial mats? In: Seckbach, J., Oren, A. (Eds.), Microbial Mats. Modern and Ancient Microorganisms in Stratified Systems. Springer, Dordrecht, pp. 5–28.

Gerdes, G., Claes, M., Dunajtschik-Piewak, K., Riege, H., Krumbein, W.E., Reineck, H.E., 1993. Contribution of microbial mats to sedimentary surface structures. Facies 29, 61–74.

Gerdes, G., Klenke, T., Noffke, N., 2000. Microbial signatures in peritidal siliciclastic sediments: a catalogue. Sedimentology 47, 279–308.

Gingras, M., Hagadorn, J.W., Seilacher, A., Lalonde, S.V., Pecoits, E., Petrash, D., Konhauser, K.O., 2011. Possible evolution of mobile animals in association with microbial mats. Nature Geoscience 4, 372–375.

Groisman, A., Kaplan, E., 1994. An experimental study of cracking induced by desiccation. Europhys 25, 415–420.

Hagadorn, J. W., Bottjer, D. J., 1999. Restriction of a Late Neoproterozoic Biotope: Suspect-Microbial Structures and Trace Fossils at the Vendian-Cambrian Transition. PALAIOS 14, 73–85.

Hagadorn, J.W., McDowell, C., 2012. Microbial influence on erosion, grain transport and bedform genesis in sandy substrates under unidirectional flow. Sedimentology 5, 795–808.

Harazim, D., Callow, R.T., McIlroy, D., 2013. Microbial mats implicated in the generation of intrastratal shrinkage ('synaeresis') cracks. Sedimentology 60, 1621–1638.

Harrison, J.E., 1972, Precambrian Belt basin of northwestern United States: its geometry, sedimentation, and copper occurrences. Geol. Soc. Am. Bull. 83, 1215–1240.

Harrison, J. E., Kleinkopf, M. D., Wells, J. D., 1980. Phanerozoic thrusting in Proterozoic Belt rocks, northwestern United States. Geology [Boulder] 8, 407–411.

Horodyski, R. J., 1993. Paleontology of Proterozoic shales and mudstones; examples from the Belt Supergroup, Chuar Group and Pahrump Group, Western USA. Precambrian Research, 61(3-4), 241-278.

Kidder, D. L., 1988. Syntectonic sedimentation in the Proterozoic upper Belt Supergroup, northwestern Montana. Geology [Boulder] 16, 658–661.

Kilias, S. P., 2012. Microbial mat-related structures in the Quaternary Cape Vani manganese-oxide (-barite) deposit, NW Milos Island, Greece. Special Publication - Society For Sedimentary Geology 101, 97-110.

Konhauser, K., 2007. Introduction to geomicrobiology. Malden, MA: Blackwell Pub. 425 pp.

Krumbein, W.E., 1983. Stromatolites – the challenge of a term in space and time. Precambrian Res 20, 493–531.

Krumbein, W.E., Brehm, U., Gorbushina, A.A., Levit, G., Palinska, K.A., 2003. Biofilm, biodictyon and biomat – biolaminites, oolites, stromatolites – geophysiology, global mechanism and parahistology, In: W.E. Krumbein, D.M. Paterson and G.A. Zavarzin (Eds.) Fossil and Recent Biofilms. Kluwer, Dordrecht, pp. 1–27.

Laflamme, M., Schiffbauer, J. D., Narbonne, G., M, 2012. Dee-Water Microbially Induced Sedimentary Structures (MISS) in Deep Time: The Ediacaran Fossil *Ivesheadia*. Special Publication - Society For Sedimentary Geology 101, 111-124.

Lund, K., 2008. Geometry of the Neoproterozoic and Paleozoic rift margin of western Laurentia; implications for mineral deposit settings. Geosphere 4, 429–444.

Macke, D. L., 1993. Cambrian through Mississippian rocks of the Powder River basin, Wyoming, Montana, and adjacent areas. U. S. Geological Survey Bulletin, pp. 174.

Mangano, M. G., Buatois, L. A., Rindsberg, A. K., 2002. Carboniferous Psammichnites: Systematic Re-Evaluation, Taphonomy and Autecology. Ichnos -Chur-9, 1–22.

Meert, J.G., Torsvik, T.H., 2003. The making and unmaking of a supercontinent: Rodinia revisited. Tectonophysics 375, 261–288.

McMechan, M.E., 1981. The Middle Proterozoic Purcell Supergroup in the southwestern Rocky and southeastern Purcell Mountains, British Columbia and the initiation of the Cordilleran miogeocline, southern Canada and adjacent United States: Bulletin of Canadian Petroleum Geology 29, 583–621.

Noffke, N., 1998. Multidirected ripple marks rising from biological and sedimentological processes in modern lower supratidal deposits (Mellum Island, southern North Sea). Geology 26, 879–882.

Noffke, N., 1999. Erosional remnants and pockets evolving frombiotic–physical interactions in recent lower supratidal environment. Sedimentary Geology 123, 175–181.

Noffke, N., 2009. The criteria for the biogeneicity of microbially induced sedimentary structures (MISS) in Archean and younger, sandy deposits. Earth-Science Reviews 96, 173–180.

Noffke, N., Gerdes, G., Klenke, T., Krumbein, W. E., 2001. Microbially induced sedimentary structures; a new category within the classification of primary sedimentary structures. Journal Of Sedimentary Research 71, 649–656.

Noffke, N., Knoll, A.H., and Grotzinger, J.P., 2002, Sedimentary controls on the formation and preservation of microbial mats in siliciclastic deposits: A case study from the Upper Neoproterozoic Nama Group, Namibia: PALAIOS 17, 533–544.

Noffke, N., Gerdes, G., Klenke, T., 2003, Benthic cyanobacteria and their influence on the sedimentary dynamics of peritidal depositional systems (siliciclastic, evaporitic salty, and evaporitic carbonatic): Earth-Science Reviews 62, 163–176.

Noffke, N., Beukes, N., Gutzmer, J., Hazen, R., 2006a. Spatial and temporal distribution of microbially induced sedimentary structures: a case study from siliciclastic storm

deposits of the 2.9 Ga Witwatersrand Supergroup, South Africa. Precambrian Research 146, 35–44.

Noffke, N., Eriksson, K.A., Hazen, R.M., Simpson, E.L., 2006b. A new window into Early Archean life: microbial mats in Earth's oldest siliciclastic tidal deposits (3.2 Ga Moodies Group, South Africa). Geology 34, 253–256.

Noffke, N., Christian, D., Wacey, D., Hazen, R.M., 2013. Microbially induced sedimentary structures recording an ancient ecosystem in the ca. 3.48 billion-year-old Dresser Formation, Pilbara, Western Australia. Astrobiology, 13, 1103–1124.

Owttrim, G.W., 2012. RNA helicases in cyanobacteria: biochemical and molecular approaches. Methods In Enzymology 511, 385–403.

Parizot, M., Eriksson, P.G., Aifa, T., Sarkar, S., Banerjee, S., Catuneanu, O., Altermann, W., Bumby, A.J., Bordy, E.M., Rooy, J.L.V., Boshoff, A.J., 2005. Suspected microbial mat-related crack-like sedimentary structures in the Palaeoroterozoic Magaliesberg Formation sandstones, South Africa. Precambrian Research 138, 274–296.

Pearson, R.C., 1996. Cambrian (?), Middle Proterozoic, and Archean Rocks Penetrated in a Borehole near Argenta. U. S. Geological Survey Bulletin 2121-B, pp. 21.

Pecoits, E., Konhauser, K.O., Aubet, N.R., Heaman, L.M., Veroslavsky, G., Stern, R. A., Gingras, M. K., 2012. Bilaterian burrows and grazing behavior at >585 million years ago. Science 336, 1693–1696.

Pflüger, F., 1999. Matground Structures and Redox Facies. Palaios 14, 25–39.

Pflüger, F., Gresse, P.G., 1996. Microbial sand chips — a non-actualistic sedimentary structure. Sedimentary Geology 102, 263–274.

Plummer, P.S., Gostin, V.A., 1981. Shrinkage cracks: desiccation or synaeresis? Journal Of Sedimentary Petrology 51, 1147–1156.

Parizot, M., Eriksson, P.G., Aifa, T., Sarkar, S., Banerjee, S., Catuneanu, O., Altermann, W., Bumby, A.J., Bordy, E.M., Rooy, J.L.V., Boshoff, A.J., 2005. Suspected microbial mat-related crack-like sedimentary structures in the Palaeoroterozoic Magaliesberg Formation sandstones, South Africa. Precambrian Research 138, 274–296.

Porada, H., Loeffler, T., 2000. Microbial shrinkage cracks in siliciclastic rocks of the Neoproterozoic Nosib Group (Damara Supergroup) of central Namibia. Communications Of The Geological Survey Of South West Africa/Namibia 12, 63–72.

Porada, H., Bouougri, E.H., 2007. 'Wrinkle structures' – a critical review. In: Schieber, J., Bose, P.K., Eriksson, P.G., Banerjee, S., Altermann, W., Catuneanu, O. (Eds.), Atlas of Microbial Mat Features Preserved Within the Clastic Rock Record. Elsevier, pp. 135–144.

Porada, H., Bouougri, E.H., Ghergut, J., 2007. Hydraulic conditions and mat-related structures in tidal flats and coastal sabkhas. In: Schieber, J., Bose, P.K., Eriksson, P.G., Banerjee, S., Altermann, W., Catuneanu, O. (Eds.), Atlas of Microbial Mat Features Preserved Within the Clastic Rock Record. Elsevier, pp. 258–265.

Porada, H., Ghergut, J., Bouougri, E.H., 2008. Kinneyia-Type Wrinkle Structures: Critical Review and Model of Formation. Palaios 23, 65–77.

Porada, H., Druschel, G., 2010. Evidence for participation of microbial mats in the deposition of the siliciclastic 'ore formation' in the Copperbelt of Zambia. Journal Of African Earth Sciences, 58, 427–444.

Pratt, B. R., 1998. Syneresis cracks; subaqueous shrinkage in argillaceous sediments caused by earthquake-induced dewatering. Sedimentary Geology 117, 1–10.

Pratt, B. R., 2001. Calcification of cyanobacterial filaments; girvanella and the origin of lower Paleozoic lime mud. Geology [Boulder] 29, 763–766.

Reineck, H. E., Gerdes, G., Claes, M., Dunajtschik, K., Riege, H., Krumbein, W. E., 1990. Microbial modification of sedimentary surface structures. In: Federal Republic of Germany, Springer-Verlag, Berlin, Federal Republic of Germany, 254-278.

Ross, G. M., Villeneuve, M., 2003. Provenance of the Mesoproterozoic (1.45 Ga) Belt basin (western North America): another piece in the pre-Rodinia paleogeographic puzzle. The Geological Society Of America Bulletin 10, 1191–1217.

Sarkar, S., Banerjee, S., Samanta, P., Jeevankumar, S., 2006. Microbial mat-induced sedimentary structures in siliciclastic sediments; examples from the 1.6 Ga Chorhat

Sandstone, Vindhyan Supergroup, M. P., India. Journal Of Earth System Science, 115, 49–60.

Sarkar, S., Bose, P.K., Samanta, P., Sengupta, P., Eriksson, P.G., 2008. Microbial mat mediated structures in the Ediacaran Sonia Sandstone, Rajasthan, India, and their implications for Proterozoic sedimentation. Precambrian Research 162, 248–263.

Sarkar, S., Banerjee, S., Samanta, P., Chakraborty, N., Chakraborty, P. P., Mukhopadhyay, S., Singh, A. K., 2014. Microbial mat records in siliciclastic rocks; examples from four Indian Proterozoic basins and their modern equivalents in Gulf of Cambay. Journal Of Asian Earth Sciences 91, 362–377.

Schieber, J., 1998. Possible indicators of microbial mat deposits in shales and sandstones; examples from the mid-Proterozoic Belt Supergroup, Montana, U.S.A. Sedimentary Geology 120, 105–124.

Schieber, J., 2004. Microbial mats in the siliciclastic rock record; a summary of diagnostic features. Developments In Precambrian Geology 12, 663–673.

Schieber, J., 2007. Mats on Sandy Substrates – Diagenetic Features Related to Mat Metabolism and Decay. In: Schieber, J., Bose, P.K., Eriksson, P.G., Banerjee, S., Altermann, W., Catuneanu, O. (Eds.), Atlas of Microbial Mat Features Preserved Within the Clastic Rock Record. Elsevier, pp. 72–75.

Schieber, J., Bose, P.K., Eriksson, P.G., Banerjee, S., Altermann, W., Catuneanu, O. (Eds.), 2007. Atlas of Microbial Mat Features Preserved Within the Clastic Rock Record. Elsevier, Amsterdam, Netherlands. 324 pp.

Seilacher, A., 1999. Biomat-related lifestyles in the Precambrian. Palaios 14, 86–93.

Seilacher, A., 2008. Biomats, biofilms, and bioglue as preservational agents for arthropod trackways. Palaeogeography, Palaeoclimatology, Palaeoecology 270, 252–257.

Shepard, R.N., Sumner, D.Y., 2010. Undirected motility of filamentous cyanobacteria produces reticulate mats. Geobiology 8, 179–190.

Shorlin, K.A., de Bruyn, J.R., Graham, M., Morris, S.W., 2000. Development and geometry of isotropic and directional shrinkage-crack patterns. Physical Review E 61, 6950–6957.

Smith, A. G., Barnes, W. C., 1966. Correlation of and facies changes in the carbonaceous, calcareous, and dolomitic formations of the Precambrian Belt-Purcell Supergroup. Geological Society Of America Bulletin 77, 1399–1426.

Tang, D., Shi, X., Jiang, G., Wang, X., 2012. Morphological association of microbially induced sedimentary structures (MISS) as a paleoenvironmental indicator; an example from the Proterozoic succession of the southern North China Platform. Special Publication - Society For Sedimentary Geology 101, 163–175.

Tanner, P. G., 1998. Interstratal dewatering origin for polygonal patterns of sand-filled cracks; a case study from late Proterozoic metasediments of Islay, Scotland. Sedimentology 45(1), 71–89.

Tanner, P. G., 2003. SYNERESIS. Encyclopedia Of Sediments & Sedimentary Rocks, 718–720.

Thomas, K., Herminghaus, S., Porada, H., Goehring, L., 2013. Formation of Kinneyia via shear-induced instabilities in microbial mats. Philosophical Transactions. Series A, Mathematical, Physical, And Engineering Sciences 371, 20120362.

Walcott, C.D., 1914. Cambrian geology and palaeontology III, no. 2: Precambrian, Algonkian algal flora: Smithsonian Miscellaneous Collections 64, 77–156.

Walter, M. R., Oehler, J. H., Oehler, D. Z., 1976. Megascopic algae 1300 million years old from the Belt Supergroup, Montana; a reinterpretation of Walcott's Helminthoidichnites. Journal Of Paleontology 50(5), 872-881.

White, W. A., 1961. Colloid phenomena in sedimentation of argillaceous rocks. Journal Of Sedimentary Petrology 31, 560–570.

Yonkee, W.A., C.D. Dehler, P.K. Link, E.A. Balgord, J.A. Keeley, D.S. Hayes, M.L. Wells, C.M. Fanning, S.M. Johnston, 2014. Tectono-stratigraphic framework of Neoproterozoic to Cambrian strata, west-central U.S.: Protracted rifting, glaciation, and evolution of the North American Cordilleran margin. Earth-Science Reviews 136, 59–95.

Appendix A:
Experimental Gas Domes

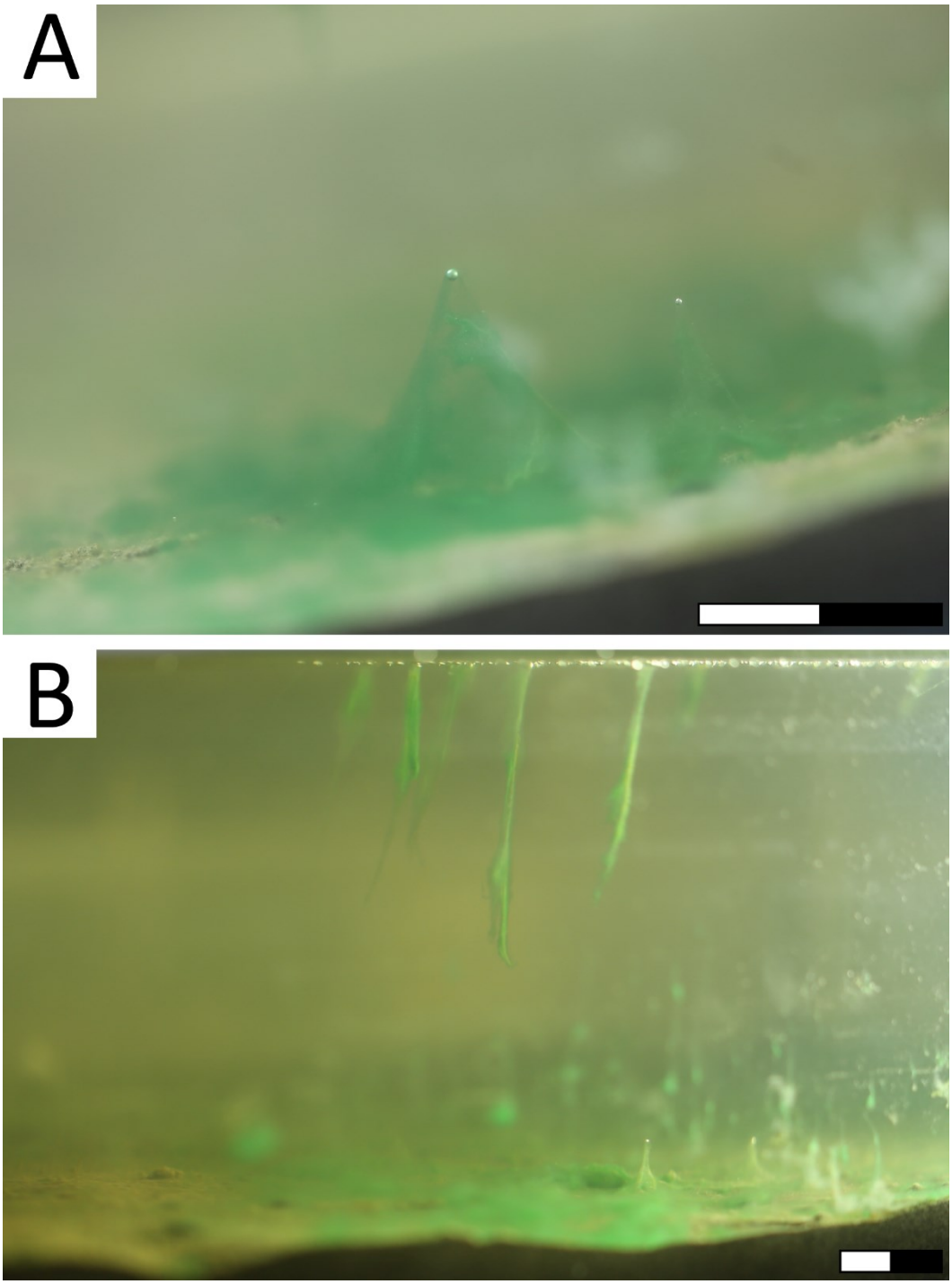

A-1. Sand-rich substratum. (A) Biofilm cone features produced by ascending gas bubbles, 5 day old biomat. (B) Cones detach and float at top of the water, held in place by entangled gas bubbles, 6 day old biomat. Scale bar is 2 cm.

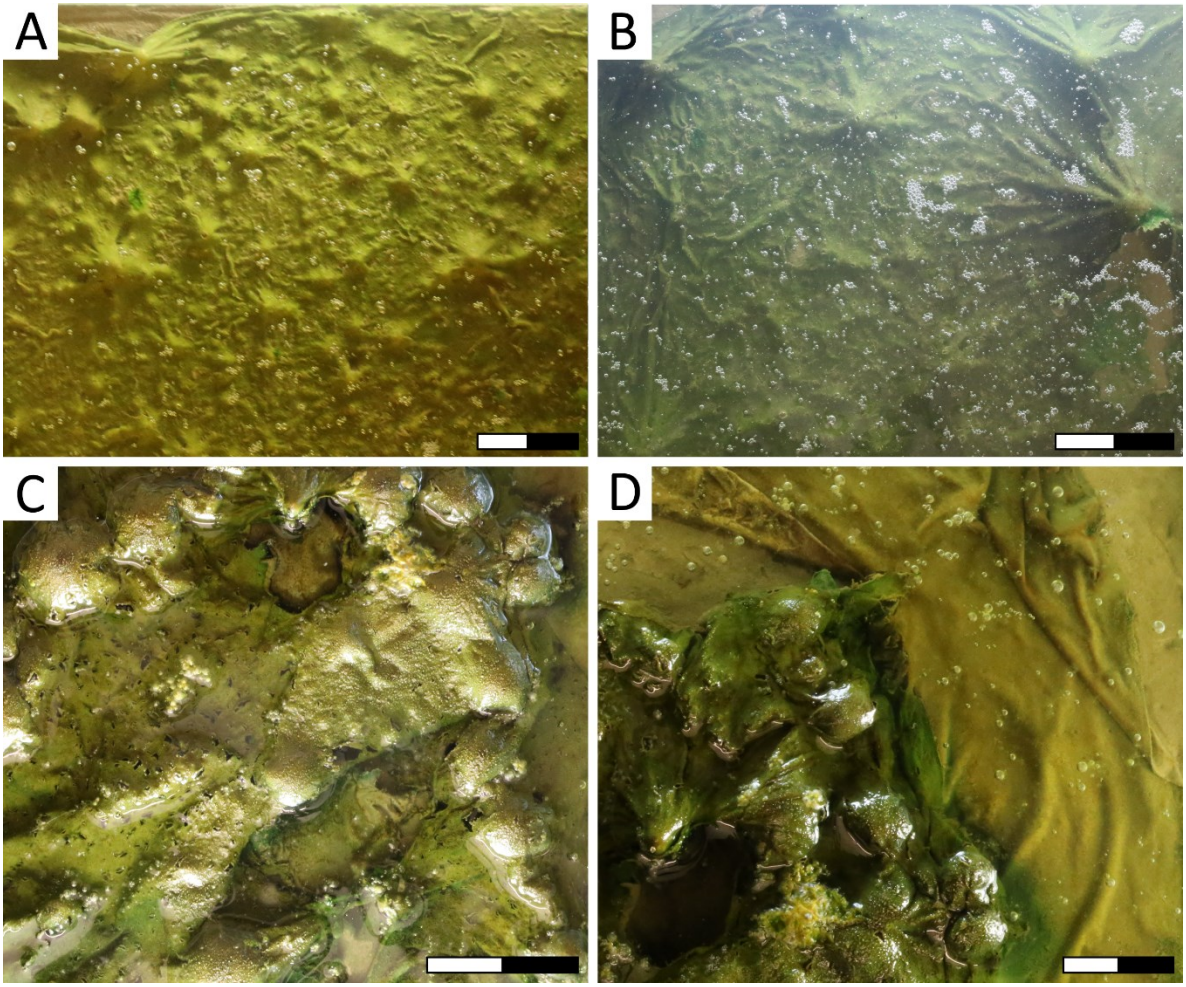

A-2. Clay-rich substratum. (A) Small gas domes produced in a young, 7 day old biofilm. (B) Long-lived gas domes in 20 day old biomat. (C) Some gas domes remain intact, while others deflate and produce wrinkles, 30 day old biomat. (D) Close-up view of the gas domes. Scale bar is 2 cm.

Appendix B:
SEM Elemental Maps

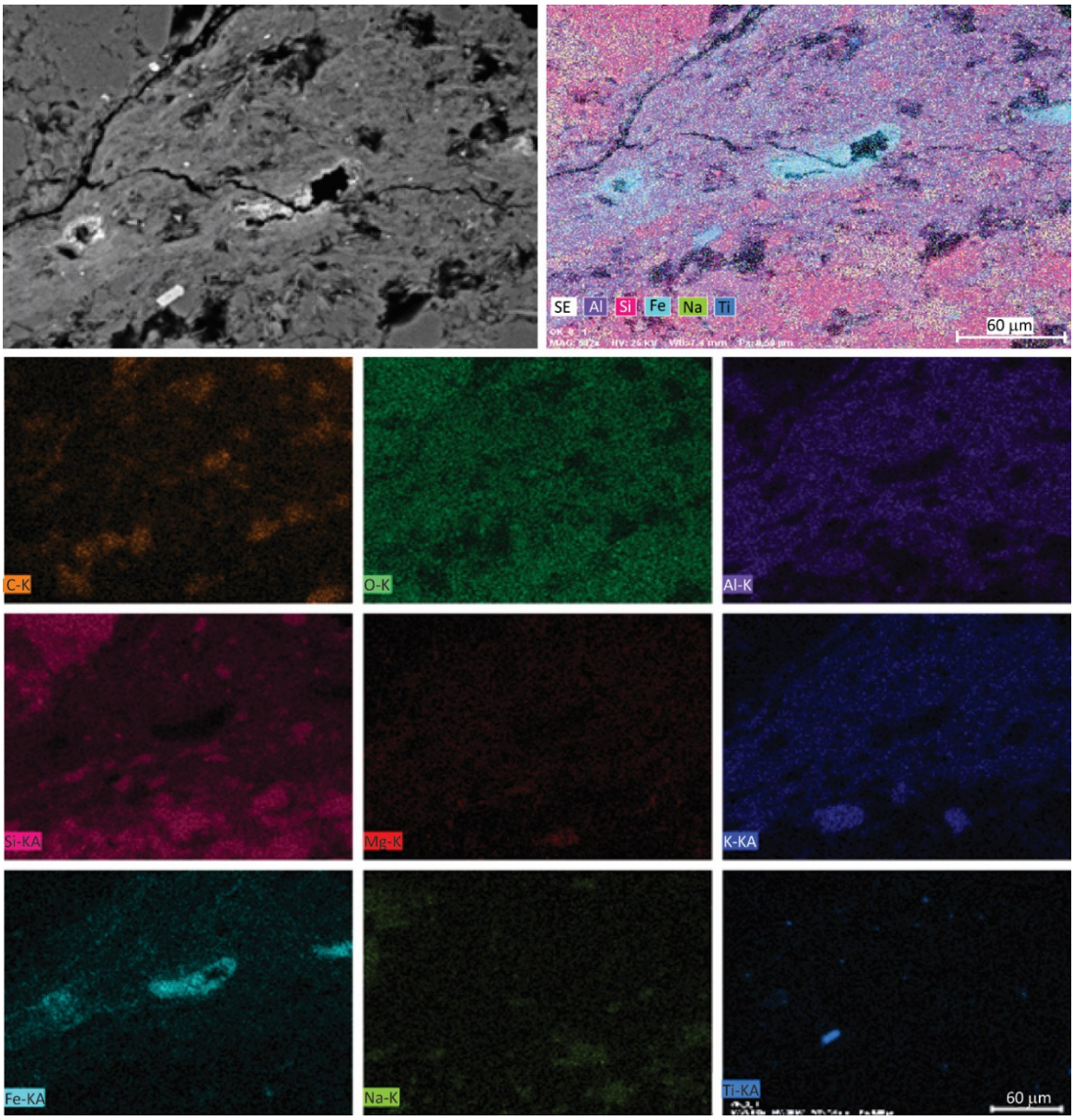

B-1. SEM elemental analysis of biolamina 1. Biolamina is enriched in Al, K, Fe, C, Ti.

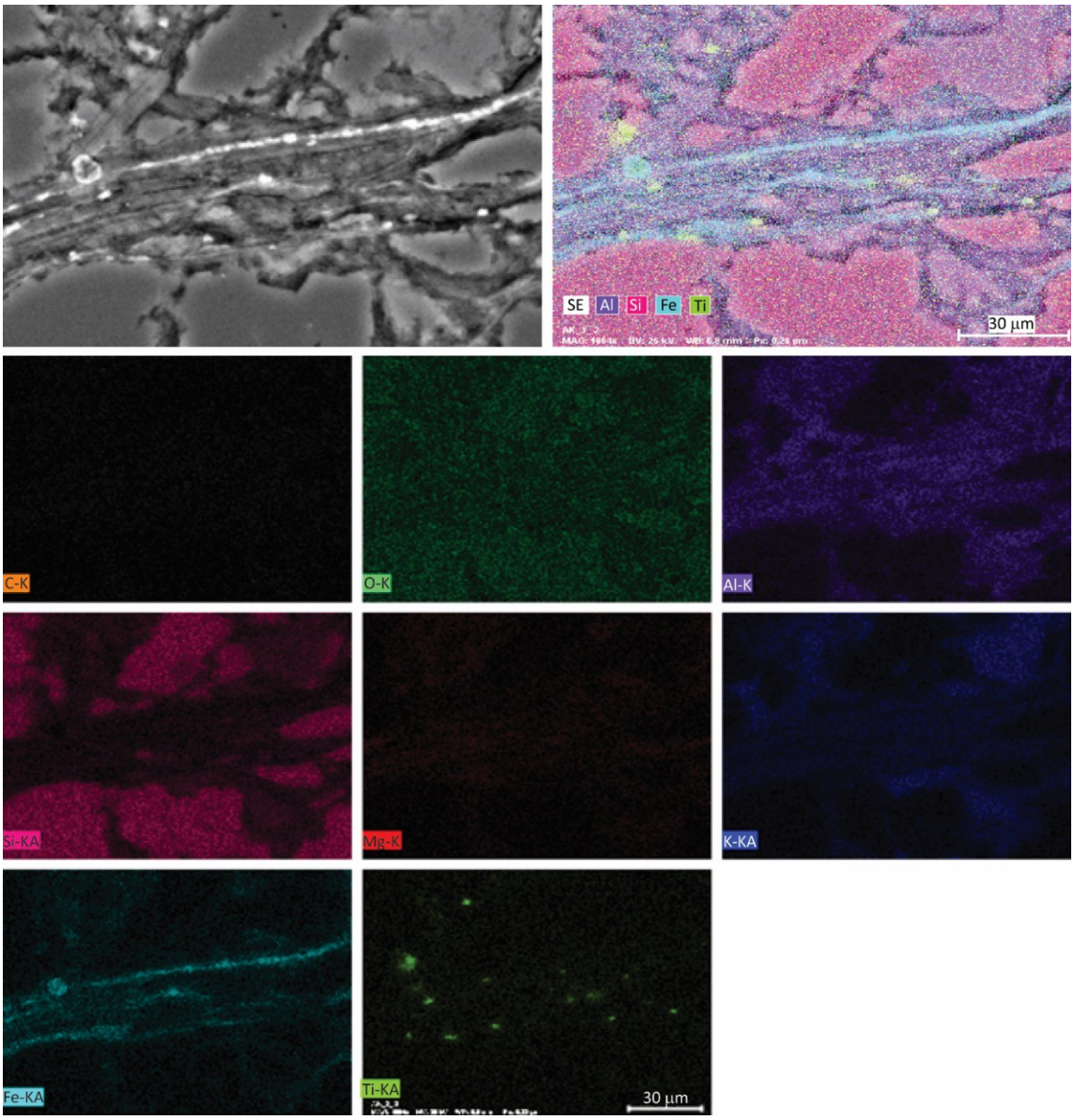

B-2. SEM elemental analysis of biolamina 2. Biolamina is enriched in Al, K, Fe, Ti, and Mg(?).